Takeoff of a hydrofoil vessel in Panship

Prediction of lift and drag of a hydrofoil vessel during the takeoff in a Boundary Element Method

J. E. Lotz

MARIN

TUDelft

Takeoff of a hydrofoil vessel in Panship

Prediction of lift and drag of a hydrofoil vessel during the takeoff in a Boundary Element Method

by

J.E. Lotz

to obtain the degree of Master of Science

at the Delft University of Technology,

to be defended publicly on Tuesday January 28, 2019 at 15:00 AM.

An electronic version of this thesis is available at `http://repository.tudelft.nl/`.

TUDelft

Abstract

Recently the interest in hydrofoil vessels using a fully submerged hydrofoil increased. Hydrofoil vessels experience a resistance hump and possible instabilities during their takeoff of which both are influence by waves. In order to determine the required power during the takeoff to overcome the resistance hump and to investigate whether the hydrofoil vessel is stable during the takeoff numerical simulations or experiments have to be performed. Experiments covering the full takeoff require a long towing tank and high towing velocities and therefore these experiments are costly. The alternative, performing numerical simulations, is favorable but requires a suitable numerical code. As no validated code is available in which a takeoff can be performed in waves, in this research Panship, a potential flow code suitable for high speed craft and adapted for use with hydrofoil craft, is validated for the takeoff of a hydrofoil vessel.

In this research the results of Panship are compared with results of experiments and other numerical codes in four different stage as little validation data is present for the takeoff of a hydrofoil vessel. The four different stages are: a foil without the influence of the free surface, a foil with the influence of the free surface, two foils with the influence of the free surface and the hull and foil system near during the takeoff. In these four stages the lift and drag determined in Panship is compared with available experimental results and numerical codes.

As the simulations in Panship require a vast amount of input parameters, the influence of these parameters is studied first to ensure the reliability of the results. Comparing the results of Panship for a deeply submerged foil with another potential flow solver shows that the lift is predicted correctly, but that the induced drag is underpredicted. If viscous effects are required in the solution, the quality of the results of Panship is dependent on the type of hydrofoil used. As some foils have a large viscous effect on lift, the lack of viscosity on Panship, leads to a low quality of the results for lift and induced drag as they are overpredicted. The trends for interaction of a foil with the free surface are predicted correctly but the underprediction of induced drag influences the quality of the results. Panship is able to predict the effects of foil interaction for lift correctly, but the results for foil interaction for drag are poorer. During the takeoff Panship is able to predict the lift fairly correct but the total drag is underpredicted severely. Recommendations are given to improve the results of Panship and for future work.

Preface

Getting to the end of this project I realize how much fun I had during this project. Maritime Research Institute Netherlands (MARIN) definitely provides a challenging working environment in which the knowledge of many experts is available. Looking back, I see how many I have learned from these experts.

I would like to thank my supervisors Francisco and Ido for their guidance during this project. Francisco provided great help by guiding me through the different stages of this thesis and providing a fresh view on my work. Ido was always able to keep me on track and helped me with his welcome critics to improve my work. Furthermore, at MARIN Frans, although not being my supervisor, was able to help me with all my questions on the use of Panship which gave me insight into the details of Panship.

Furthermore I would like to thank Michiel, Michel, Wick, Maarten and Derk for their company during the many coffee breaks. As the projects of Michel and mine were closely related, we were able to cooperate which gave insight into the behavior of foils. I had a lot of fun with the members of the Henhouse, the student room of MARIN, during the breaks and evenings. Thank you all for that. I would like to thank my parents for letting me stay at their place and providing advice as well. At last I would like to thank the cluster manager for providing a motivating and friendly cooperation.

J.E. Lotz
Delft, January 2020

Contents

Glossary

BEM Boundary Element Method. 2, 17, 21

LLXM Lifting Line - XFoil Method. 2, 18, 20–23, 25, 26, 33–37, 43–45, 47–52

MARIN Maritime Research Institute Netherlands. 21, 55

RANS Reynolds-averaged Navier-Stokes. 43

VLM Vortex Lattice Method. 42, 48

1

Introduction

A hydrofoil craft is a vessel which is supported by hydrodynamic forces of foils such that its hull is completely clear above the water surface and that its resistance is reduced. Hydrofoil vessels can be subdivided in two classes, hydrofoil vessels using a surface piercing hydrofoil and hydrofoil vessels using a fully submerged hydrofoil. These types of hydrofoils are also called V-shaped hydrofoils and T-shaped hydrofoils respectively [8]. Both types of hydrofoils can be seen in figure 1.1. The advantage of a surface piercing hydrofoil is that it does not require a control system to regulate the required lift, as the lift is regulated by submerging the foil deeper or less deep. However, under influence of waves this system does not perform well as the waves influence the system severely by having the same effect. Therefore, vessels with a fully submerged foil, although requiring a complex control system, have a benefit since they are less affected by waves.

Figure 1.1: A hydrofoil vessel with surface piercing foils on the left and a hydrofoil vessel with fully submerged hydrofoils on the right. Figure based on [25].

In the 1960s a broad interest in hydrofoil vessels lead to the development of several hydrofoil vessels using a fully submerged hydrofoil, but due to its complexity and high costs the interest in hydrofoil vessels weakened. However, recently the interest in hydrofoil vessels using a fully submerged hydrofoil increased again

1

due to their use in the latest events of the America's Cup. The level of competitiveness in the America's Cup demands for faster sailing ships and innovation plays a significant role. As a result, hydrofoil technology is applied to decrease the resistance of the vessel. The application of this technology to sailing vessels led to a renewed interest within the shipping market to apply it in the transportation of passengers using high speed vessels. Problems which lead to a declined interest in hydrofoil craft can now be overcome due to present-day technologies like composites and high quality control systems.

Moreover, hydrofoil vessels have hydrodynamic advantages over normal high speed vessels. The first benefit is the reduced resistance in foil borne conditions where the vessel is able to travel more energy efficient and can attain higher speeds. The second benefit is that hydrofoil vessels have good sea-keeping characteristics in both hull borne and foil borne conditions. Since the wave excitation of the vessel decreases as the hull is lifted above the water, the motions of hydrofoil vessels are greatly reduced when sailing in foil borne mode. Motions can also be reduced when sailing in hull borne mode since the hydrodynamic lift of the submerged foils can be used as control force [15]. Due to the reduction in motions of the vessel, passengers experience less seasickness and experience the trip as more pleasant. This is for instance relevant for offshore windmill mechanics who will be less tired when arriving at their destination and work more efficiently.

The application of high speed foiling vessels for the transportation of passengers has several other benefits. For example, the benefits of high speed vessels versus airplanes for passenger transportation in the Canary Islands is discussed by Grisolia and de Dios Ortuzar [9]. In this case, the high speed vessel was able to sail directly into the city whereas using an airplane requires at least an extra 40 minutes transit from and to the airport. In addition, transportation using fast vessels from and to cities across bodies of water does not require an extensive infrastructure. Therefore, the infrastructure needed for transportation with high speed vessels may be cheap to realize compared to the infrastructure needed for airplanes. As a hydrofoil vessel is more energy efficient it can play a role in the reduction of emissions.

In order to have the described advantages, the hull of the hydrofoil vessel has to be lifted out of the water and therefore the hydrofoil vessel has to perform a takeoff. The takeoff of a hydrofoil vessel consists of a transition from the hull borne to foil borne condition as the hydrofoil vessel produces more lift with increasing speed. This takeoff has several challenges. First, the vessel should have enough power to overcome a resistance hump, induced by the resistance of the hull and the foil system, which the vessel experiences just before the takeoff. Only after the takeoff the resistance is reduced as the hull is risen out of the water. The hump the hydrofoil vessel has to overcome is larger than that of a non-foiling craft as the wet area is increased due to the presence of the foil system. Furthermore, at low velocities the foil system provides little lift and therefore is not able to lift the vessel out of the water to have a benefit. Second, when performing a takeoff, difficulties arise with the stability of the vessel at the moment the hull rises out of the water. The presence of free surface waves influences the resistance and stability of the hydrofoil vessel as well and cannot be neglected.

Two options are available to analyze the stability and resistance during the takeoff: performing towing tank tests and performing numerical calculations. The first, performing towing tank tests is difficult and costly due to the high towing speed, requiring a large towing tank, and the required control system. The second, performing numerical calculations, requires a suitable numerical code. This thesis focuses on the second.

The numerical methods used for the takeoff study have four requirements. First, during the transition from hull borne to foil borne condition, the submerged geometry of the vessel changes drastically. Therefore the numerical method has to be able to cope with changes of the submerged geometry. Remeshing of the geometry is required for some methods during the takeoff and a simple definition of the geometry is favorable. Second, the influence of external waves should be included in the solution and therefore the numerical code should be unsteady. Third, the solution must include ride control for lifting surfaces to be able to actively stabilize the hydrofoil vessel. Last, to reduce computational costs and for it to be practical in (early) design stage, the method has to be fast.

Determining the hydrodynamical forces of a hydrofoil vessel during the takeoff using a detailed CFD-solver is unfavorable as a large amount of time steps is required leading to long simulation time and thus high computational costs. However, a much faster solution is obtained by neglecting viscosity and compressibility and therefore resorting to potential flow. Several unsteady potential flow codes are available, but few are suitable for the takeoff of a hydrofoil vessel.

For this research, two suitable potential flow codes for a takeoff of a hydrofoil vessel are available: Unvlm and Panship. Unvlm uses the Vortex Lattice Method (VLM) and consists of an unsteady and a steady part, Unvlm and Hydres. Unvlm does not incorporate hull forces and therefore cannot be used for the takeoff of a hydrofoil vessel. In Hydres the hull forces are incorporated, but the method is not able to cope with unsteady flow and therefore can only be used to perform a takeoff without disturbance of waves [25]. The hull forces are determined by interpolation of the results of the Series 65 model tests. This limits the use of Hydres as only hull forms with a close resemblance with the Series 65 models can be used. The foil forces can be calculated separately by without the influence of the hull in the subprogram Hydvlm. Panship is a Boundary Element Method (BEM) and is mainly developed for assessment of seakeeping behaviour of high speed craft. The program is relatively fast but computationally more intensive than Hydres. Flow corrections for fast ships have been implemented in Panship, including a transom flow condition, forces of propellers and motion control appendages. Due to these implementations the results of Panship are realistic for high speed craft despite neglecting viscosity and compressibility [3]. In Panship, in contrast to Hydres, the full geometry is discretised and not only the foil system. Therefore Panship can be used for a wide variety of hull forms.

Hydres has been validated extensively for its purpose, the takeoff of a hydrofoil vessel, but Panship has not. As it is possible to perform a takeoff in waves in Panship and in Panship a wide variety of hull shapes can be used, but not in Hydres, in this thesis Panship is validated for the takeoff of a hydrofoil vessel. The ultimate goal is to validate Panship for the takeoff of a hydrofoil vessel in waves, but due to the complexity of the problem and the little available validation data, this research is limited to calm water is used. This is considered as a first step in the validation process of Panship. Furthermore, since Hydres is much less computationally intensive, the question arises what the benefit of using Panship in calm water is. In other words, what is the quality of results of Hydres versus Panship in calm water. Therefore the research question in this thesis is:

> *What is the quality of the results for the hydrodynamical forces during the takeoff of a hydrofoil vessel in Panship in calm water, and how does this compare to the results of Hydres?*

Due to the simplifications and linearizations in Panship, the code should be validated thoroughly to ensure the reliability of its results. This validation process should be done carefully, and therefore the validation process is split up into four parts which are represented by the following subquestions:

1. *What is the quality of the results for the hydrodynamical forces for a deeply submerged hydrofoil in Panship with a constant forward speed?*

2. *What is the quality of results for the hydrodynamical forces for a foil near the free surface in Panship in calm water with a constant forward speed?*

3. *What is the quality of the results for the hydrodynamical forces for two foils towed behind each other in Panship in calm water with a constant forward speed, and how does this compare to the results of Hydvlm?*

4. *What is the quality of the results for the hydrodynamical forces of a foil and ship system in Panship during the takeoff in calm water, and how does this compare to the results in Hydres?*

The hydrodynamical forces consist of the lift and drag, or a ratio of these. The total drag consists of the lift induced drag and parasitic drag of which the latter is a viscous effect. In the four different validation steps the complexity of the problem is increased with every step to end with the most complex step, the takeoff of a hydrofoil vessel. The four subquestions represent four different phenomena: lift and drag of a foil without the presence of the free surface, interaction between the foil and the free surface, interaction between two foils near the free surface and interaction between the hull and the foil system near the free surface.

The first subquestion has the purpose of validating the result of Panship in a very controllable environment, without the free surface. In this straight forward solution is determined if the lift and drag are determined correctly before the complexity of the problem is increased. The effect of changing the input parameters of Panship is studied in this environment as well. In the second subquestion the free surface is added to the

solution. As the free surface influences the performance of the hydrofoil, it is investigated if Panship is able to correctly predict the free surface effects on a hydrofoil. The interaction between two foils without the presence of a hull is studied in the third subquestion since if a foil is towed in the wake of a different foil, its performance is influenced. This interaction is also influenced by the free surface and therefore is complex. As the hull influences the performance of the foils and vice versa, in the last subquestion the interaction between the hull and the foil is studied during different stages of the takeoff.

The subquestions and the research questions are answered using five different sources of validation data consisting of experimental results and four numerical flow solvers. The results of numerical flow solvers are an extension to the experimental results. The used numerical flow solvers are: the Lifting Line - XFoil Method (LLXM), XFoil, Unvlm and Refresco. An overview of the validation data sources is given in table 1.1 which also indicates which source is used to give an answer to the subquestion. The LLXM, XFoil and Unvlm will be described in this work but for a description of Refresco is referred to [1], many other sources are available.

The used experimental results consist of results of foils in three configurations and sources. The three different foil system configurations are: a foil towed near the free surface [27], two foils towed near the free surface showing interaction effects [19] and a hull-foil system with the presence of the free surface. The last consists of experiments performed in the early 90s at MARIN.

As the induced drag is difficult to predict in experiments, a model is developed in which the induced drag can be determined separately from the total drag. As the induced drag can be determined separately from the total drag, this method is very suitable. This model is called the LLXM and uses lifting line theory and results of XFoil to determine three dimensional foil forces. The background of the LLXM will be given. In this work the LLXM is used to determine foil forces for a deeply submerged foil and for foil-foil interaction coefficients for two deeply submerged foils. As the LLXM is developed during this thesis, its results have to be validated before it can be used. This validation process is also performed in this work.

XFoil is a numerical tool developed in the early 90s which is able to determine the 2D foil forces in a very efficient manner. The method is based on the BEM and viscous effects can be included or neglected in the solution. XFoil is used as an input for the LLXM and to compare the pressure distribution of Panship to.

As little validation data is present on foil-foil interaction, the results of Hydvlm and Hydres, marked as Unvlm in the table, provide a welcome extension of validation data. As Hydvlm and Hydres are validated in earlier work, Panship can be validated using their results as an extension to the experimental results [25].

The four different subquestions will be answered in the conclusions of four different chapters. As can be seen in table 1.1 not every source of validation data is used for every subquestion but each subquestion uses a selection.

To provide an answer to the first subquestion, numerical results of two numerical flow solvers are used to compare the lift and drag of Panship to. In the comparison viscous effects are first excluded, to see if the results of Panship are correct with respect to other inviscid solvers, and later included to see what the effect of neglecting viscous effects is on the quality of the results of Panship. The used flow solvers are the LLXM and Refresco. Furthermore, the lift distribution of Panship is compared to the lift distribution of XFoil.

The second subquestion is answered using experimental results and numerical results of the LLXM and Refresco. A comparison of results of Panship with experimental results is performed to see whether Panship is able to correctly predict the effects of the interaction between the free surface and a foil. This comparison has been performed earlier but is redone here as more computational power is available and Panship has been developed over time [3].

The third subquestion is answered using experimental results, an extension of the LLXM for two foils and the results of Unvlm. First, the free surface is excluded from the solution, to create a controllable environment, and the results for foil interaction in Panship are compared to the LLXM. Second, the foil interaction in Panship is studied near the free surface by comparing the results of Panship to experimental results and Hydvlm. The effect of adding a strut to the solution is studied as well.

An answer to the last subquestion is formulated using experimental results and the results of Unvlm. The re-

Table 1.1: Table indicating if experimental results are used and which models are used to give an answer to the subquestion. The subquestions are represented by a short description and the numbers refer to the subquestions.

	1. A deeply submerged foil	2. A foil near the free surface	3. Foil-foil interaction	4. Hull-foil interaction
Experiments		●	●	●
LLXM	●	●	●	
XFoil	●			
Unvlm			●	●
Refresco	●	●		

sults of forces on a hull and foil system in Panship and Hydres are compared to experimental results. Furthermore, to find the source of the differences between the results of Panship and the experiments, the interaction coefficients are studied.

The aim of this thesis is to provide insight into the quality of the results of Panship and to see if a Boundary Element Method is suitable for prediction of the hydrodynamic forces during the takeoff of a hydrofoil vessel. Furthermore, it was noticed that in earlier work not all findings were documented thoroughly and results were difficult to reproduce. Therefore, during the current research unnecessary research was redone. To avoid the same in future work this thesis provides a thorough description of the used input parameters and detailed findings such that the work can easily be reproduced in future work, for instance, the takeoff of a hydrofoil vessel in waves. For readers which are not interested in these details is referred to the introductions and conclusions of the chapters.

The following structure is adopted in this work. First, this thesis starts with the physical background of foils and hydrofoil vessels and continues with the used numerical codes, Panship, Unvlm, XFoil and the LLXM in chapter 2. Second, Panship is validated for a single hydrofoil without a free surface in chapter 3. Third, Panship is validated for a foil in the proximity of a free surface in chapter 4. Fourth, the hydrodynamics of two hydrofoils in Panship, of which the second hydrofoil comes in the wake of the first hydrofoil, is validated in chapter 5. Fifth, the transition from the hullborne to the foilborne condition of a foiling vessel and the interaction between the hull and the foil are studied in chapter 6. Last, a conclusion is drawn and an answer to the research question is provided in chapter 7.

The structure of the four chapters which provide an answer to a subquestion is as follows. First the used validation source, consisting of experimental and numerical results, is described. Second the results of Panship are described and compared to the results of the used validation source. Last, based on the used validation source and the results of Panship a conclusion is formulated.

2

Fundamentals

In this chapter the fundamental theories are given on how a foil and a hydrofoil vessel work, followed by an introduction to four computational models. The theory behind hydrofoils and hydrofoil vessels can be split into four different parts. First is started with a single foil without free surface effects, a deeply submerged hydrofoil. Second, by adding a free surface, the performance of the hydrofoil is influenced. Therefore, free surface effects on hydrofoil performance have to be accounted for as well and therefore are introduced. Third, as most hydrofoil vessels have two hydrofoils, the hydrofoil which is placed in the aft of the hydrofoil craft is influenced by the most forward foil. This means that the interaction between two foils near the free surface has to be considered and introduced as well. Fourth and last, during the takeoff (a part of) the hull is in the water which also influences the performance of the foils. Therefore the hull foil interaction has to be accounted for as well.

Four different computational models are introduced in this chapter. These computational models are: Panship, Unvlm, XFoil and the LLXM. In order to introduce these computational models, the governing equations and fundamental theories are provided as well.

The structure of this chapter is as follows. First the behaviour of a deeply submerged foil is described in section 2.1, which is followed by the behaviour of a foil in the proximity of a free surface in section 2.2. Section 2.3 then treats the effect of the wake of a forward foil on a trailing foil. The foil interaction is described next in section 2.4. In order to introduce the numerical methods, first the governing equations are given in section 2.5 then the numerical methods Panship, Unvlm, XFoil and the LLXM are introduced in sections 2.6, 2.7, 2.8 and 2.9 respectively.

2.1. Lift and drag for a deeply submerged foil

A hydrofoil is curved or flat fin like device which is attached to the vessel using struts. A comparison to a wing of an aeroplane is easily made, but three important differences should be noted. The first is that a hydrofoil operates in the presence of free surface, which influences the performance of the hydrofoil. The second is that a hydrofoil operates in conditions where cavitation can occur which also influences the performance severely. The last is that a hydrofoil, due to the difference in viscosity, operates at a different Reynolds number than the wings of an airplane [8].

If the right angle of attack is used, a hydrofoil generates substantially more lift than drag, such that it can lift a vessel out of the water. The foil generates a low pressure at the top side, the suction side, and a high pressure at the lower side, the pressure side, leading to a pressure difference over the two sides of the foil. The pressure difference between the suction and the pressure side leads to a resulting force which can be split in a lift and drag component.

At the moment a foil starts to move, the flow starts to circulate around the foil and a starting vortex is created. This can be explained using Kelvin's theorem, where the time rate of change of circulation around a closed curve is zero [13] and therefore a starting vortex is required to compensate for the circulation around the foil. When the motion of the foil stops, a stopping vortex is created such that no vortex lines end in the fluid.

To describe the lift and drag on a hydrofoil it is possible to use dimensionless coefficients. These dimensionless coefficients are the lift coefficient C_L and the drag coefficient C_D. The definitions of the drag and lift coefficient are [2]:

$$C_L = \frac{L}{\frac{1}{2}\rho U^2 S} \tag{2.1}$$

$$C_D = \frac{D}{\frac{1}{2}\rho U^2 S} \tag{2.2}$$

where S is the wing area of the hydrofoil, L is the lift of the hydrofoil, D is the drag of the hydrofoil, ρ is the free stream density and U is the free stream velocity. The two-dimensional lift (C_l) and drag coefficients (C_d) for a foil section are given by:

$$C_l = \frac{L}{\frac{1}{2}\rho U^2 c} \tag{2.3}$$

$$C_d = \frac{D}{\frac{1}{2}\rho U^2 c} \tag{2.4}$$

where the wing area S is replaced by the chord c and the lift L and drag D are per unit meter.

With an increasing angle of attack the lift coefficient increases linear until the maximum lift coefficient is reached. This region can be described using a lift curve slope, defined as:

$$a_0 = \frac{dc_l}{d\alpha} \tag{2.5}$$

At higher angles than the maximum lift coefficient, the flow around the foil starts to separate due to viscous effects, leading to a reduction in lift. The effect of separation cannot be seen in inviscid fluids and therefore the lift slope curve is fully linear in inviscid flow.

Since a foil is not infinite over span, the flow around a foil behaves in a 3-dimensional manner. As described earlier, the wing generates lift as result of the pressure difference between the upper and lower side of the foil. This pressure difference also generates a tip vortex, a flow from the lower side to the top side at the tip of the foil. This flow is called the downwash and influences the local angle of attack of the foil. As the local angle of attack is increased, the local produced lift reduces. This reduction in lift leads to larger velocities in the wake of the foil which becomes the largest at the tip of the foil. Due to the self-induced velocities of the downwash, the wake of a hydrofoil rolls up into two down moving trailing vortices behind the wing which contain all the circulation in the wake, and therefore the wake is not flat. According to experiments, at length e the trailing vortices are fully rolled up, such that their shape becomes stationary, and the wake stops to move downwards [23]. The length e behind the foil where the wake has fully rolled up, such the wake only consists of two cores near the tips of the foil, depends on the aspect ratio AR and the lift coefficient C_L. The following formula for the length e divided by the chord c is provided [23]:

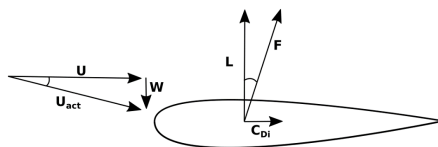$$\frac{e}{c} = 0.28\frac{AR^2}{C_L} \tag{2.6}$$

Figure 2.1: Induced drag and lift on a foil

This relation shows that for low AR foils the wake sheet is rolled up much faster than for high aspect ratio foils.

A wing experiences multiple types of drag: induced drag and parasitic drag. The first, the induced drag is result of the change of direction of the lift force due to induced velocities described earlier in this section. As the inflow angle changes due to the downwash w, the lift force is rotated backwards as it is perpendicular to the inflow angle. A horizontal force arises which should be added to the drag, as can be seen in figure 2.1. A different name for this type of drag is drag due to lift. The induced drag is very sensitive to the local inflow angle and therefore may be difficult to predict in numerical methods.

The second, the parasitic drag is result of viscous effects and can be split up in form drag and skin friction drag. Form drag results from the pressure differences at the leading and trailing edge of the foil due to the shape of the foil. Skin friction drag is resultant of the frictional forces of the skin of the foil.

2.2. Free surface effects on hydrofoil performance

If a hydrofoil is positioned near a free surface it will experience velocity disturbances which lead to the formation of free surface waves. As the submergence of the foil decreases and the foil gets closer to the free surface, the streamlines around the foil will be curved downwards and an additional down wash will be generated around the foil leading to an increase in induced drag and a decrease in lift forces. The result is an increase of induced drag over lift ratio and the effect is dependent on the Froude submergence number Fn_h:

$$Fn_h = \frac{U}{\sqrt{gh}} \tag{2.7}$$

This effect is most extreme on a Froude submergence number of 1.4 [27]. However, for very low Fn_h, the free surface acts as a wall which leads to the opposite, an increase in lift. It should be noted that as the foil gets closer to the free surface, cavitation and ventilation might occur in reality, causing a reduction in lift. The downwards curving of the streamlines leads to a change in zero-lift angle where it decreases as the submergence decreases [8].

The effect of the free surface on drag can be described by means of the drag over lift coefficient C_D/C_L^2 which is visualized over the submergence Froude number (Fn_h) for different submergences in figure 2.2. This figure contains experimental data and numerical simulations and is produced in [3].

The figure clearly shows the submergence effect as at a Fn_h of 1.4 a clear peak in drag over lift can be seen for low submergences, and at very low Fn_h and submergences the increase in lift also can be seen. The figure indicates that the free surface effects are less abundant for realistic submergences for hydrofoil vessels as the difference between the lines $h/c = 2.0$ and $h/c = 4.0$ is small. Hydrofoil vessels generally operate at a Fn_h higher than 4, where free surface effects are even smaller [8].
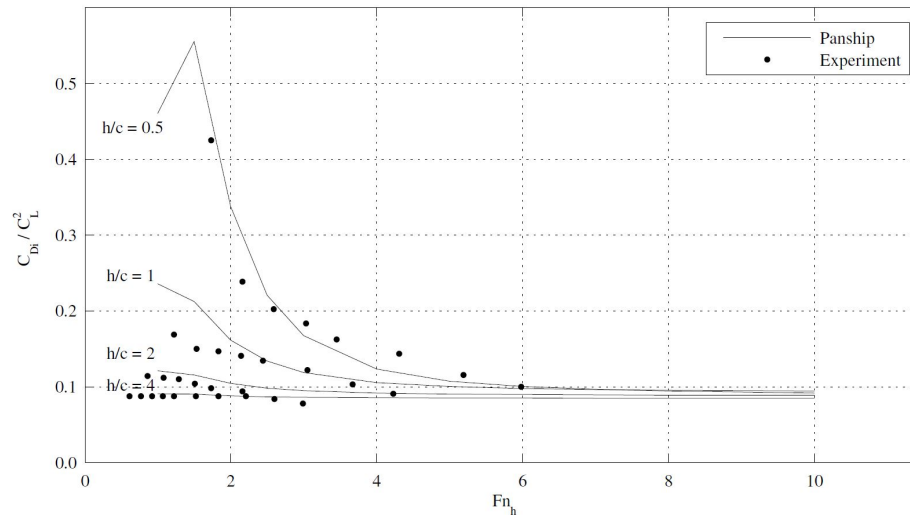
Figure 2.2: Effect of submergence on $\frac{C_{Di}}{C_L^2}$ for 4 submergences determined in Panship and towing tank tests over the submergence Froude number [27][3]. Figure reused with permission from [3].

2.3. Interaction between two foils

As described, a foil produces a trailing wake which rolls up at distance e behind the foil (2.6). In case two foils towed behind each other, a leading foil and a trailing foil, this trailing wake also influences the trailing foil by generating additional downwash on the trailing foil additionally to the downwash of the trailing foil on itself. Roll up does not seem to play an important role in foil interaction as simulations show that the effect of roll up does not have a large effect on the foil interaction[25]. However, it should be noted that this might be a foil specific case.

As the leading foil generates a wave system, since it is translating in the proximity of the free surface, the downwash of the leading foil in the trailing foil might not be the only effect in foil interaction. The free surface waves generated by the leading foil can also influence the performance of the trailing foil. Experiments have been performed, showing a reduction of lift and increase in drag for small foil spacing due to downwash of the leading foil but showing an increase in lift for specific larger foil spacing. Therefore, the effect of the leading foil on the trailing foil is not always negative, indicating that not only downwash plays a role here but free surface effects as well[19].

Coefficients are used to see what the effect of the forward foil on the leading foil is. The used subscripts are: r indicating that the coefficient is a ratio of two other coefficients, af indicating that the influence of the leading/forward foil f is accounted for when determining the lift or drag of the trailing/after foil a and a only indicating that the lift and drag of the trailing/after foil is considered without influences of the forward foil. By dividing the lift and drag of the trailing foil with influences of the leading foil (C_{Laf} and C_{Daf}) by the lift or drag of the trailing foil without the influences of the leading foil (C_{La} and C_{Da}) the increase or decrease of lift and drag can be seen easily:

$$C_{Lr} = \frac{C_{Laf}}{C_{La}}$$
$$C_{Dr} = \frac{C_{Daf}}{C_{Da}}$$

(2.8)

These formulations are commonly used throughout the current work.

2.4. Interaction between the foil system and a hull

The hull and foil system contains three components: the leading foil, the trailing foil and the hull. The influence on the first, the leading foil, is very small since the foil is in front of the ship. The influence of the forward foil on the hull can be large as the wake of the forward foil induces a reduction of pressure on the hull such that the lift of the hull is reduced [25]. The effect of the leading foil on the trailing foil is described in section 2.3, but the effect might be amplified due to the presence of the hull as the hull can induce an increase in pressure on the suction side of the foil, such that the lift of the trailing foil is reduced and induced drag is increased[17].

The effects of the interaction between the hull and the foils depend on the velocity of the vessel, the distance between the hull and the foil system and the shape of the hull [17]. Experimental and numerical results showed that the lift produced by a foil of a hydrofoil assisted catamaran can be reduced more than 25% [11]. In this case the distance between the hull and the foil was 0.5 chords thus the interaction effect is expected to be strong. Other calculations show that the interaction effects can be small as the foil is placed further away from the hull. The reduction in lift of the total system was approximately 3% [25].

2.5. Governing equations

In this section the foundations of the used computational methods are given. First the equation for conservation of mass in an incompressible fluid is given in section 2.5.1 which is followed by the derivation of the conservation of momentum in section 2.5.2. In section 2.5.3 the potential is introduced and in section 2.5.4 the boundary conditions are elaborated. At last, section 2.5.5 provides the Kutta condition.

2.5.1. Conservation of mass for an incompressible fluid

Conservation of mass for a volume V with a surface S in a flowing fluid is given by [14]:

$$\int_V \frac{\partial \rho}{\partial t} dV + \int_A \rho \mathbf{u} \cdot \mathbf{n} \, dA = 0 \tag{2.9}$$

stating that the sum of the rate of change of mass in V and the net flux of mass over the surface S should be zero. Applying the Reynolds transport theorem (A.19) to the left-hand side of the equation results in:

$$\int_V \left(\frac{\partial \rho}{\partial t} + \nabla \cdot \rho \, \mathbf{u} \right) dV = 0 \tag{2.10}$$

of which the second term at the right-hand side vanishes for an incompressible fluid. The statement of conservation of mass is given by:

$$\int_V \nabla \cdot \mathbf{u} \, dV = 0. \tag{2.11}$$

2.5.2. Conservation of momentum in potential flow

The derivation of the momentum equations as given in [3] is used where the momentum equation is derived from Newton's second law applied to a volume V with a surface area A. The rate of change of momentum within V and the flux of momentum through A then should equal the external force. This is directly stated as:

$$\frac{d}{dt} \int_V \rho \, \mathbf{u} \, dV + \int_A \rho \, \mathbf{u} \, (\mathbf{u} \cdot \mathbf{n}) \, dA = \sum \mathbf{F} \tag{2.12}$$

where $\rho \mathbf{u}$ is the momentum per unit volume. Now the boundary integral can be eliminated using the Reynolds transport equation (A.19) and the equation is rewritten using the chain rule:

$$\int_V \mathbf{u} \left(\frac{\partial \rho}{\partial t} + \nabla \cdot \rho \, \mathbf{u} \right) + \rho \left(\frac{\partial \, \mathbf{u}}{\partial t} + \mathbf{u} \cdot \nabla v \right) dV = \sum \mathbf{F} \tag{2.13}$$

By using the statement of conservation of mass (2.11) the left part of the integral is eliminated and assuming constant density ρ the following result is obtained:

$$\int_V \rho \left(\frac{\partial \, \mathbf{u}}{\partial t} + \mathbf{u} \cdot \nabla \, \mathbf{u} \right) dV = \sum \mathbf{F}. \tag{2.14}$$

The external forces $\sum F$ can be described assuming an incompressible and inviscid fluid. The remaining forces are the gravity and the pressure on the surface, which are substituted for $\sum \mathbf{F}$:

$$\int_V \rho \left(\frac{\partial \mathbf{u}}{\partial t} + \mathbf{u} \cdot \nabla \mathbf{u} \right) dV = -\int_A p \, \mathbf{n} \, dA + \int_V \rho \, \mathbf{g} \, dV. \tag{2.15}$$

Rewriting the right-hand side of the equation using the Divergence theorem (A.2) results in:

$$\int_V \rho \left(\frac{\partial \mathbf{u}}{\partial t} + \mathbf{u} \cdot \nabla \mathbf{u} \right) dV = \int_V (\rho \mathbf{g} - \nabla p) \, dV \tag{2.16}$$

which is Euler's equation for inviscid fluids. Next, by assuming irrotational flow, $(\mathbf{u} \cdot \nabla)\mathbf{u}$ can assumed to be $\nabla \left(\frac{1}{2} |\mathbf{u}|^2 \right)$, the following result is obtained:

$$\int_V \rho \left(\frac{\partial \mathbf{u}}{\partial t} + \nabla \left(\frac{1}{2} |\mathbf{u}|^2 \right) \right) dV = \int_V (\rho \mathbf{g} - \nabla p) \, dV. \tag{2.17}$$

2.5.3. Potential flow

For inviscid, incompressible and irrotational flow the problem can be reduced to a potential flow problem. Potential flow has the advantage that the velocities are the derivatives of the potential Φ which can be used to describe a fluid:

$$\mathbf{u} = \nabla \Phi \tag{2.18}$$

The potential can be split up in two parts:

$$\Phi = \Phi_\infty + \phi \tag{2.19}$$

where Φ_∞ is the undisturbed potential and ϕ is the disturbance potential. Using the potential, the conservation of mass can be rewritten to the continuity equation or Laplace's equation:

$$\nabla^2 \Phi = 0 \tag{2.20}$$

Using (2.19) the result derived in the previous section (2.17) can be rewritten, after removing the integrals, to:

$$\nabla\left(\frac{\partial\Phi}{\partial t} + p + \frac{1}{2}\rho\left|(\nabla\Phi)^2\right| + \rho g z\right) = 0 \tag{2.21}$$

Which can again be simplified to the Bernoulli equation in a potential flow:

$$\frac{\partial\Phi}{\partial t} + p + \frac{1}{2}\rho\left|(\nabla\Phi)^2\right| + \rho g z = c \tag{2.22}$$

where c is a constant. Φ can be defined using singularities such as sources and dipoles.

2.5.4. Boundary conditions

In order to simulate a foil submerged in a potential flow, five different boundary conditions are required. These boundary conditions are the linearized free surface boundary condition, the Kutta condition, the linearized body boundary condition, condition at infinity and the initial condition. The Kutta condition is introduced in section 2.5.5.

The first boundary condition, the linearized free surface boundary condition, is a result of the kinematic free surface boundary condition and the dynamic free surface boundary condition. Both these boundary conditions are imposed on the water surface as the kinematic surface boundary condition relates the velocity of the motion of the surface to the motion of the particle and the dynamic boundary condition imposes a zero pressure jump at the water surface [7]. The kinematic free surface boundary condition is obtained by taking the material derivative of $F = z - \zeta(x, y, t) = 0$ and is given by

$$\frac{\partial\Phi}{\partial z} - \frac{\partial\Phi}{\partial x}\frac{\partial\zeta}{\partial x} - \frac{\partial\Phi}{\partial y}\frac{\partial\zeta}{\partial y} = 0 \quad \text{on} \quad z = \zeta(x, y) \tag{2.23}$$

where ζ represents the wave elevation. The dynamic free surface boundary condition is the result of applying the Bernoulli equation (2.22) to the free surface, given by:

$$\frac{1}{2}\left(\left(\frac{\partial\Phi}{\partial x}\right)^2 + \left(\frac{\partial\Phi}{\partial y}\right)^2 + \left(\frac{\partial\Phi}{\partial z}\right)^2\right) + \frac{\partial\Phi}{\partial t} + g\zeta = 0 \quad \text{on} \quad z = \zeta(x, y) \tag{2.24}$$

Linearizing the kinematic and dynamic free surface boundary condition can be done by removing all the terms with a higher order. The linearized kinematic boundary condition (2.23) can be written as:

$$\frac{\partial\zeta}{\partial t} = \frac{\partial\Phi}{\partial z} \quad \text{on} \quad z = 0 \tag{2.25}$$

and the linearized dynamic boundary (2.24) condition can be written as:

$$g\zeta + \frac{\partial\Phi}{\partial t} = 0 \quad \text{on} \quad z = 0 \tag{2.26}$$

By combining (2.25) and (2.26) and by time derivation of equation 2.26 the following result is obtained:

$$g\frac{\partial\Phi}{\partial z} + \frac{\partial^2\Phi}{\partial t^2} = 0 \quad \text{on} \quad z = 0 \tag{2.27}$$

The third boundary condition is the body boundary condition. As a requirement for mass conservation, the normal component of a flow on a solid surface must be equal to normal component of the velocity of the solid surface. The solid surface cannot be penetrated. This is stated by

$$\boldsymbol{n} \cdot \boldsymbol{U}_s = \boldsymbol{n} \cdot \boldsymbol{u} \tag{2.28}$$

where $\boldsymbol{U}_s$ is the velocity of the solid surface, $\boldsymbol{n}$ is the normal of the surface and $\boldsymbol{u}$ is the velocity of the flow. The body boundary condition is linearized as described by Timman and Newman in [24]. The result is a formulation in a general form for small displacements around the steady translating body orientation. For full details is referred to [3].

The last two boundary conditions are the condition at infinity, the radiation boundary condition and the initial condition. The initial condition states that the fluid is at rest at the start of the process. In order to do so, the waves, if present, can for instance be started with a ramp-up function at t = 0 and the ship can be set in motion impulsively. In order to do so:

$$\Phi = 0 \quad \text{at} \quad t = 0$$
$$\frac{\partial \Phi}{\partial t} = 0 \quad \text{at} \quad t = 0 \tag{2.29}$$

At last the condition at infinity is considered. The result of the moving body on the velocity of the flow should disperse when going far away from the ship and foil. This can be written as:

$$\lim_{\bar{x} \to \infty} \phi = 0$$
$$\lim_{\bar{x} \to \infty} \frac{\partial \phi}{\partial t} = 0 \tag{2.30}$$

where ϕ is the disturbance potential of the ship and foil.

2.5.5. The Kutta condition and the shape of the wake

The Bernoulli equation (2.22) does not necessary specify the location the flow leaves the foil. If the flow leaves the foil physically correct, the flow around the foil has the right amount of circulation and therefore produces the correct lift. In order to make the flow leave the foil correct, the Kutta condition is required to make the flow leave the foil physically correct.

Experiments show that the flow should leave the foil at the trailing edge along the bisector line at the stagnation point. Therefore a stagnation point has to be imposed at the trailing edge [13]. In order to do so, the pressure difference at the trailing edge must be zero:

$$\Delta p_{T.E.} = 0 \tag{2.31}$$

Imposing a zero pressure difference across the trailing edge can be done by choosing the strengths of the singularities such that the pressure difference is zero. However, this requires an iteration and therefore it is computationally intensive. To avoid an iteration, the Kutta condition can be imposed differently in 2D, the two dimensional Kutta condition. In order to do so, the velocity and vorticity are integrated over the wake sheet as illustrated in figure 2.3. This figure contains the trailing edge on the left and the wake sheet on the right. For clarity the trailing edge and the wake sheet are separated but in reality the wake sheet is attached to the trailing edge.

Two derive the two dimensional Kutta condition first is started with the definition of the circulation:
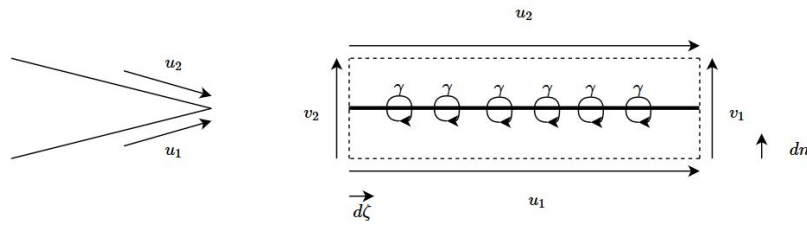
Figure 2.3: Trailing edge of a foil and its wake sheet

$$\Gamma = \oint \mathbf{U} \cdot \mathbf{ds} = \gamma d\zeta \tag{2.32}$$

Now using the velocities as described in figure 2.3 this equation can be rewritten to:

$$\Gamma = -(u_1 d\zeta + v_1 dn - u_2 d\zeta - v_2 dN) = \gamma d\zeta \tag{2.33}$$

It is assumed that dn is very small, therefore the limit of $dn \to 0$ can be taken, such that:

$$\lim_{dn \to 0} \Gamma = -(u_1 - u_2)d\zeta = \gamma d\zeta \tag{2.34}$$

Which can be simplified to:

$$u_2 - u_1 = \gamma \tag{2.35}$$

The zero pressure difference across the the upper and lower part of the trailing edge and the flow leaving the foil over the bisector line, imposed by the Kutta condition, provides $u_2 = u_1$, therefore:

$$\gamma_{TE} = 0 \tag{2.36}$$

which is the two dimensional Kutta condition.

A simple way to apply the Kutta condition on a three-dimensional foil is to apply this two-dimensional Kutta condition on the three-dimensional trailing edge. In order to do so, the foil can be discretised using a doublet distribution. In that case a change in doublet strength can be described as[13]:

$$\frac{\partial \mu}{\partial x} = -\gamma \tag{2.37}$$

In combination with the two dimensional Kutta condition (2.36), this means that:

$$\mu_{T.E.} = constant = \mu_w \tag{2.38}$$

This condition can be easily imposed at the trailing edge.

The wake should not produce lift, therefore the wake sheet should be force free. This means that if the Kutta-Joukowski formula (A.23) is applied on the wake sheet, the result should be zero:

$$\mathbf{F} = \rho \mathbf{U} \times \mathbf{\Gamma} = 0 \tag{2.39}$$

Which means that:

$$\mathbf{U} \times \boldsymbol{\gamma} = 0 \tag{2.40}$$

This condition is satisfied if the vorticity vector is parallel to the velocity vector.

2.6. Panship

As written earlier in this work, Panship is a potential flow code where viscous forces and compressibility are neglected and therefore the governing equations reduce to (2.20) and (2.22). This section elaborates on how the solution in Panship is obtained. This section is based on [3] and for the full description of the model is referred to this source. The method uses a three-dimensional time domain Green's function and has linearized free surface boundary conditions. Furthermore, the body boundary condition is retained on the actual submergence and is linearized. The method is able to deal with significant forward speed and large amplitude motions and due to the use of a panel method and linearized boundary conditions the code is relatively fast.

The structure of this section is as follows. The first section, 2.6.1, describes the transient Green function and its features followed by a description of the transient integral equation, derived from Green's second identity in 2.6.2. The third section continues with the discretisation of the problem in 2.6.3. Section 2.6.4 elaborates on the wake model used in Panship and 2.6.5 describes an important feature for high speed craft in Panship, the transom flow. Furthermore, the Trefftz plane is in section 2.6.6. Last, the viscous forces in Panship are treated in 2.6.7.

2.6.1. Transient Green function

An important part of Panship is the transient Green Function. This function is used to find the influence of a singularity at a field point in the domain while respecting the boundary conditions. In other words, the free surface Green function is required to impose the boundary conditions. Many types of Green functions have been derived but for this purpose a function given by Newman [20] is used. This Green function specifies the influence of a transient moving singularity on the potential field and satisfies the Laplace equation, the free surface boundary condition and the condition at infinity. This transient Green function G consists of two parts. The biplane image G^0 and the free surface part of the Green function G^F:

$$G(p, q, t - \tau) = G^0 + G^f \tag{2.41}$$

The biplane image depends on the distance of the field point to the location of the singularity R and the distance of the field point to the mirror image of the singularity R_0:

$$G^0 = \frac{1}{R} - \frac{1}{R_0} \tag{2.42}$$

This biplane image is relatively easy to determine, but the free surface part of the Green function is harder to evaluate. As the free surface part of the Green function is rather complex and there is no gain in showing it here, for details is referred to [3]. The function consists of an integration over the elapsed time and therefore it requires a vast amount of computational power, therefore an effort is made to reduce the computational burden of this function and its derivatives.

The computational requirements of this function are reduced severely by linearization of the position of the geometry around an average position such that the free surface part of the Green function can be calculated prior to the time simulation and stored in interpolation tables of the values of free surfaces Green functions and its derivatives required to solve (2.46) for the nearest history and asymptotically approximations for further history. After a certain history length the integrals are cut off, leading to a truncation error. This cut off length is:

$$t_{cut} = \text{NHIST} \cdot \Delta t \tag{2.43}$$

where NHIST is a chosen integer and Δt is the time step. Based on this equation it is favorable to use a large time step Δt to avoid truncation errors, however as the free surface part of the Green function shows strong oscillatory behavior, the time step should be small enough to be able to evaluate it correctly.

2.6.2. Transient integral equation

To find the solution of the potential flow problem, Green's second identity can be used to determine the transient integral equation of the problem. With the transient integral equation the potential Φ of the problem can be determined which can be used in Bernoulli's equation 2.22 to find the pressure on the body of the geometry.

To derive the transient integral equation first is started with Green's second identity which is derived in appendix A.2:

$$\iiint_V \left(\psi \nabla^2 \phi - \phi \nabla^2 \psi \right) dV = \oiint_S (\psi \nabla \phi - \phi \nabla \psi) \cdot \mathbf{n} \, dS \tag{2.44}$$

where ψ and ϕ are two functions that satisfy the boundary conditions. ψ and ϕ will be replaced by the potential Φ and the green function G which both satisfy the Laplace equation (2.20). And therefore 2.44 can be reduced to:

$$\oiint_S (\psi \nabla \phi - \phi \nabla \psi) \cdot \mathbf{n} \, dS = 0 \tag{2.45}$$

Where the fluid is bound by S consisting of:

- S_∞: Surface boundary at infinitely far in the fluid from the object
- S_ϵ: Surface of small sphere around a singularity to ensure it is excluded from the domain
- S_F: Surface of the free surface of the fluid
- S_H: Surface of the hull of the ship
- S_L: Surface of the foil
- S_W: Surface of the wake

The contributions of the far field S_∞ and the sphere around the singularity S_ϵ become zero due to the boundary condition at the far field and the sphere around the singularity taken very small. As the evaluation of (2.45) over S_F undesirable, it is removed from the integration by rewriting. For the full derivation is referred to [3], where it should be noted that in the process of removing the integration over S_F from (2.45), the equation has to be integrated over time.

The result is given in (2.46) where the equation is split up in four terms. The first, third, and fourth term are result of the elimination of the free surface and the second term is a remainder of (2.45).

$$\overbrace{4\pi T\Phi(\mathbf{x}_0,t)}^{1} = \overbrace{-\int_{S_{HLW(t)}} \Phi(\boldsymbol{\xi},t)\,G_n^0 - G^0\,\Phi_n(\boldsymbol{\xi},\tau)\,dS}^{2}$$

$$+ \overbrace{\int_0^t \int_{S_{HWL(\tau)}} \Phi(\boldsymbol{\xi},\tau)\,G_{\tau n}^f - G_\tau^f\Phi_n(\boldsymbol{\xi},\tau)\,dS\,d\tau}^{3}$$

$$+ \overbrace{\frac{1}{g}\int_0^t \int_{l_w(\tau)} \Phi(\boldsymbol{\xi},\tau)\,G_{\tau\tau}^f - G_\tau^f\,\Phi_\tau(\boldsymbol{\xi},\tau)\,V_N\,dL\,d\tau}^{4} \quad (2.46)$$

In this equation ξ represents the location of the singularity, G represents the Green's function, τ the elapsed time and V_N the normal velocity of the body at the body waterline intersection. T is defined as 1 in the fluid domain, $\frac{1}{2}$ at the hull of the ship and 0 at other locations. The subscripts of G and Φ denote the derivatives in the direction of τ and n. The G^f terms depend on time whereas the G^0 are time independent.

2.6.3. Discretisation of the hull and foil

To find a solution of 2.46, the hull and lifting surfaces are discretized use a combination of a dipole and source distribution whereas the wake sheets are implemented as thin volumes, using vortex rings to impose the Kutta condition at the trailing edge and the transom flow conditions. The wake sheet behind the foil consists of vortex rings instead of dipole panels as their influence on the domain can be determined more easily and therefore reducing computational requirements. Changing from dipole panels to vortex rings does not influence the physical problem [13].

As every panel has two unknowns, a dipole and a source distribution, the source strength is set equal to the normal velocity on the panel first to eliminate one unknown per panel:

$$\Phi_n^+ - \Phi_n^- = \sigma \quad (2.47)$$

Now the amount of unknowns and equations are equal and the no flow boundary condition is maintained by the dipole strengths such that the difference between the potential on the inner side is the potential on the outer side:

$$\Phi^+ - \Phi^- = -\mu \quad (2.48)$$

In this way the system with double the unknowns as equations can be solved. For the wake sheets, the circulation strength is set by the Kutta condition, described in the next section.

2.6.4. Wake model in Panship

The wake sheet behind the foil is visualized in figure 2.4 in two ways in the XZ-plane. The first representation (I) shows the full vortex distribution over the wake whereas the second representation (II) only shows the vortices of the first wake panel. In both these representations the circulations around the x-axis are not visualized for clarity.

For the lifting surfaces and the transom flow at the stern extra boundary conditions have to be solved to obtain a unique solution. For the wake sheet of the lifting surfaces three different conditions should be satisfied: the Kutta condition, the Kelvin's circulation theorem and the wake sheet being force free.
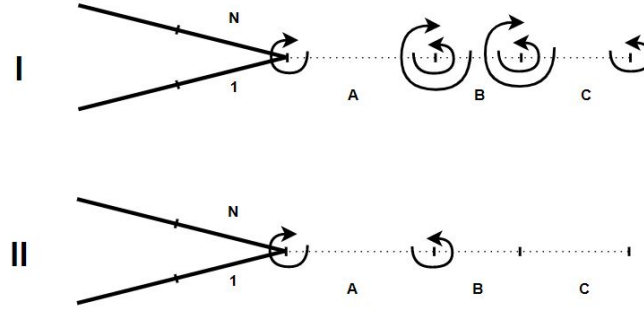
Figure 2.4: 2D representation of the wake in Panship in the XZ-plane

The first condition for the wake sheet, the Kutta condition, is introduced in section 2.5.5 and is satisfied by the first panel of the wake sheet. As the foil moves forward in a time step, the gap is filled with a wake panel which becomes the first wake panel of the wake sheet. Rewriting (2.38) for a dipole distribution over the foil and the wake sheet gives:

$$\mu_w = \mu_{upper} - \mu_{lower} \tag{2.49}$$

where μ_w is the dipole strength of the first wake panel and μ_{upper} and μ_{lower} are the circulation strengths of the upper and lower panels at the trailing edge, such that $\gamma_{TE} = 0$. However, as this implementation of the Kutta condition did not perform well on high angles of attack, the pressure Kutta condition from equation 2.31 is used. The pressure difference over the trailing edge, panels 1 and N in figure 2.4, becomes zero by choosing the circulation strength of the first wake panel, panel A, such that the pressure difference is zero.

In determining the pressure on the two trailing edge panels, only the influence of the first wake panel is used, as can be seen in representation II in figure 2.4. Therefore, choosing the length of the first wake panel too short might result in errors in the result of the simulation. The parameter FAKTWE can be used to influence the length of the first wake panel l_{w1}:

$$l_{w1} = \text{FAKTWE} \cdot U \cdot \Delta t. \tag{2.50}$$

The second condition, as result of the Kelvin's circulation theorem, is that the vortex lines cannot end in a fluid. The Kelvin's circulation theorem is defined as

$$\frac{D\Gamma}{Dt} = 0 \tag{2.51}$$

where $D\Gamma/Dt$ represents the total time rate of change of circulation following the fluid in a closed curve [14]. The Kelvin's circulation theorem is satisfied by using vortex rings in the wake sheet such that no vortex line ends in a fluid.

The last requirement is that the wake sheet should be force free as the wake is not a solid surface. The force on a vortex sheet can be determined by the Kutta-Joukowski equation in (A.23) which states that the vorticity vector should be in the same direction as the velocity vector in order to be force free. This requirement is not satisfied to reduce computational requirements as the wake sheet is not deformed by the motion of the flow, the roll up, as described in section 2.5.5.

To reduce the computational burden of the wake sheet, a maximum number of wake panels is limited to NHISTW. If this maximum number of wake panels is reached, the last wake panel is removed as a new wake panel is created.

2.6.5. Transom flow model

Fast vessels fitted with a cut-off or transom type stern experience smooth flow separation at the transom at high Froude numbers. However, extremely high velocities may occur at the transom when simulating this problem in potential flow, depending on forward speed and local panel distribution. In Panship this problem can be solved by adding a transom flow model.

In the transom flow model, the pressure just forward of the transom edge is equal to the pressure just after the transom edge. These pressures are linked to each other using the Bernoulli equation (2.22), the hydrostatic pressure, the total pressure resultant of motions and the wave incidence pressure at one side and the free surface pressure on the other side. This results in

$$g \, z_T = U \left(\frac{\partial \Phi}{\partial x} + \frac{\partial \Phi_w}{\partial x} \right) - \left(\frac{\partial \Phi}{\partial t} + \frac{\partial \Phi_w}{\partial t} \right) \tag{2.52}$$

where z_T is the local immersion at the transom edge. Equation 2.52 is satisfied using a source-doublet distribution over the hull in front of the transom edge and a trailing wake sheet extending aft from the transom edge.

2.6.6. Trefftz plane

During the late stage of this project the Trefftz plane is introduced in Panship to determine the induced drag in an alternative way then by pressure integration. The benefit of this method is that it is less susceptible for the orientations of the panels at the leading edge to determine the drag. The method is described in [22].

In order to apply a Trefftz plane it, is assumed that the induced drag can be determined in a transverse plane in the far field behind the foil. This plane, the Trefftz plane, is only affected by the velocity disturbances in the wake of the foil crossing this plane. In order to determine the induced drag, first a control volume is defined such that the box shaped control volume uses this plane and such that the other planes of the control volume are placed far away from the foil and the wake. If the momentum equation is applied to the control volume in x-direction in potential flow now, only two contributions remain. These two remaining contributions are the pressure on the foil, leading to the induced drag, and the velocity disturbances to the free stream in the far field behind the foil.

Unfortunately, in Panship this method can currently only be used for deeply submerged foils without free surface effects. Since this method is applied in the late stage of this thesis, it is only used in chapter 4 and referenced to in the conclusions of chapters 5 and 6 and the takeoff.

2.6.7. Viscous forces

As provided in the derivation of equation 2.22, viscous forces are neglected in potential flow. However, in real flow, viscous effects influence the drag and lift as boundary layers are created due to the no-slip boundary condition. In this case the flow around a foil consists of a rotational inner region, a boundary layer, and a laminar outer region. For the inner region and the boundary layer is not accounted in potential flow since the no-slip condition at the body is not applied and the laminar outer region remains. As in this laminar flow no separation occurs, this results in an overprediction of lift and therefore an overprediction of induced drag. The laminar inviscid flow also leads to a lack of parasitic drag, introduced in section 2.1.

For the overprediction of lift and induced drag no correction is applied, but the parasitic drag R_v, the viscous resistance, can be determined empirically using the ITTC '57 convention frictional correlation line to determine C_f and a form factor $(1 + k)$:

$$R_v = \frac{1}{2} \rho U^2 \cdot S_{wet} \cdot C_f (1 + k). \tag{2.53}$$

The ITTC '57 convention frictional correlation line is given by:

$$C_f = \frac{0.075}{\left(\log_{10} Rn - 2\right)^2}$$ (2.54)

where Re is the corresponding Reynolds number. The form factor k can be determined using the empirical formula based on experimental results provided by [10]:

$$1 + k = 1 + 2\frac{t}{c} + 60\left(\frac{t}{c}\right)^4$$ (2.55)

2.7. Unvlm

Unvlm was developed in four different parts in the late 1990s and can be seen as a predecessor of Panship. The code uses the same free surface Green function. The code consists of three different parts: Hydvlm, Hydres, Unvlm and Hydsim. The first, Hydvlm, is able to determine the lift and drag forces on a foil near a free surface in a steady flow using a VLM. In the second part, Hydres, the hull resistance and lift and effects of other appendages are modelled empirically and added to the first part. Hydres can be used for optimisation of the takeoff characteristics and to determine the performance of a ship in foilborne mode. The third and fourth part are called Unvlm and Hydsim respectively. These codes use an unsteady Vortex Lattice Method and have the main purpose of determining the seakeeping and manoeuvring characteristics of hydrofoil craft operating in unsteady foilborne conditions [25].

As the main goal of using this code is validation of a takeoff of a hydrofoil vessel in steady conditions, Hydres is the most suitable for use in this research. As Hydres is based on Hydvlm, Hydvlm and Hydres both will be described in this section. These methods are described by van Walree in [25] but a summary is given here.

2.7.1. Hydvlm

As described earlier, Hydvlm is used to determine the lift and drag forces on the foil without accounting for cavitation aspects. The hydrofoils are assumed to be thin and are represented by their reference planes consisting of a vortex system.

As described in section 2.5.3, potential flow does not account for viscous effects. However, the viscous forces on hydrofoils play a significant role and should be accounted for. In Hydvlm viscous effects are taken into account by using a viscosity correction factor which can be determined by the program XFoil or empirical, and correcting for a change in zero lift angle. The viscosity correction factor has the form of:

$$C_{lv} = C_{lp} f_a$$ (2.56)

where f_a is the viscosity correction factor. Viscous drag is added by means of empirical formulations, as described in section 2.6.7.

2.7.2. Hydres

To simulate the full dynamics of a hydrofoil vessel, the hull, propulsor and appendage force components should be added to the model. This is done in Hydres. Since the use of panel methods for this purpose required too much computational demands, the hull, propulsor and appendage forces are added empirically.

The hull forces are determined using the results of the Series 65 model tests. These results are used to determine the hull force components, the hull trimming moment, and the hull draft using interpolation of the

independent variables. This limits the use of Hydres as only hull forms with a close resemblance with the Series 65 models can be used.

2.7.3. Validation of Hydvlm and Hydres

In order to check if the results of Hydvlm and Hydres are valid, the results of both methods have been compared to the results of multiple experiments [25]. This section starts with a summary of the validation of Hydvlm followed by a summary of the validation of Hydres.

The free surface effects and lift and drag forces are well predicted by Hydvlm for practical submergence. It should be noted that the prediction of the effect of viscosity on the lift curve slope might be too strong in some cases as the results of Hydvlm are compared to experimental results. For larger incidence angles the drag is underestimated if compared to experimental results, this might be due to the start of a boundary layer transition. For low aspect foils, the differences between calculated and experimental results are a bit higher for both the lift and the drag coefficient. The effects of foil interaction are qualitatively predicted well in Hydvlm for lift and drag for variations in foil spacing and submergence.

Hydres has been validated is performed using scaled model ships of hydrofoil craft consisting of a hull, forward foil and after foil. For a model of a hydrofoil vessel using a TT-shaped hydrofoil, the experiments have been performed for vessel speeds from 18 to 32 knots in which the vessel performs a takeoff. In the experiments the maximum vessel speed was limited to 32 knots as on higher velocities the motions of the ship became unsteady and the results cannot be trusted. The trim angle and draft are well predicted, but in the calculations the takeoff was a little too early. For speeds higher than 26 knots, the equilibrium equations in the numerical model were difficult to solve due to instability of the configuration.

2.8. XFoil

XFoil is a design and analysis tool for 2D foils. The program is able to determine viscous and non-viscous forces on a foil using a source and vortex distribution in a two-dimensional Boundary Element Method (BEM). The program is based on the ISES code but was further improved to reduce computational requirements and is described in [4] and [5]. A summary of these sources is given in the current work but for details, which are considered out of scope for this project, is referred to these sources.

In the inviscid formulation the foil is discretized in using N panels on the chord of the foil and N_w panels on the wake. Each airfoil panel consists of a constant source distribution and a linear vortex distribution. Each wake panel consists of a constant source distribution. The flow field is now constructed using a free stream flow and the effects of the vortex and source distributions.

The Kutta condition is defined such that the sum of the strengths of the vortex sheets at the two panels at the trailing edge is zero as provided in (2.36). The solution is obtained by finding the streamline along the nodes of the foil. As the streamline has the same value at each node of the foil, the system of sources an vortex distributions can be solved linearly in combination with the Kutta Condition [4].

If viscous effects are included in the solution, the boundary layer equations have to be solved as well. The boundary layer equations have to be solved for two different regions: the viscous laminar region and the separation bubble. The viscous laminar layer is solved using the boundary layer equations only, whereas the separation bubble requires an additional stress-transport equation. Crucial in this analysis is to determine where the laminar region ends and the separation bubble starts. The transition is based upon the growth of the Tollmien-Schlichting wave, which is initiated by external turbulence, surface roughness, noise and vibration. As the wave grows as it becomes unstable, due to, for instance, surface roughness, the velocities it induces on the velocity field grow as well. The disturbances in the velocity field become that large that the viscous laminar flow collapses into a turbulent flow and the separation bubble starts [21]. To determine the transition point, the amplification factor of the Tollmien-Schlichting wave N is used. At the point the Tollmien-Schlichting wave and thus the amplification factor have grown by the critical amplification factor N_{crit}, the viscous laminar flow collapses. The value of N_{crit} is set by the user and influences the viscous solu-

Situation	N_{crit}
Sailplane	12-14
Motorglider	11-13
Clean wind tunnel	10-12
Average wind tunnel	9
Dirty wind tunnel	4-8

Table 2.1: Values for N_{crit} as suggested by [6] based on experiments

tion of XFoil severely [4]. The XFoil manual suggest values of the critical amplification factor for five situations in table 2.1 based on experimental results, but not for a hydrofoil [6]. As the viscosity of water is higher than the viscosity of air, it is suggested that separation occurs earlier than in air and therefore a lower value of N_{crit} than in table 2.1 is expected. Little is known on the choice for N_{crit} for hydrofoils and therefore in this thesis the critical amplification factor will be chosen by means of a comparison with the solution of Refresco in chapter 3.

2.9. The Lifting Line - XFoil method

The (viscous) results of XFoil can be used to determine the lift and drag on a deeply submerged 3D foil by using lifting-line theory. The lifting-line theory is used to determine the local downwash, which can be used to determine the local lift on the foil using the results of XFoil. The method is called the LLXM.

In order to determine the local downwash, the foil is discretized using M spanwise elements having their own inflow angle. As a vorticity line cannot end in the fluid, the foil is discretized by means of horseshoe vortices. Using this discretisation in horseshoe vortices, it is possible to have different circulations over the entire lifting line of the foil and therefore a lift distribution. In this way a difference in circulation strength between two adjacent vortices on the lifting line is compensated with a circulation strength in the trailing vortices. This can be explained by the fact that the trailing vortex between two vortices on the lifting line is the difference between these two vortices, as one is in the opposite direction. This is clarified in figure 2.5.

In figure 2.5 the discretisation of the foil using $M = 5$ can be seen. In this figure, the two trailing vortices of two adjacent horseshoe vortices are drawn side by side for clarity, but they are actually on the same location. The length of the trailing vortices l_{trail} is theoretically never ending but it ends in the model a converged length. The trailing vortices stay in the xy-plane and do not roll up. The direction of the circulation is provided by a minus sign.

The total lift of the foil can be found by iteration of three different steps. First the local circulation (Γ_m) as result of the local angle of attack (α_m) should be determined. Second, the influence coefficients of the trailing vortices on the collocation points of the elements are determined and used to find the local downwash ($w_{m,ind}$) at the collocation points. Third, the new local angle of attack (α_{init}) is determined. This process is displayed in figure 2.6 and repeated until a converged solution is found.

To determine the circulation Γ around an element, step 1, the Kutta-Joukowski law (A.22) and the definition
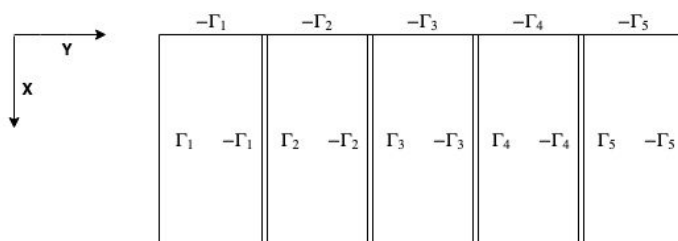
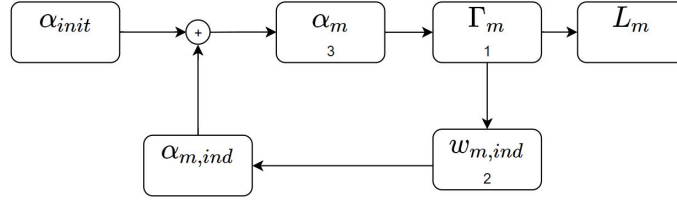Figure 2.5: Discretisation of the foil using $M = 5$

Figure 2.6: Followed solution procedure

of the two-dimensional lift coefficient are used (2.3):

$$L = -\rho U \Gamma \tag{2.57}$$

$$C_l = \frac{L}{\frac{1}{2}\rho U^2 c} \tag{2.58}$$

Substituting (2.57) in (2.58) gives a relation between the circulation around the foil, the lift coefficient, the free stream velocity and the chord of the foil:

$$\Gamma = -\frac{1}{2}U c C_l \tag{2.59}$$

XFoil is used to determine the lift coefficient C_l as function of the angle of attack α. The lift coefficient as function of alpha is stored in an interpolation table and is used to create a relation between C_l and α:

$$\Gamma = -\frac{1}{2}U c C_l(\alpha) \tag{2.60}$$

To determine the downwash resultant of the trailing vortices, step 2, the Biot-Savarts law is used (A.34) and rewritten to a convenient form (A.48):

$$\mathbf{q}_{1,2} = \frac{\Gamma}{4\pi} \frac{\mathbf{r}_1 \times \mathbf{r}_2}{|\mathbf{r}_1 \times \mathbf{r}_2|^2} \mathbf{r}_0 \cdot \left(\frac{\mathbf{r}_1}{r_1} - \frac{\mathbf{r}_2}{r_2} \right) \tag{2.61}$$

This equation is used to determine the induced velocities at the collocation points of the elements. By setting Γ to one in (2.61), the influence coefficient a is obtained:

$$a_{1,2} = \frac{1}{4\pi} \frac{\mathbf{r}_1 \times \mathbf{r}_2}{|\mathbf{r}_1 \times \mathbf{r}_2|^2} \mathbf{r}_0 \cdot \left(\frac{\mathbf{r}_1}{r_1} - \frac{\mathbf{r}_2}{r_2} \right) \tag{2.62}$$

Now a system of equations can be set up to determine the downwash w_m at all collocation points as result of the circulation at all collocation points:

$$\begin{pmatrix} w_1 \\ w_2 \\ w_3 \\ \vdots \\ w_m \end{pmatrix} = \begin{pmatrix} a_{11} & a_{12} & \dots & a_{1m} \\ a_{21} & a_{22} & \dots & a_{2m} \\ a_{31} & a_{32} & \dots & a_{3m} \\ \vdots & & \ddots & \vdots \\ a_{m1} & a_{m2} & \dots & a_{mm} \end{pmatrix} \begin{pmatrix} \Gamma_1 \\ \Gamma_2 \\ \Gamma_3 \\ \vdots \\ \Gamma_m \end{pmatrix} \tag{2.63}$$
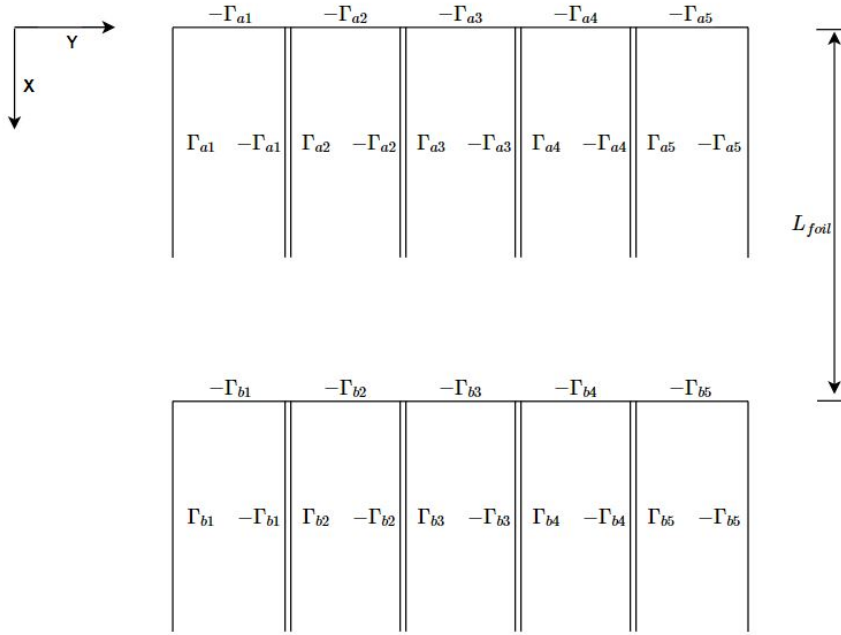
Figure 2.7: Discretisation of two foils using $M = 5$

The collocation point is chosen at the halve width of the leading edge of the horseshoe vortex. Using the downwash w_m the new angle of attack can be determined for each element using:

$$\alpha_m = \alpha_{init} + \arctan\left(\frac{w_m}{U}\right) \tag{2.64}$$

The process is iterated using a relaxation procedure until a converged solution is found. In the relaxation procedure the solution consists of 90% of the preceding step and 10% of the new solution. As the iteration procedure took one second for 1000 iterations, increasing the amount of iterations for the relaxation procedure did not require much more computing time and therefore this (inefficient) method was very suitable. Finally, the lift L and drag D are found by integration of the lift and drag distribution over the foil.

The LLXM can be extended for use with two foils by extending the influence matrix **a** in (2.63) (now **aa**) with three sub matrices: **ba**, **ab** and **bb**. **ba** and **ab** determine the interaction between the two foils and the third matrix **bb** determines the influence of the trailing foil in itself:

$$\left(\begin{array}{c} \mathbf{w_a} \\ \mathbf{w_b} \end{array}\right) = \left(\begin{array}{cc} \mathbf{aa} & \mathbf{ba} \\ \mathbf{ab} & \mathbf{bb} \end{array}\right) \left(\begin{array}{c} \mathbf{\Gamma_a} \\ \mathbf{\Gamma_b} \end{array}\right) \tag{2.65}$$

where $\mathbf{\Gamma}_a$ and $\mathbf{\Gamma}_b$ are the vectors containing circulations of the discretized leading and trailing foil and $\mathbf{w_a}$ and $\mathbf{w_b}$ are the vectors containing the local down wash. The discretisation of the two foils can be seen in figure 2.7 where L_{foil} is the distance between the two foils.

3

A deeply submerged foil

As provided in the introduction, first the results for a deeply submerged foil in Panship are studied. As the free surface is neglected in the solution, this situation is very controllable and the quality of the results of this relatively simple solution can be assessed and compared with the solution of other numerical solvers to set the foundations of the validation study.

The research question answered in this chapter is:

> *What is the quality of the results for the hydrodynamical forces for a deeply submerged hydrofoil in Panship with a constant forward speed?*

In order to give an answer to this question the lift, the induced drag and total drag of Panship are compared to the results of other numerical solvers. Furthermore, the pressure distribution at midspan of the foil in Panship is compared to the pressure distribution of the foil in another numerical solver.

The quality of the results for lift and drag is determined in two parts: first without inclusion of viscous effects and second with inclusion of viscous effects. As can be seen in table 1.1 the research question is answered by using the results of the LLXM, XFoil and Refresco. The LLXM has the benefit that the total and induced drag can be evaluated separately to make an easy comparison with Panship. Furthermore, the LLXM also has the benefit that the viscous forces can be included or neglected by choosing the output of XFoil, see sections 2.8 and 2.9. Therefore the lift and drag of Panship in can be compared to results excluding viscous effects and including viscous effects easily to see what the effect of neglecting viscosity is. For the same reason the results of Panship are also compared to Refresco.

However, before being able to validate the results of Panship two other steps have to be taken: first the results of the LLXM have to be validated and second, the input parameters of Panship have to be chosen correctly. In order to do the first step, the results of XFoil and the LLXM are discussed and the results of the LLXM are compared to the results of Refresco to find the correct value of the critical amplification factor N_{crit} as introduced in section 2.8. In the second step the influence of the different input parameters is studied and chosen and furthermore the pressure distribution at midspan of a very high aspect ratio foil in Panship are compared to the results of XFoil.

In Panship the influence of the free surface is excluded from the solution by neglecting the free Surface part of the Green function G^f such that only the biplane image G^0 remains, see (2.41). Furthermore, the foil is placed far away from the free surface such that it is submerged deeply. The benefit of excluding the free surface from the solution is that the calculations are much faster and require a fraction of the RAM.

The used calculations in Refresco have been performed for the Foiling Future project of MARIN and are available for this project. Since the discretisation of the geometry of the foil required for Refresco was created

with a different tool, it was possible to include more details of the geometry. However, it was not possible to discretize the same detailed shape of the foil in the meshing tool for Panship and a much simpler shape was used, without the winglet and rounded tip. These differences in shape can be seen in figures 3.1 and 3.2. The foil is the same as used on a small foiling sailboat, the Waszp. This foil is referred to as the Waszp foil.

Figure 3.1: Representation of the foil in Refresco.

Figure 3.2: Representation of the foil in Panship

As the calculations performed in Refresco were not performed with the definition of the angle of attack being zero if the angle with the camber line is zero, high angles of attack are used in the calculations in Refresco. The difference between the definition of zero in the calculations in Refresco and the angle of the camber line being zero is +4.35°. In the plots represented in this thesis the angle of attack is 0° if the angle with the camber line is zero.

To do the computations in Panship, the clusters Marclus3 and Marclus4 at MARIN are used which are available for students. For the computations without a free surface, the memory requirements were low and the normal nodes could be used. For the computations including a free surface, the large queue was required, which had a RAM of 512GB and was still limiting the quality of the results.

Concluding, in order to give an answer to the first subquestion, first the results of XFoil and the LLXM using the critical amplification factor N_{crit} are described in sections 3.1 and 3.2. Furthermore, as Panship uses many parameters to discretize a foil and its wake, the influence of important parameters is studied in Panship in section 3.3. Next, a comparison of the pressure distribution of a very high aspect foil in Panship to the pressure distribution in XFoil is provided in section 3.4. The results of Panship are compared to the results of the LLXM and Refresco in section 3.5 and a conclusion is drawn in section 3.6.

3.1. XFoil Results

The XFoil program is described in section 2.8 and is used in this study as an input for the LLXM and to compare the lift distribution on a very high aspect ratio foil in Panship. The manual of XFoil states that the solution of XFoil is converged for the number of chordwise panels of N = 160. A convergence study for lift and drag at angles of attack of -7°, 0° and 7° verified that the results of XFoil where indeed converged at a number of chordwise panels N of 160 for the viscous solution using a cosine spacing to the leading edge. The inviscid solution was converged earlier at N = 120.

For the viscous solution a critical spatial amplification factor N_{crit} is required to induce the start of the separation bubble which is introduced in section 2.8. To study the effect of the value of the value of N_{crit} on the start of the separation bubble and choose it correctly, different values of N_{crit} are used in the calculations. The starting location of the separation bubble at the pressure and suction side of the foil for different values of N_{crit} can be seen in figure 3.3 for an angle of attack of 0°. As expected, decreasing the value of N_{crit} leads to an earlier start of the separation bubble. For the low values of N_{crit} = 0.01 and 0.1 based on table 2.1, the separation bubble starts very close to the leading edge and the solution is solved almost fully turbulent. In table 2.1 values for N_{crit} have been introduced for different situations but not for a hydrofoil. Specifying the value of N_{crit} for a hydrofoil is difficult. It is expected that the separation is started earlier than in an average wind tunnel, since the viscosity in water is higher, and therefore the expected value of N_{crit} would be lower
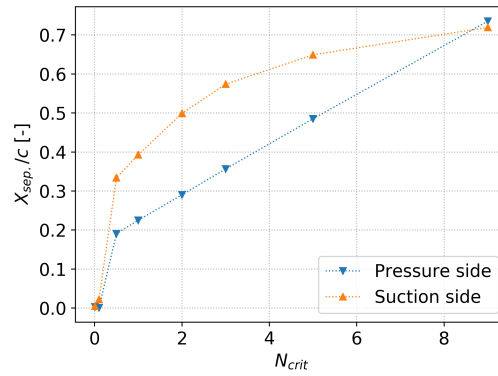
Figure 3.3: Start of the separation bubble at the pressure and suction side for different values of N_{crit} at an angle of attack of 0°

than 9.

As can be seen in figure 3.4 the lift curves show a linear part and a part where the separation influences the results and the lift curve becomes less steep and finally breaks down. The value of N_{crit}, and thus the start of the separation bubble, influences the lift curve for of a Waszp foil by displacing a hump in the lift curve from an angle of attack of -2° to 4.5° and by decreasing the slope for decreasing values of N_{crit}. Using a value of N_{crit} lower than 0.1 does not change the results as the values for C_l are the same for N_{crit} is 0.1 and 0.01 and the hump is removed completely. The inviscid solution of XFoil is linear with respect to the angle of attack, which is expected for a two-dimensional foil in potential flow. The same hump as seen in the lift curves can be seen for the drag in figure 3.5. The drag curves for the viscid solution show a quadratic form and the drag for the inviscid solution is zero for all angles of attack.

As it is difficult to choose the right value of N_{crit} for a hydrofoil based on these results, the final choice for N_{crit} is moved to the next section. In the next section the choice for the value of N_{crit} can be determined based on
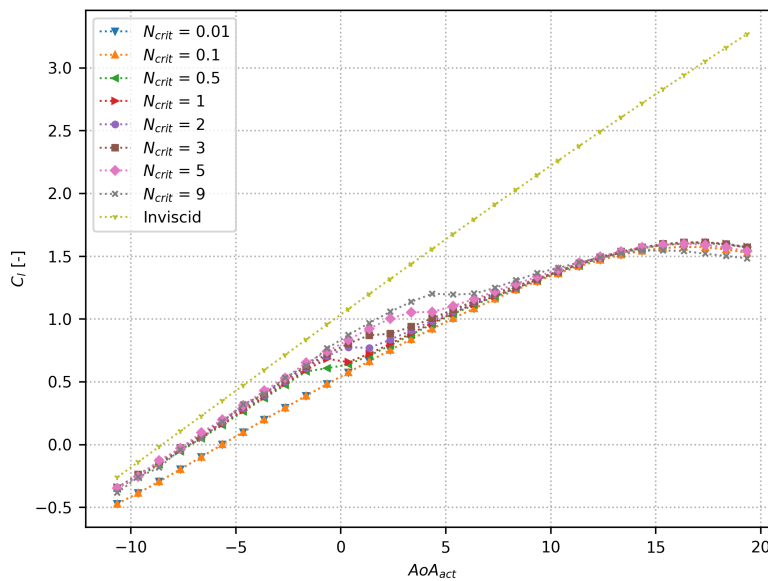
Figure 3.4: The viscid and inviscid solution for lift of XFoil
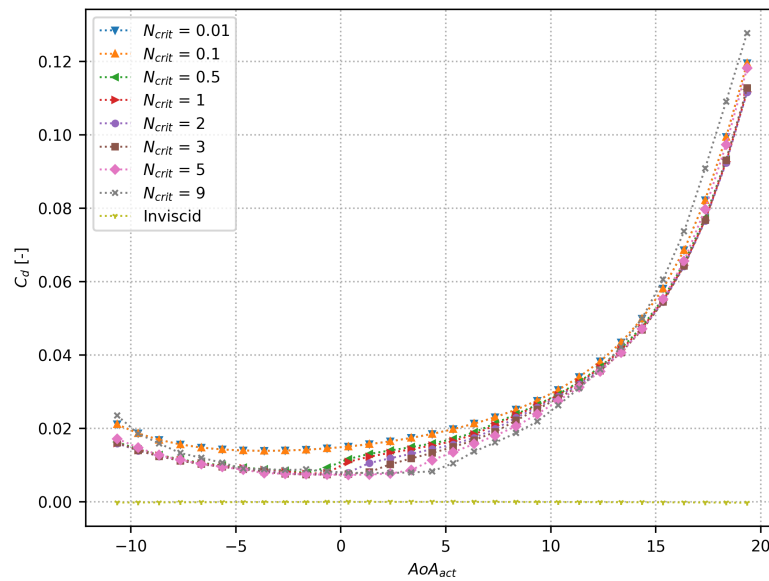
Figure 3.5: The viscid and inviscid solution for lift of XFoil

a comparison of the 3D LLXM with results of Refresco.

3.2. Lifting-Line XFoil results

In order to find a solution for the Lifting Line - XFoil Method (LLXM), a convergence study has been performed for the number of span wise elements M, the required number of iterations and the length of the trailing vortices. As the lift and drag are calculated using the local angle of attack on the foil, the drag is converged if the lift is converged. Therefore, in this section only the convergence of lift is taken into account. To create the required interpolation tables to determine the local circulation due to the angle of attack (2.60), results of XFoil using $N = 200$ and $N_{crit} = 0.1, 0.5, 1, 5, 9$ and an inviscid solution are used.

In the LLXM, the foil is discretized using three different parameters: the number of span wise elements, the length of the trailing vortices and the number of time steps. The effect of the number of span wise elements M on the lift coefficient C_L is studied first. In figure 3.6 the effect of the number of span wise elements M on the lift coefficient C_L can be seen using 1000 iterations. This figure shows that the lift coefficient converges fast and is fully converged for $M = 250$. Second, the effect of the length of the trailing vortices is studied in figure 3.7. The solution is converged at a length of four times the width. Third, the convergence for lift for the number of time steps can be seen in figure 3.8. At 600 iterations the lift is converged which means that the number of iterations used for the convergence study for the number of span wise elements and trailing vortices was enough. The lift distribution over the span of the foil for an angle of attack of zero can be seen in figure 3.9.

Calculations for values of $N_{crit} = 0.1, 0.5, 1, 5, 9$ and angles of attack of -3.65 to 12.35 have been performed to study the influence off N_{crit} on the lift and drag curves. The resulting lift and drag curves can be seen in figures 3.10 and 3.11. Figure 3.10 shows the inviscid and viscid results of the LLXM and the results of the viscous flow solver Refresco. The results show the same behaviour as seen for the results of XFoil. The lift slope and the location of the hump are influenced by the value of N_{crit} and the inviscid solution is fully linear and higher than the viscid solution. This figure shows that when the value of N_{crit} is reduced, the solution approaches the solution of Refresco. An explanation for this behaviour is that Refresco assumes a fully turbulent solution and XFoil assumes a laminar viscous and turbulent part. By reducing the value of N_{crit} separation is induced earlier and if a very low value of N_{crit} is chosen, the solution becomes fully turbulent, see figure 3.3.
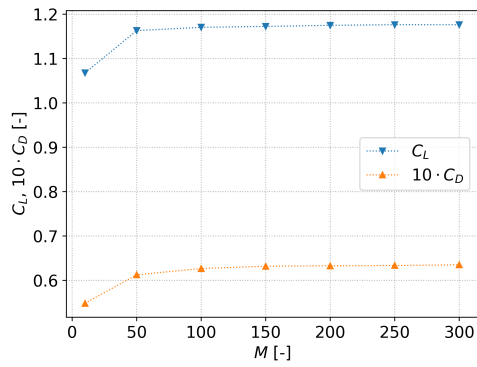
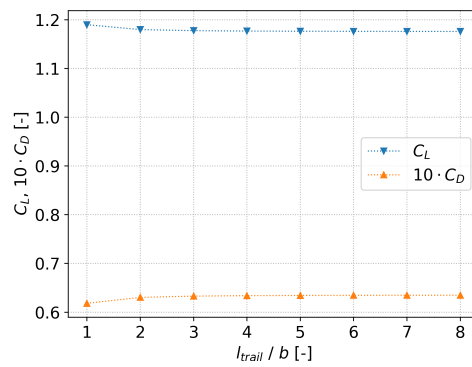Figure 3.6: Convergence for number of spanwise elements M, using 1000 iterations

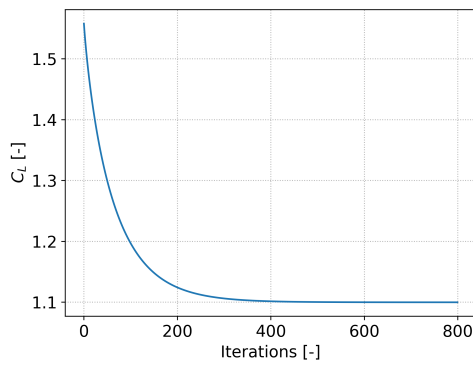Figure 3.7: Convergence of C_l for the length of the trailing vortices l_{trail}

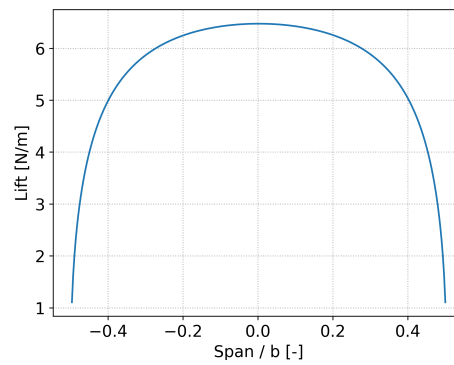Figure 3.8: Convergence of the lift per iteration

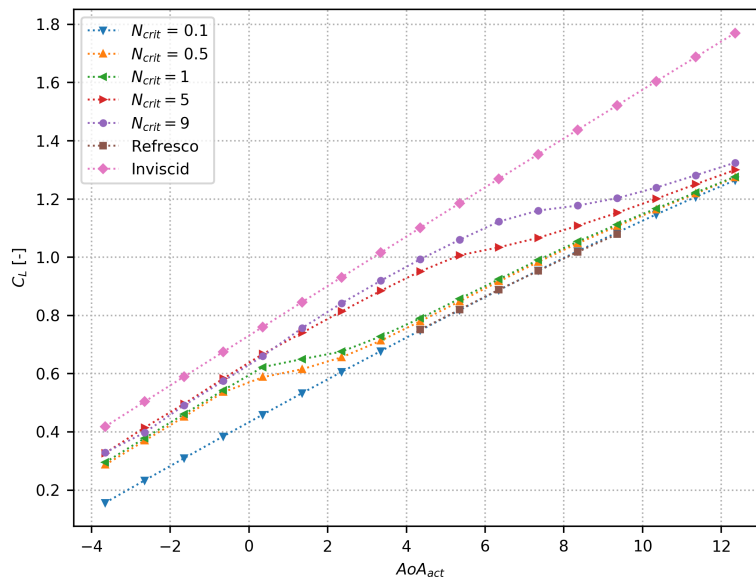Figure 3.9: Lift distribution over the span of the foil

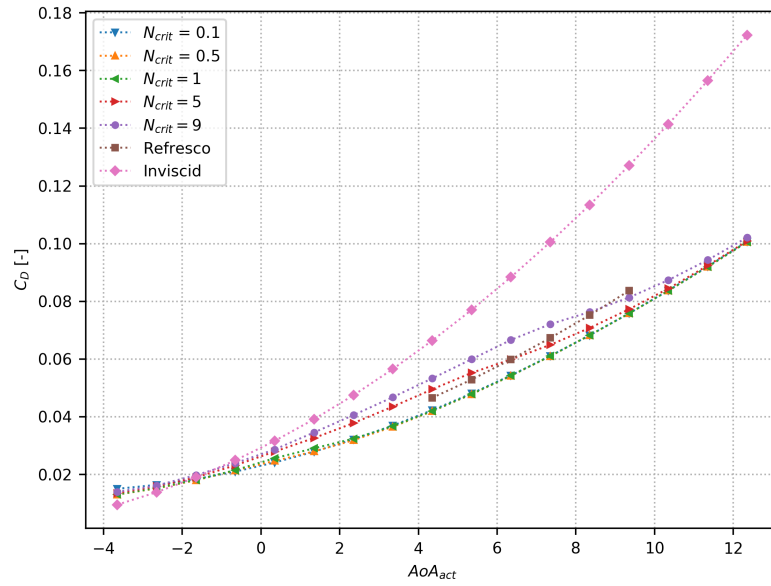Figure 3.10: Lift in the LLXM per angle of attack for different values of N_{crit} compared to Refresco.

Figure 3.11: Drag in the LLXM per angle of attack for different values of N_{crit} compared to Refresco.

The computed drag for the same angles of attack can be seen in figure 3.11. This figure shows that the solution for drag becomes smaller as the values of N_{crit} is reduced. The solution does not converge to the solution of Refresco but under predicts the drag by 9%. The inviscid drag only consists of the induced drag, which shows the expected quadratic shape. The total and induced drag are compared in figure 3.12 where it can be seen that the induced drag grows much faster than the parasitic drag for increasing angle of attack. As the value of N_{crit} decreases, induced drag decreases as well, but the parasitic increases. It should be noted that the total drag for values of N_{crit} = 0.1 and 1 are approximately the same in figure 3.11 but the induced and parasitic drag do differ.
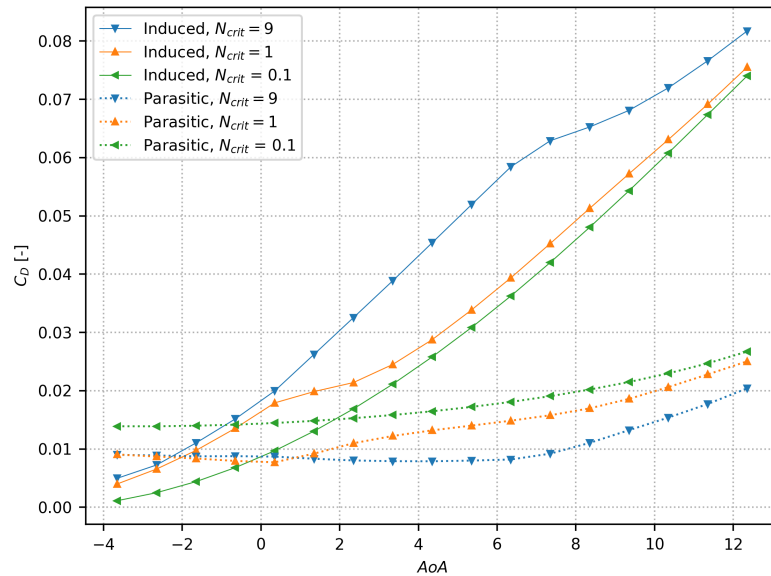

Figure 3.12: Induced and parasitic drag in the LLXM per angle of attack for different values of N_{crit} compared to Refresco.

3.3. Exploration of important parameters in Panship

As it is expected that the results of Panship highly depend on the discretisation of the foil and other input parameters, the influence of the input parameters is studied first. The most controllable environment is the situation where the free surface does not influence the solution, therefore the effect of these parameters is studied when the free surface part of the Green function G^f is turned off and the foil is submerged deeply.

In previous work for foils in Panship a trailing edge gap, a small opening at the trailing edge, was used to avoid pressure peaks near the trailing edge, it led to an invalid solution here as satisfying the Kutta condition proved to be difficult. Therefore, the trailing edge was closed.

The eight studied input parameters are:

- t: time simulation length [s]

- h: submergence [m]

- N: the number of chordwise elements

- M: the number of spanwise elements

- n_{side}: the number of panels at the side of the foil

- FAKTWE: factor influencing the length of the first element of the wake sheet

- α: the angle of the first part of the wake sheet with respect to the x-axis [°]

- DWMXA: the maximum length of the first part of the wake sheet [m]

A visual explanation of the parameters FAKTWE, the angle of the first part of the wakesheet α, the angle of the second part of the wakesheet β, the length of the first part of the wakesheet DWMXA and the length of the second part of the wakesheet DWMXB is provided in figure 3.13. The influence of changing β is not determined here as it is assumed that the wake follows the free stream far away from the foil and its starting vortex [23]. Therefore, the value for β is kept at 0°. DWMXB is held constant on a very long distance of 10 m, such that its maximum length is deep in the far field. The effect of the input parameters on the solution will be discussed now.
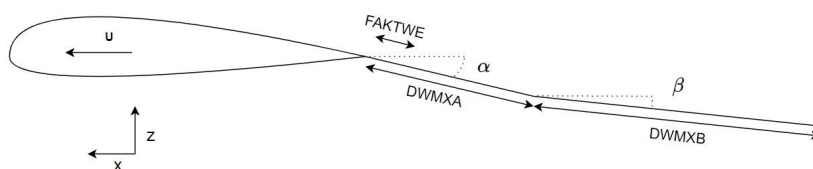

Figure 3.13: A two-dimensional view of a foil and his wake sheet in Panship

Time simulation length t
As on every time step a new wake panel is placed behind the foil, the length of the wake sheet depends on the time t the simulation is running. Therefore, a long enough time simulation length should be chosen for convergence of the influence of the wake sheet. The wake sheet extends over the two parts of the wakesheet DWMXA-DWMXB and as can be seen in figure 3.14 the lift and induced drag coefficient converge fast over time. This figure shows that the solution converges in a simulation length of 0.5 s. For this simulation a time step of 0.1s was used and therefore 5 time steps are required. For a smaller time step more time steps are required. For the following calculations at least 100 time steps are used to ensure a large enough wake length, but the amount of time steps can be reduced severely to reduce the computational time if necessary.

As in this case the maximum amount of wake panels NHISTW was set to 100, it can be assumed that it is large enough as the solution is converged after 5 time steps. It is kept at this length to ensure that the number of wake panels is not the limiting factor in the solution.
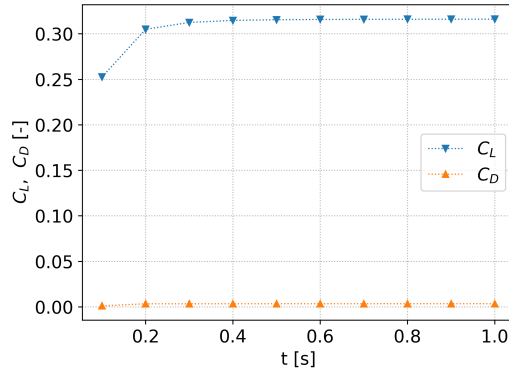
Figure 3.14: Convergence of the solution over time

Effects of increased submergence h: excluding effects of the free surface
The free surface is excluded from the solution by increasing the submergence h and therefore placing the foil further away from the free surface. If the foil is placed far enough from the free surface, a further increase of submergence does not influence the results of the foil anymore. Therefore the effect of increasing the submergence is studied in figure 3.15. In this figure the induced drag C_{Di}, viscous drag C_{Dv}, lift C_L and buoyancy coefficient C_b are plotted versus the submergence. In order to create a clear figure, the induced and viscous drag have been multiplied by 40. The figure shows that the lift and induced drag forces are converged at a submergence of 8 chords. A value of the same order was also seen by de Jong [3].
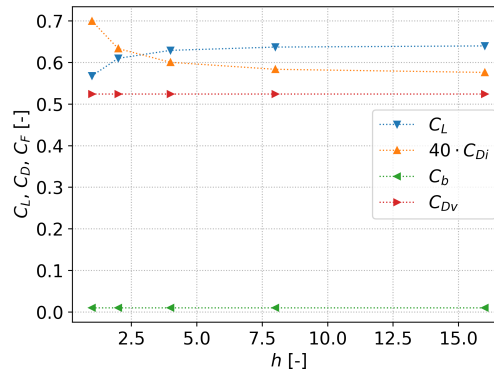
Figure 3.15: Effect of increasing submergence h of the foil using $M = 20$ and $N = 140$

As the convergence was slightly slower at different paneling, a submergence of $h = 16\ c$ is used to ensure convergence. The buoyancy force remains constant as the volume is not changed at a deeper submergence and the viscous drag forces remain constant as they are determined using the ITTC '57 convention frictional correlation line, introduced in section 2.6.7.

It should be noted that the solution breaks down at a very deep submergence due to round off errors. In the mesh input file of Panship the geometry is described using a maximum of six digits. As the foil is submerged deeper, some of these digits are used to describe the depth of the foil and the remaining precision of the digits is not satisfactory to describe the geometry of the foil. Panship uses single precision in its calculations of the free surface Green function to save memory, so round off errors could be induced in other parts of the calculation than the input as well.
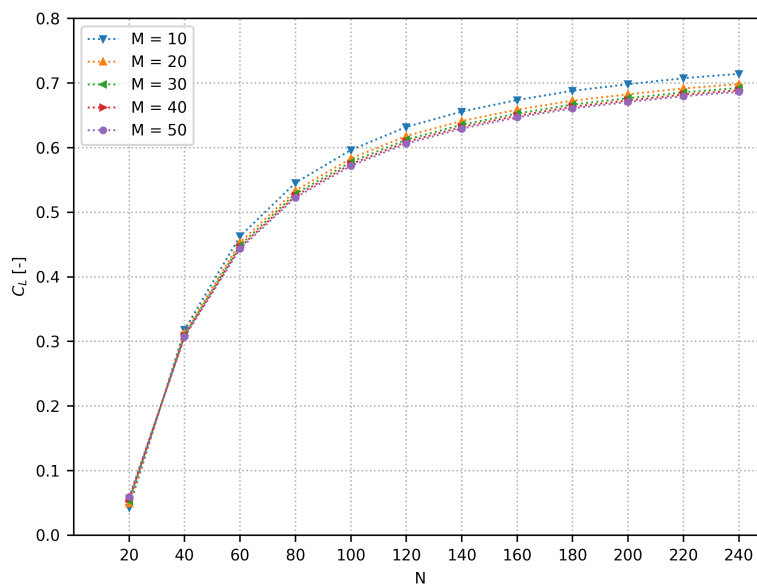
Figure 3.16: Effect of amount of spanwise M and chordwise panels N on lift

Discretisation in chordwise and spanwise panels N and M
The foil is discretized using a cosine spacing towards its leading edge over its chord and an even spacing over its span. A cosine spacing towards the leading and trailing edge of the foil has been used as well but this required more panels over the chord of the foil N. Applying a cosine spacing in both directions also led to problems in imposing the Kutta condition due to a very small last panel at the trailing edge, leading to errors in the solution for $N > 160$.

The effect of increasing the number of panels over the span and the chord on lift and induced drag can be seen in figures 3.16 and 3.17. These figures show that the lift and induced drag converge very fast for the number of spanwise panels M. The solution for lift and induced drag is almost not improved by using M higher than 20. Convergence for N is much slower than for M as the lift and drag are not yet fully converged at $N = 240$. The convergence for induced drag is slower as it depends on the angle the lift vector is rotated backwards due to downwash as described in section 2.1. As this angle may be small, small changes in the discretisation of the geometry may influence the induced drag and detailed discretisation is required to determine it correctly.

As computations with a detailed discretisation of $N = 240$ required a vast amount of computational power, a less detailed discretisation of $N = 140$ is used to study the influence of other parameters. The choice for a less detailed discretisation especially influences the quality of results of induced drag. However, for further study of the input parameters it is assumed that the same trends are seen for the results of less detailed discretisation. For the calculations which are used to compare Panship to other numerical tools, the detailed discretisation is used.

The convergence for the number of span and chordwise panels M and N for other foils is different. The same plots for M and N can be seen in figures B.1, B.2, B.4 and B.5 in appendix B for a NACA64010 and a NACA 16-008 with a modified NACA a = 0.8 camber line. For the NACA64A010 foil the convergence for N is much faster for lift and drag but the convergence for M for drag is much slower. For the NACA 16-008 with a modified NACA a = 0.8 camber line the convergence for M is just as fast as the first foil described above for both lift and drag. As the convergence behavior is different for the three different used foils, the used number of panels should be chosen carefully for each foil.
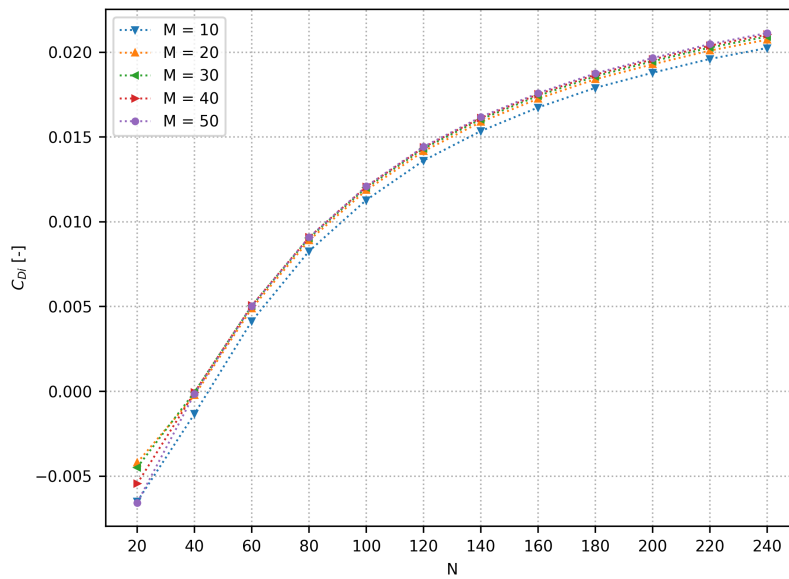
Figure 3.17: Effect of amount of spanwise M and chordwise panels N on induced drag

Applying a cosine spacing over the span of the foil
The effect of applying a cosine spacing over the span of the foil is studied in figure 3.18 for lift and drag. Applying a cosine spacing over the span may have the benefit of the panels near the tip of the foil having a smaller width and therefore the downwash near the tip of the foil can be determined more precisely. The figures show that applying a cosine spacing over the span of the foil has small benefit for lift if the number of spanwise panels $M = 10$ is used, but there is no improvement of the solution when $M = 20$ is used. For drag the improvement of the solution is bigger, especially at $M = 10$. This means that for foils with a slow convergence for lift or drag for M a cosine spacing definitely may be a benefit and reduce computational requirements.
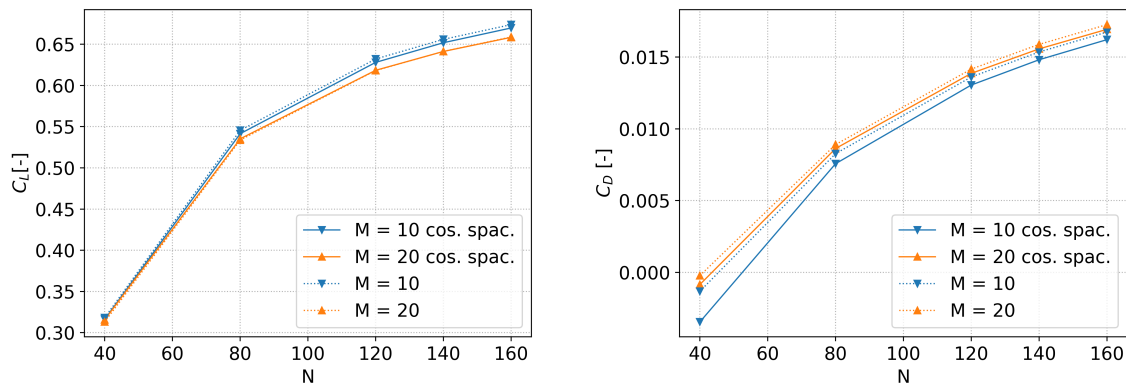

Figure 3.18: C_L and C_D using cosine spacing over the span of the foil versus normal spacing

Applying the no-flow boundary condition at sides
In order to have a better representation of the geometry of the foil, the no-flow boundary condition can be applied at the sides of the foil by placing source panels. Over the length of the foil halve the amount of chordwise panels $N/2$ panels are used such that the connection between the panels the side of the foil and

the panels over the chord of the foil is watertight and no gaps are present. In the direction of the thickness of the foil a number of panels of n_{side} of 0, 1, 2 and 3 are used. An example with $N = 100$, such that the number of panels over the chord of the side is 50, and $n_{side} = 2$ is given in figure 3.19.

Figure 3.20 shows that by adding panels to the side of the foil leads a very small change of the solution and the solution almost not improved by increasing the panel density on the sides by increasing n_{side} and N. A further increase of n_{side} was not possible as the panels near the leading and trailing edge had become too small for Panship to allow. As the results show a very small improvement of the solution by adding panels to the side of the foil and since this addition increases the required time for meshing and computational requirements, it is decided not to apply the no-flow boundary condition at the sides of the foil.

Figure 3.19: Panels on closed side of the foil with $n_{side} = 2$ and $N = 100$ such that number of panels over the chord of the side is 50.
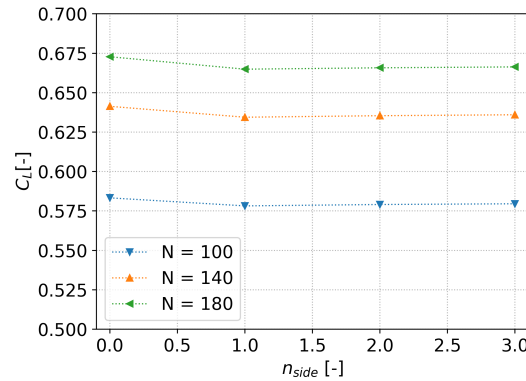

Figure 3.20: Effect of number of panels at the side of the foil

The length of the first wake panel influenced by FAKTWE
The length of the first wake panel l_{w1} depends on the forward velocity U, the time step Δt and the parameter FAKTWE. The parameter is introduced in section 2.6.4 but its relation to the first wakepanel is restated here:

$$l_{w1} = \text{FAKTWE} \cdot U \cdot \Delta \qquad (2.50)$$

In the manual the value of FAKTWE is recommended to be such that the length of the first wake panel l_{w1} is the same as the length of the last panels at the trailing edge of the foil $l_{T.E.}$:

$$\text{FAKTWE} = \frac{l_{T.E.}}{U \cdot \Delta t} \qquad (3.1)$$

However, the length of the first wake panel severely influences the lift and drag if it is chosen too low. In figure 3.21 the lift is plotted versus time step Δt for different values of FAKTWE for a NACA64A010 foil. The value of FAKTWE is specified by 3.1 and is a factor which influences the length of the first wake panel. Therefore, by using a low value of FAKTWE, the length of the first wake panel is very short, and by using a large value of FAKTWE, the length of the first wake panel is long.

As the length of the first wake panel is determined using equation 2.50, for a very small time step the length of the first wake panel is short and Panship is not able to find a correct solution. Figure 3.21 shows that if a very small time step is used, a very high value of FAKTWE is required to find a correct solution. The requirement for a large first wake panel can be explained by part II of figure 2.4 and is introduced in section 2.6.4. Since the Kutta condition is imposed by the influence of the first wake panel only, the sum of the circulation at the intersection of the first and the second wake panel is not zero as the circulation of the second panel is not taken into account. Therefore, if the length of the first wake panel is chosen too short, the stagnation point is influenced by this circulation, which should have been canceled out.

Another benefit of using a high value of FAKTWE is that it leads to a fast growth of the wake sheet during the first time step and therefore the solution is converged faster over time. However, as FAKTWE is chosen too large, the wakesheet is not able to follow the prescribed shape of the wake.
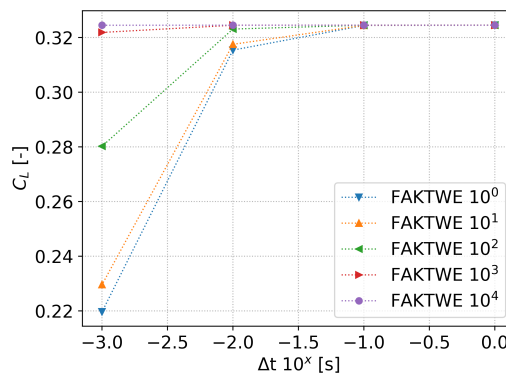
Figure 3.21: Influence of time step and FAKTWE on solution of a NACA64A010 foil.

The angle of the first part of the wake: α
The effect of the angle of the first part of the wake, α, on lift and induced drag can be seen in figure 3.22. For $\Delta\alpha = 0°$, the wake goes straight out of the trailing edge as prescribed by the Kutta condition in equation 2.35. Increasing and decreasing α both gives an increase of lift as the induced velocities of the wake sheet change due to rotation of the wake sheet. The induced drag is increased for decreasing α and decreased for increasing α. The effect on induced drag is bigger than for lift. It should be noted that for coarse grids the effect of α on the lift and induced drag is not smooth and bumps arise in the curve. For further calculations an α imposed by the Kutta condition is used.
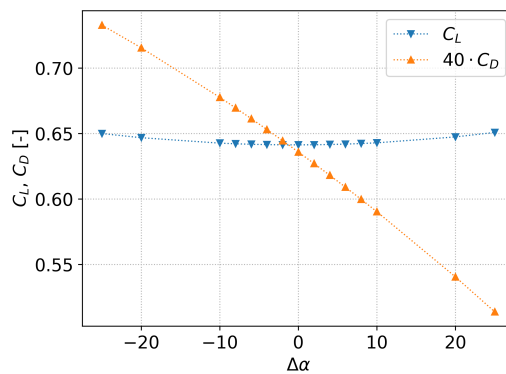
Figure 3.22: Influence of the angle α on the lift and induced drag using N = 200 and M = 56

The length of the first part of the wake: DWMXA

In order to investigate the effect of the length of the first part of the wake, DWMXA, the length of the second part of the wake, DWMXB, is kept constant at 10 *m* such that the wake sheet ends in the far field and a further increase of DWMXB does not influence the results.

Increasing DWMXA has a small effect on the solution if a large first wake panel is used, as can be seen in figure 3.23. As the first wake panel is very large, decreasing DWMXA does not affect the result as it cannot be smaller than the length of the first wake panel. However, for smaller first wake panels, the effect of DWMXA is much stronger as can be seen in figure 3.24 where a much smaller first wake panel is used. It should be noted that for this plot a different angle of attack is used, leading to different values of lift and drag. In the last case the shape of the wake sheet therefore clearly influences the lift and the induced drag on the foil.

The length of the first part of the wakesheet, DWMXA, has to be chosen realistically. In reality the wake sheet rolls up into two trailing vortices near the tips of the foil, but for this effect is not accounted in Panship. In order to find a realistic value for the length of DWMXA, the start of DWMXB is chosen at the point the wake sheet should have been fully rolled up and the trailing vortices move with the free stream velocity. Choosing the length of DWMXA as such, implies that the height of the wake sheet is at the height of the cores of the trailing vortices.

The roll up of the wake sheet is described by equation 2.6 in section 2.1 where the wake sheet is fully rolled up at length e behind the foil depending on the chord c, the aspect ratio AR and the lift coefficient C_L:

$$\frac{e}{c} = 0.28 \frac{AR^2}{C_L} \tag{2.6}$$

For this foil, having an aspect ratio of 5 and a lift coefficient varying from 0.4 to 1.6 for angles of attack of -8 ° to 8 °, based on 2.6 e/c varies from 23.5 to 6.2. As can be seen in figure 3.23, the induced drag is not influenced by choosing a value of DWMXA in this range but the lift is. It should be noted that this effect is different for lower aspect ratios, the value of e/c will be lower and the value of DWMXA might have a large influence on the results.
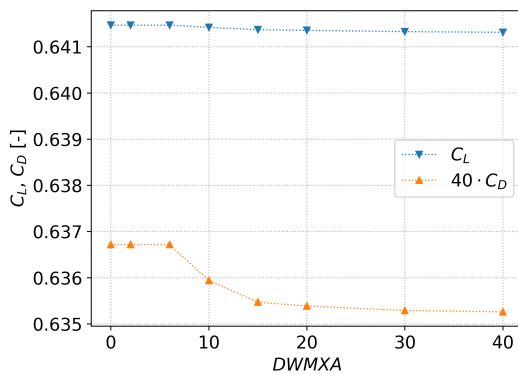

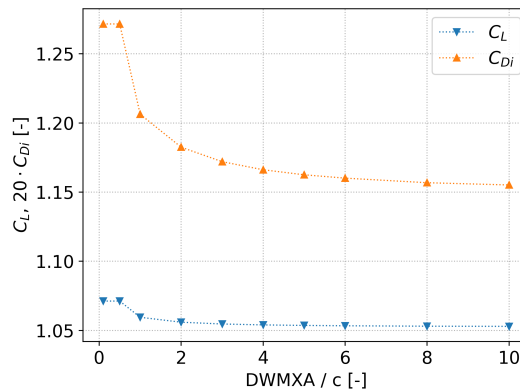Figure 3.23: Effect of changing DWMXA on lift

Figure 3.24: Effect of changing DWMXA on lift, using a small first wake panel

Conclusion

Based on this study the following parameters are used for the calculations comparing the results of Panship to the results of the LLXM and Refresco:

- a simulation length t of 10 s and a time step of 0.1 s to ensure convergence over time;

- a submergence h of 16 chords, such that the free surface effects do not influence the results;

- a number of chordwise panels N of 240 and a number of spanwise panels M of 20, to ensure convergence;

- zero panels at the sides, as it did not improve the results significantly;

- FAKTWE = 10, such that the length of the first wake panel is long enough for a stationary condition;

- an α-angle imposed by the Kutta condition;

- a DWMXA imposed by equation 2.6.

3.4. Comparing a very high aspect ratio foil in Panship to XFoil

To check if the panel method is correctly implemented in Panship, de Jong compared a very high aspect ratio NACA 0012 foil in Panship to the 2D calculations in XFoil [3]. In order to do so, it was assumed that 3D effects at mid span of the foil have disappeared as the aspect ratio is very high and the foil is very wide. In the present study, these results are reproduced and extended for two extra foils. In figure 3.25 the results for three different foils is plotted using spanwise panels $M = 50$, chordwise panels $N = 160$ and aspect ratio $AR = 50$ can be seen. The discretisation is different than one would expect based on the conclusion of the previous section as due to the large width of the foil the amount of used spanwise panels had to be increased from $M = 20$ to $M = 50$. Due to the large memory requirements therefore the amount of chordwise panels had to be reduced from $N = 240$ to $N = 160$. The three used foils are a NACA 4412 foil under an angle of attack of 7 degrees, a NACA 0012 foil under an angle of attack of 5 degrees and the Waszp foil under an angle of attack of 4.34 degrees. Of these foils the NACA 4412 and the Waszp foil have a camber.

For the NACA 0012 foil a slight underprediction of the pressure at the leading edge can be seen with respect to XFoil, which was also seen by de Jong [3]. This underprediction is bigger for the NACA 4412 and the Waszp foil at the suction side, especially at the peak near the leading edge. The NACA 4412 also shows a deviation near the trailing edge on the pressure side. It seems that the prediction of the pressure distribution in Panship is better for symmetrical foils than for cambered foil, but the underprediction of the pressure decreased as AR and M increased and these results can still be improved. It should be noted that the results may be influenced by the round off errors described earlier. Increasing the amount of chordwise panels N did not give improved results.
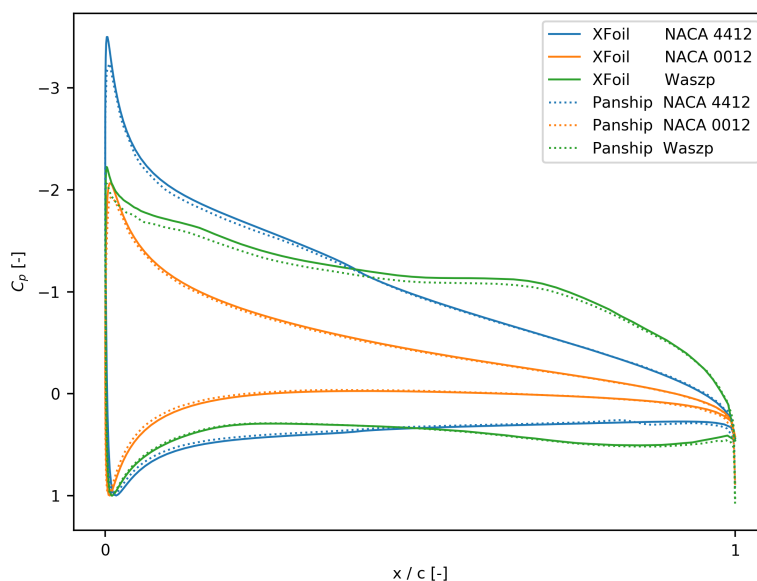
Figure 3.25: Pressure distribution of a NACA 4412, NACA 0012 and a Waszp foil in XFoil and at midspan of a very high aspect ratio foil in Panship

3.5. Comparing the result of Panship to the LLXM and Refresco

To compare the behavior of a foil under an angle of attack in Panship, the results of a foil in Panship under different angles of attack are compared to the results of the Lifting Line - XFoil Method (LLXM) and Refresco. The inviscid solution of Panship is compared to the inviscid solution of the LLXM first, after which the solution of Panship, in which the viscous drag is included empirically, is compared to the viscous solution of the LLXM and Refresco. In figure 3.26 the solution of Panship, without empirical viscous drag forces, is given for angles of attack of -4° to 10°. In the same figure, the inviscid solution of the LLXM is given for the angles of attack of -3.65° to 10.35°.

The figure shows that the lift obtained in Panship agrees with the lift of the LLXM for the lower angles of attack of -4° to 4° but for higher angles of attack the lift starts to deviate from the LLXM as to the lift curve slope in Panship is slightly lower. The same was seen in earlier work where de Jong compared the lift of a very high aspect ratio NACA 0012 foil in Panship for the angles of attack of 0 to 12 with XFoil and found a slightly lower lift curve slope in Panship [3]. In that case, the difference was expected to be result of 3D effects and unrealistic panel shaping [3]. In this case the results of Panship should be almost completely converged panel wise but can be improved slightly and therefore it is assumed that this effect arises due to errors in the representation of the 3D effects in the LLXM.

The difference between the induced drag determined in Panship and the LLXM is larger than for the lift. As the induced drag is highly dependent on 3D effects, a small error in the local angle of attack might lead to a large error in induced drag. Therefore, the errors in the 3D effects of the LLXM play a larger role here. As the LLXM also was not able to predict the drag matching to the correctly predicted lift in figures 3.10 and 3.11, a difference between the results of the LLXM and Panship for drag is also expected here. In the next chapter, under the free surface effects the induced drag treated again. Based on these results, it can be expected that Panship is able to predict the lift in potential flow if no free surface is included in the solution. The drag determined in Panship should be used with more care.

As in real flow the viscous effects influence the lift and drag, the results of Panship are compared to the viscous results of Refresco and the LLXM. In figure 3.27 the results of Panship are compared to the viscous solutions of the LLXM using N_{crit} = 0.1 and Refresco. To determine the viscous drag in Panship, the ITTC'57 con-
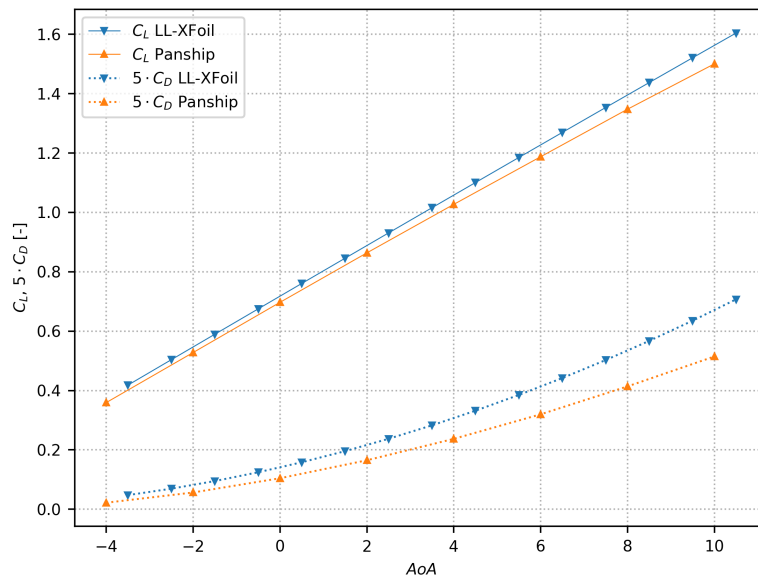
Figure 3.26: Results for C_L and C_D, Panship using N = 200 and M = 56 versus the inviscid solution of the LLXM

vention frictional correlation line is used as introduced in 2.6.7. This figure shows that the drag and lift are overpredicted severely in Panship as the lift in Refresco is 70% of the lift in Panship. The overprediction of lift is resultant of the lack of viscous effects in the solution of Panship, see for instance 3.10 and 3.11 where the introduction of viscous effects leads to a reduction of lift and an increase in drag. As the lift and induced drag are closely related, an overprediction of lift leads to an overprediction of drag.
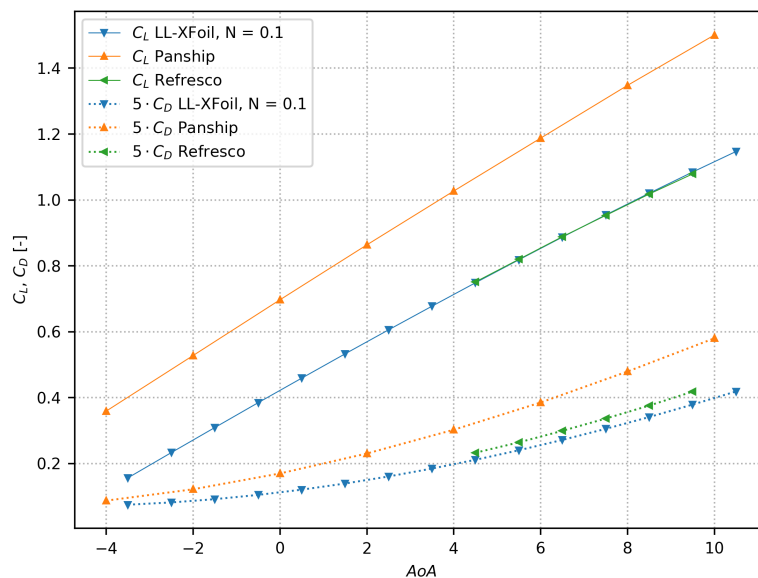

Figure 3.27: Results for C_L and C_D, Panship using N = 200 and M = 56 and the ITTC'57 convention frictional correlation line, Refresco versus the viscid solution of the LLXM using N_{crit} = 0.1

The overprediction of lift is logic as for this type of foil, having a large trailing edge closure angle, the effects of viscosity are strong. For a foil with a large trailing edge closure angle of 20° in a flow with a Reynolds number of

$6 \cdot 10^5$ the reduction of lift due to viscous effects, separation for instance, could be 70 % based on experiments [16] [25]. Which is approximately the same as seen in this case.

3.6. Conclusion

The value of N_{crit}, inducing the start of a separation bubble, has a large influence on the viscous results of Lifting Line - XFoil Method (LLXM). Choosing N_{crit} close to zero, and therefore imposing a fully turbulent solution gives the same results as Refresco for lift, of which the solution is fully turbulent as well. The results for drag, for the same N_{crit} are in less agreement with Refresco. This might be result of incorrect representation of 3D effects in the LLXM.

The results of Panship are highly dependent on the discretisation of the foil. The solution is converged fast for the number of spanwise panels M but much slower for the number of chordwise panels N. The length of the first wake panel l_{w1} should be long enough such that the Kutta condition is imposed correctly. The discretisation of the wake does have an influence on the performance of a foil near the free surface, only in the extreme cases a big difference is seen.

The results of XFoil, the LLXM and Refresco can be used to give an answer to the question provided at the beginning of this chapter:

> *What is the quality of the results for the hydrodynamical forces for a deeply submerged hydrofoil in Panship with a constant forward speed?*

The pressure distribution on midspan of a very high aspect ratio foil in Panship is very similar to the pressure distribution determined in XFoil. The results for lift in Panship are similar to the results of the LLXM but show a slightly lower lift curve slope, such that the results for higher angles of attack are in less agreement. The result for lift for a deeply submerged foil in Panship is qualitatively good. The results for induced drag have a poorer quality if compared with the LLXM as they show an underprediction. The results for drag should be used with more care.

For foils with a large influence of viscous effects on lift, the quality of the results of Panship is of poorer quality and should be used with great care as the lift and induced drag are overpredicted. In this case the results of the LLXM are in much better agreement with the results of the viscous flow solver Refresco.

4

A foil near the free surface

In this chapter the second stage of the validation process, studying the influence of the free surface on a foil, is performed. After comparing the results of a deeply submerged foil in Panship to the results of other numerical solvers, the complexity of the situation is increased by adding free surface effects. The presence of the free surface influences the performance of a hydrofoil vessel and the aim of this chapter is to see if Panship is able to correctly predict the influence of free surface on a hydrofoil. The influence of the free surface on the performance of the foil is introduced earlier in section 2.2.

In the second chapter is described that a foil will experience ventilation and cavitation near the free surface. Due to limits of the model it is not taken into account here. The question to be answered in this chapter is:

> *What is the quality of results for the hydrodynamical forces for a foil near the free surface in Panship in calm water with a constant forward speed?*

An answer to this question will be given by making a comparison between the results of Panship, experiments, the LLXM and Refresco. The comparison of Panship with experimental results has been performed in earlier work by de Jong but is partly redone to see whether the results can be reproduced and then improved as limited memory was available in the earlier work [3]. The experiments and the earlier work are described in this chapter.

In the comparison of the results of Panship with the experimental results the C_{Di}/C_L^2-curves are used. These curves are introduced in section 2.2. Furthermore, the lift and drag of a foil in Panship near the free surface are compared with results of Refresco to verify if the same is seen as in chapter 3 with respect to the inclusion of viscous effects. A comparison with the LLXM is made to see if the inclusion of viscous effects is more important than the inclusion of free surface effects. These comparisons are used to give an answer to the research question in a conclusion.

The free surface part of the Green function G^f in (2.41) was neglected earlier to speed up the calculations of the deeply submerged foil in Panship but is reintroduced here. Therefore the effect of a new input parameter is studied, the number of time steps NHIST in the history of the free surface part of the Green function. Furthermore, a second grid convergence study is performed to verify if the same behavior is seen as when the free surface is neglected in the solution.

Summarizing, first the used experimental data and the earlier are described in sections 4.1 and 4.2 respectively. As for the numerical simulations near a free surface history in the Green function is required, the required history NHIST is studied in section 4.3. Also, to ensure convergence, a grid convergence is performed and the effect of the length first wake panel on the solution is studied again in sections 4.4 and 4.5. Last, in sections 4.6 and 4.7 the earlier work is reproduced and the results of Panship are compared to Refresco and the Lifting Line - XFoil Method (LLXM).

4.1. Experimental data

The experimental data is obtained by Wilson and is published in [27]. This work contains results of towing tank tests where foils are towed for different foil submergences, velocities and angles of attack for steady and unsteady cases. For the current study the steady cases are of interest.

The foils are towed using a support system with a forward leading sting to minimize its influence and using a piano wire for turbulence stimulation at the leading edge. The influence of the support on the foil is expected to be minimal and the hydrodynamical forces of the support are excluded from the experimental result by determining these forces by towing the support without the foil. The foil is rectangular with a NACA64A010 section shape, a chord of 0.406 m and a width of 2.438 m.

The towing velocities vary from 2.44 to 8.53 m/s and the submergences vary from 0.25 to 4 chords. In this work only the submergences of 0.5, 1 and 2 chords are used and therefore the Froude submergence numbers (2.7) vary from 0.86 to 8.55. The used angles of attack vary from 0° to 10°. For the current research the results for an angle of attack of 4° are used as the author stated that the results for lift for the angle of attack of 2° were small and might contain errors. The induced drag is determined by extracting the parasitic drag from the total drag where the parasitic drag is determined empirically using the 1957 frictional correlation line, described in 2.6.7.

4.2. Earlier work in Panship

de Jong compared the results of a foil near a free surface in Panship, to the same experimental results as described in section 4.1 [3]. The main purpose of this research was to verify if the panel method was implemented correctly. A summary of the work of this work is provided here [3].

In order to find a converged solution in Panship, convergence is ensured for the number of chordwise panels N, the number of spanwise panels M, the free surface memory truncation NHIST and the length of the wake sheet at conditions with a strong free surface influence. Based on a convergence study values of $N = 40$ and $M = 16$ for the number of span and chordwise panels are chosen, while taking memory limitations in account. Due to these limitation is was not possible to use a more detailed discretization.

The results obtained in Panship are compared to the experimental results by means of the lift curve slope, the zero-lift angle and the C_{Di}-C_L^2-curve over the submergence Froude number (2.7). The first, the lift curve slope varying over submergence, determined in Panship shows good agreement to the results of the experiment except for lower Fn_h (2.7) and low submergence.

The second, the zero-lift angle, is overpredicted severely for low submergence but the right trends, as described in section 4, are predicted. The results for deeper submergence are in better agreement with the experiments. The differences in results for low foil submergences could be result of the linearization of the free surface boundary condition and the possibility that the results were not converged yet and are influenced by discretization errors. The third, the C_{Di}-C_L^2-curve, seen in figure 2.2, shows agreement for the deeper submergences.

4.3. Effects of history in the free surface part of the Green function

To determine the effect of a free surface on the foil, the free surface part of the Green function G^f (2.41) is introduced and the foil is placed closer to the free surface. If G^f is used, a number of time steps in its history NHIST has to be specified. NHIST is introduced in section 2.6.1 and its effect on the solution of Panship is studied in this section.

Since the used history influences the required memory and the computational speed of the calculation severely, it is important to keep the used history as low as possible. However, to get correct results NHIST should be chosen long enough. The Panship manual recommends NHIST to be [26]:
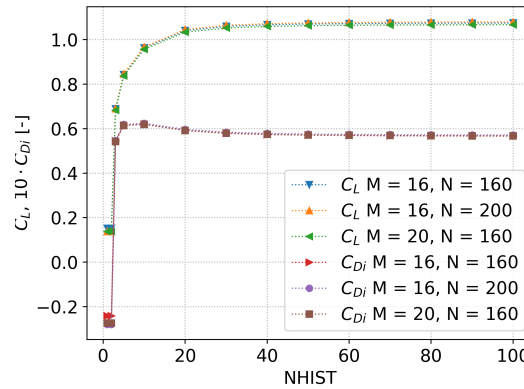
Figure 4.1: Effect of increasing number of time steps taken into account for history in the free surface Green function

$$\text{NHIST} = \frac{L}{\Delta t \cdot U} \tag{4.1}$$

where L is the length of the ship/foil. For a foil with a chord of 0.406 m, time step $\Delta t = 0.1$ s and a forward velocity $U = 5$ m/s, the value of NHIST should be 1 based on this approximation for ships.

In figure 4.1 the effect of increasing NHIST on lift and induced drag can be seen for foils with three different paneling. The results show that the lift and induced drag need at least a value of NHIST of 50 for convergence but the solution is still improved as NHIST is increased to 100. This clearly shows that this approximation is not valid for foils as it is much more than the suggested value of NHIST by the manual. Another indicator for the required amount of history is the behaviour of the derivatives of G^f, as on a long enough history the fluctuations of these derivatives flatten out. Figure 4.1 shows that changing the paneling on the foil does not influence the required amount of time steps in the history. Based on the results for increasing values of NHIST and the flattening of the derivatives of G^f, a history length of 100 time steps is chosen.

4.4. Grid convergence

A grid convergence study is performed near the free surface to see what the influence of the free surface is on the required amount of panels. In figures 4.2 and 4.3 the results for increasing number of spanwise M and chordwise panels N are shown. These figures show that the convergence is approximately the same for the lift C_L without a free surface in figure 3.16 but when taking a very close look, it can be seen that the convergence without a free surface is slightly faster for increasing N, compared to figure 3.16. For the induced drag C_{Di} the required M near the free surface is lower than for the solution without a free surface, as it converges faster. The rate of convergence for N is approximately the same.

Both figures 4.2 and 4.3 show fluctuations for curves for increasing N. As these foils are placed very close to the free surface, it is assumed that these fluctuations arise due to the formation of waves. The maximum values of M and N due to memory limits where $M = 72$ and $N = 260$ if 100 history steps in the free surface part of the Green function G^f are used.

4.5. Length of the first wake panel

In section 3.3 the effect of changing l_{w1} using FAKTWE (2.50) is studied for a deeply submerged foil. In this section is shown that l_{w1}, depending on the time step, should be long enough to get correct results. For the case of a time step of 0.01 s, the first wake panel was not long enough should be compensated with a FAKTWE of at least 100. However, for the case of a time step of 0.1 s the value of 1 for FAKTWE was enough.
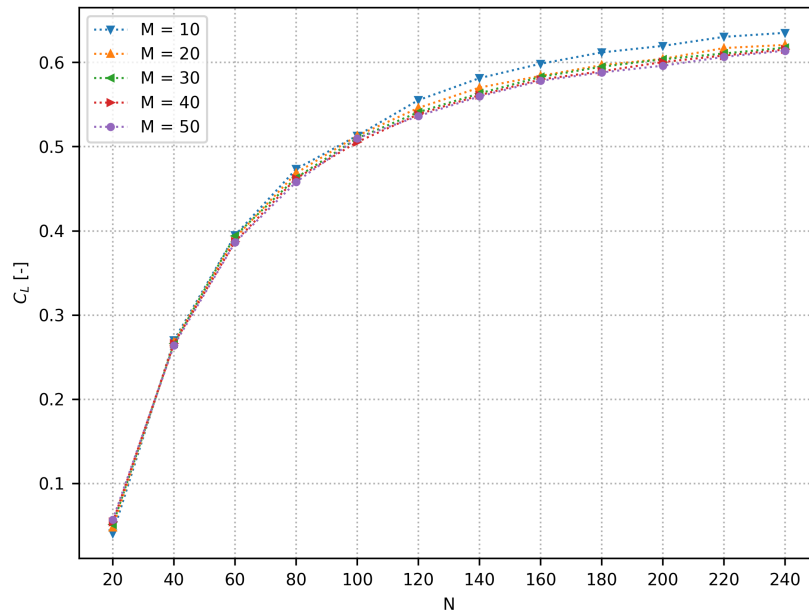
Figure 4.2: Effect on lift of increasing the number of panels in span and chordwise direction at a submergence of $h = 0.8c$
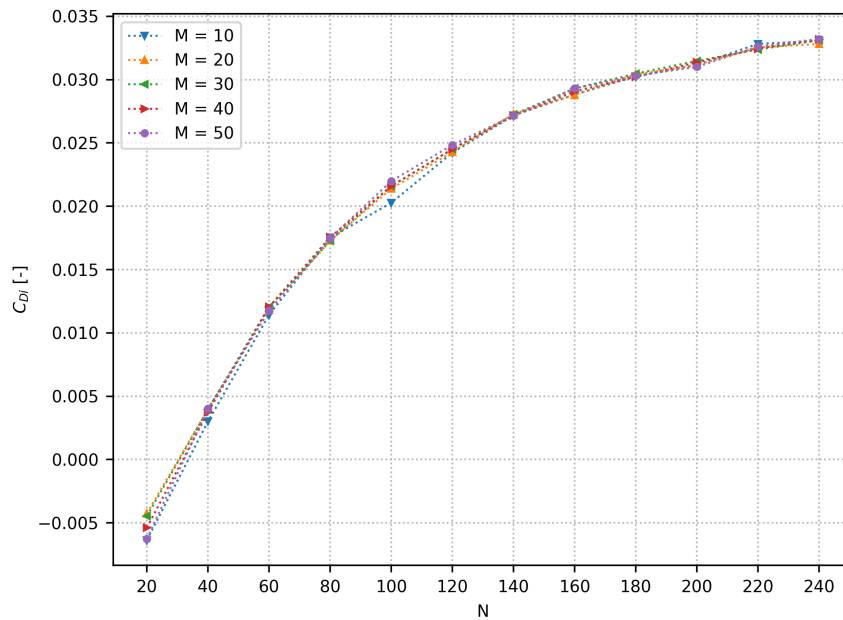

Figure 4.3: Effect on induced drag of increasing the number of panels in span and chordwise direction at a submergence of $h = 0.8c$

Results show that l_{w1} influences the results even more for a foil near the free surface than for a deeply submerged foil. This might be a result of the used Green function which imposes the free surface boundary condition. The simulations in Panship corresponding to the experimental results in the next section have been performed for the values of FAKTWE of 0.1, 0.5, 1, 2.5 and 10 and can be seen in appendix B.2. These simulations show that l_{w1} is long enough if a value of FAKTWE of 10 is used since a further increase does not improve the results.

4.6. Reproduction of results of earlier work

In the previous research the quality of the discretization was very limited by the available memory [3]. Therefore, using a higher quality of discretisation could give new insights. It is also interesting to see if the results of the earlier work can be reproduced. As described in section 4.2, in the earlier work the simulations where performed using a number of chordwise panels $N = 40$ and a number of spanwise panels $M = 16$. Figures 4.2 and 4.3 show that these values should show poor convergence. Interesting is that in the earlier work convergence plots show that the solution was converged faster than in this study.

In the previous work it was proven to be difficult to extract the experimental data from the original source, therefore it was redone using a digital data extractor in this work. In this way the data could be extracted more precisely than by hand. Comparing the re-extracted data to the data extracted in the earlier work, significant differences were found. As mentioned earlier, the results of the C_{Di}/C_L^2-curve for the angle of attack of 2 ° might be influenced by measurement errors, therefore the experimental results for an angle of attack of 4° are used in this case [27].

Figure 4.4 shows the C_{Di}-C_L^2-curves for submergence h/c of 0.5, 1 and 2 chords for Panship and the experiments. The results for Panship for a submergence of 16 chords, where the free surface effects are negligible and the result for an elliptical lift distribution in an analytic lifting line method are shown as well, defined by:
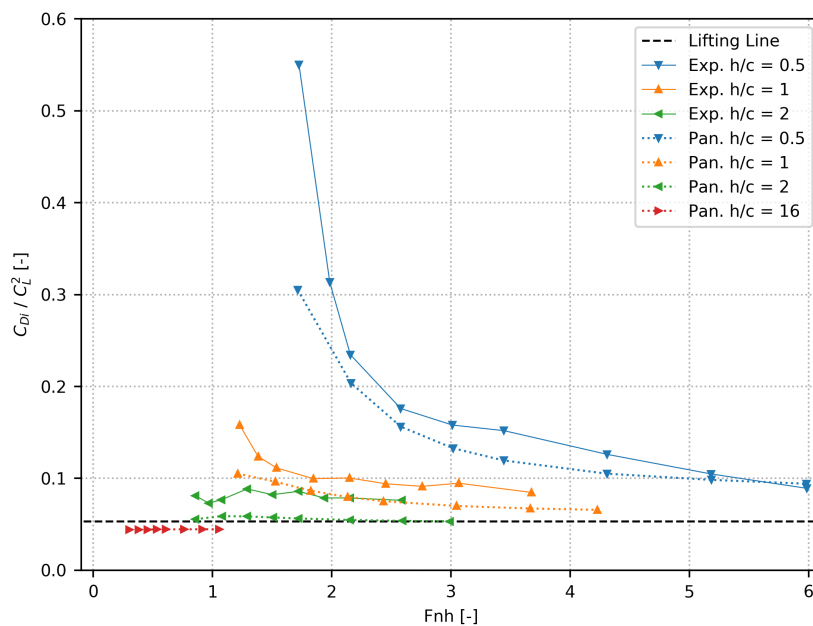

Figure 4.4: Results of Panship and experiments [27] for the C_{Di}/C_L^2-curve for an angle of attack of 4°, the results for an elliptical lift distribution in an analytic lifting line method are shown as well.

$$\frac{C_{Di}}{C_L^2} = \frac{1}{\pi AR} \tag{4.2}$$

For the simulations in Panship, a value for FAKTWE, influencing the length of the first wake panel, of 10 is used and, as described in the previous section, a further increase did not lead to different results.

In general, it can be said that the results of Panship show the same trends as the experiments, but there are clear differences. The results of Panship for $h/c = 0.5$ are in good agreement with the experimental results but are slightly lower. The difference is the highest for the lowest Froude submergence number Fn_h. For the submergence of $h/c = 1$ and 2 the results are lower than the experimental results over the entire used range of Fn_h as well. Comparing the results for $h/c = 16$, where all free surface effects are negligible, to the analytic lifting line results (4.2) it can be seen that the results of Panship are slightly lower.

Based on these results it can be said that the C_{Di}-C_L^2-curve determined in Panship is different for all submergences h/c compared to the experimental results and (4.2). The differences, logically, may arise from two origins: the results of Panship may be underpredicted and the results of the experiments and (4.2) may be overpredicted. Reasons for both origins and a conclusion will be given now.

Panship
The underprediction of the C_{Di}/C_L^2-curves in Panship may arise from five different origins: the used history in the free surface part of the Green function NHIST, the wake model, the linearization of the free surface boundary condition, the lack of viscosity and the discretisation of the foil.

For the used history in the free surface Green function and the length of the wake sheet is made sure that a further increase does not improve the results. This should not play a role here. Also by adjusting the angle of the first part of the wake sheet α, see figure 3.13, to 0,° instead of 4°, such that the wake sheet flows with the free stream, did not give an improvement of the result. The linearization of the free surface boundary condition may play a role but it would be expected that it would induce more errors closer to the free surface, which is not the case here. The lack of viscosity in Panship influences the results here as well. As viscosity leads to a reduction in lift curve slope, the lift in Panship is overpredicted. This might lead to an under prediction of the C_{Di}/C_L^2-curve.

As shown in sections 3.3 and 4.5, the results of Panship can be influenced severely by the discretization of the foil and wake and the used history in the free surface Green function. The underprediction may be a result of the lack of panels in spanwise direction as for the calculations only $N = 140$ is used, to decrease computational requirements. Figure B.3 shows the convergence for N and M on C_{Di}/C_L^2. The result of (4.2) is shown as well, such that an easy comparison can be made with figure 4.4. The figure shows that by increasing the number of spanwise elements from $N = 140$ to $N = 240$, an increase of 3% is obtained and it seems that the solution is not fully converged yet. However, it can be seen that the convergence is very slow and the converged solution cannot be reached due to limits in the available memory.

In the late stage of this thesis, a new method to compute the induced drag is introduced in Panship. This method uses a Trefftz plane, as introduced in [22]. This method determines the induced drag in the wake of the foil as it is the only disturbance if the control volume is chosen correctly. Therefore this method is less susceptible for the orientations of the panels at the leading edge to determine the drag. The computations of this method give a higher value of induced drag and the C_{Di}/C_L^2-ratio is very similar of that of the result of the analytic lift line. Unfortunately this method can currently only be used for deeply submerged foils without free surface effects.

Experimental results and lifting line
The possible underpediction of the lifting line and the experimental results can arise from two origins: the lack of thickness effects in the lifting line model and a wrong prediction of viscous drag in the experimental results.

First, the difference between the results of an elliptical lift distribution in an analytic lifting line method (4.2) and Panship can be explained by the fact that in the lifting line method only the effect of the planform area

on lift and drag is included and the effect of the camber and thickness of the foil are neglected, whereas it is included in Panship. For the effect of thickness on induced drag and lift it is shown that it can influence the C_{Di}/C_L^2-curve where it is increased by decreasing thickness [18]. The same is seen in Panship, decreasing the thickness leads to an increase in C_{Di}/C_L^2. Therefore the results of the analytic lifting line might give a too high value of C_{Di}/C_L^2.

Second, as described in section 4.1, the induced drag is calculated by subtracting the estimated viscous drag from the total drag as it cannot be measured directly from the experiments. A wrong estimation of viscous drag can easily lead to a wrongly calculated induced drag. Therefore, the difference between the experimental results and result of Panship may arise due to an overprediction of induced drag from the experimental data.

The first argument plays a role here as well since the same experimental results have been used in [25] to check if the same free surface Green function G in Hydvlm was implemented correctly. In this work the agreement between the experimental results and numerical results was good for the submergences of h/c = 2 and 4 and in lesser extent for the shallower submergences. In the same work it was mentioned that the outer most singularities are smaller to leave a free tip width such that convergence was faster. In this way the aspect ratio is smaller and an overprediction of induced drag may arise. The numerical results of the VLM are influenced by the lack of thickness as well, which also leads to an overprediction of C_{Di}/C_L^2. As the VLM may contain an overprediction of C_{Di}/C_L^2, the experimental results also may contain an overprediction of C_{Di}/C_L^2.

Conclusion
Based on the discussion in the two previous sections, it can be concluded that the prediction of lift induced drag is difficult in both numerical solvers and experiments. There are indications that the C_{Di}/C_L^2-curve is overpredicted in the experiments and therefore these results should be used with care. In Panship a detailed discretization is required to avoid discretization errors in the induced drag. Interesting is that in previous work in Panship the predicted C_{Di}/C_L^2-curve was higher but it might be possible that these results were influenced by a lack of panel density or use of different input parameters. A new method to determine the induced drag in Panship gives results much better agreement with the analytic lifting line results and therefore the current results of Panship should be used with great care.

4.7. Comparing Panship to Refresco and the LLXM

The results of Panship are compared to the results of the (viscous) Reynolds-averaged Navier-Stokes (RANS) solver Refresco and the Lifting Line - XFoil Method (LLXM) to compare their quality of results. The simulations are performed on the same foil of the Waszp sailer used in the previous chapter.

The lift and total drag are calculated in Panship for angles of attack of 0° to 20° can be seen in figures 4.5 and 4.6 for submergences of 0.8 and 1.5 chords. The same figures show the results for Refresco for angles of attack of 4.35° to 19.35° and the inviscid and the viscous results of the LLXM. The inviscid solution of the LLXM is added to the plot to make an easy comparison with figure 3.26 such that it can easily be seen that the Panship results are influenced by the free surface as in the LLXM no effect of a free surface is present in the solution.

It is assumed that the free surface does not influence the behavior of the parameters studied in section 3.3, except for the length of the first wake panel. Therefore, the same values for simulation length t, side paneling n_{side}, angle of the first part of the wake α and length of the first part of the wake DWMXA are used. The same discretization, a number of spanwise panels of M = 20 and a number of chordwise panels of N = 240, as in section 3.5 for a deeply submerged foil is used. As determined in section 4.3, and verified here again, 100 time steps in the history NHIST where enough.

Figure 4.5 shows that the lift determined in Panship is overpredicted severely when comparing to the results of Refresco. At the angle of attack of 19.35° it can be seen that the results of Refresco have reached the point where the separation starts and the lift is reduced. This reduction cannot be seen in Panship as viscosity is neglected in potential flow and separation does not occur. As described in section 3.5 the viscosity influences the results severely, especially for a foil with a high trailing edge angle, therefore the lack of viscosity results in an overprediction of lift. The overprediction is approximately the same as for the deeply submerged foil in section 3.5, approximately 70 %, which is expected for a foil with a trailing edge closure angle of 25° [16].
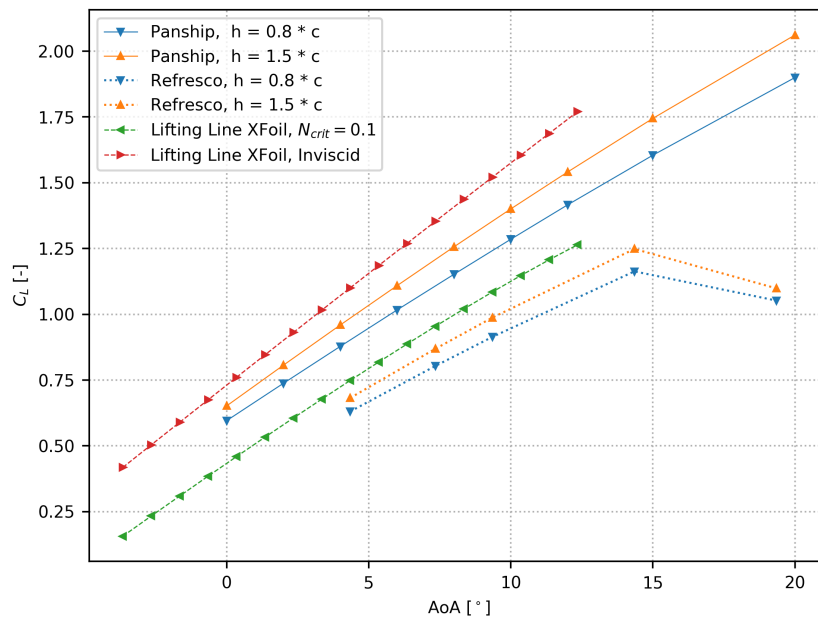
Figure 4.5: Lift in Panship, Refresco and the LLXM for different angles of attack.

The effect of submergence is slightly higher for the lift determined in Panship. Whereas the reduction for a shallower submergence in Refresco is 93%, the reduction in Panship is 90%. The lift curve slope is lower for the results of Refresco results, but it should be noted that the results of Refresco are not fully linear yet and therefore the lift curve slope could be in agreement for lower angles of attack. For the solutions of both Refresco and Panship it can be seen that the lift curve slope is influenced by the submergence, where a deeper submergence leads to a steeper lift curve slope and an increase in lift.

The drag in Panship is determined using the induced drag determined by the panel code, and the viscous drag, determined using the ITTC '57 convention frictional correlation line, described in section 2.6.7. This viscous drag is constant for all angles of attack at $C_{D,v} = 0.014$ and in the plot can be seen that the induced drag is reaching zero as the zero lift angle is reached in figure 4.5 and the value of $C_{D,v} = 0.014$ is subtracted from C_D.

In figure 4.6 it can be seen that the drag determined in Panship shows a different trend for increased submergence than in Refresco. With increasing submergence the drag in Panship is, as expected, reduced where in Refresco the drag is increased. As described in section 2.2 the lift of a foil closer to the free surface is expected to decrease, but on the contrary the induced drag is expected to decrease. The origin of the problem should be in Refresco but the exact source is unknown. A possible explanation could be that the reduction in induced drag is higher than the increase of wave making drag. The influence of the submergence is much smaller on drag than on lift in both the calculations in Refresco and Panship. The same is seen in section 3.5, an overprediction of drag due to the overprediction of lift resultant of inviscid effects, leading to an overprediction of induced drag.

Comparing both the results of the LLXM to the results of Panship and Refresco, it can be seen that the lack of free surface effects in the solution leads to an overprediction of lift and an underprediction of drag but the same trends are followed. However, in this specific situation the inclusion of viscous effects leads to a better prediction of lift and drag than the inclusion of the effects of the free surface.
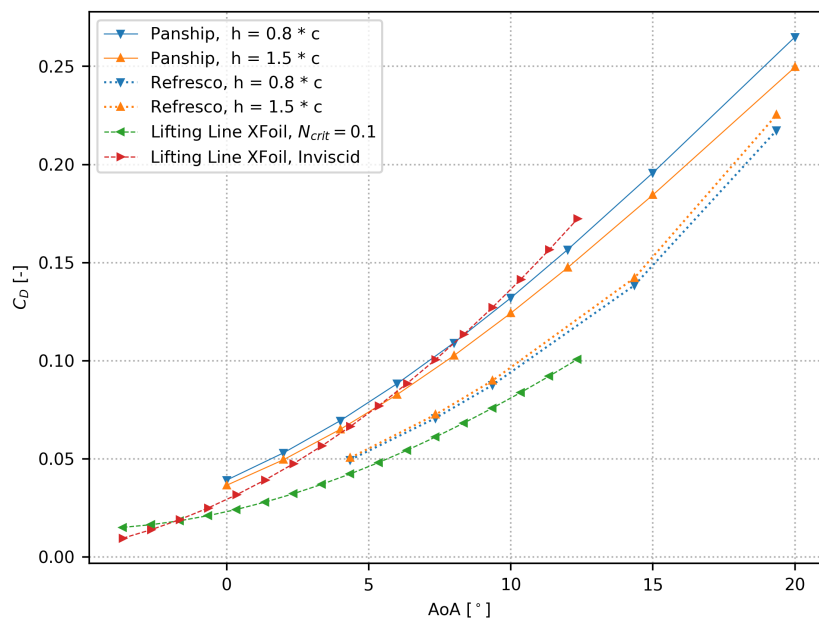
Figure 4.6: Drag in Panship, Refresco and the LLXM for different angles of attack.

4.8. Conclusion

An answer can be formulated to the subquestion provided at the beginning of this chapter. This subquestion is:

> *What is the quality of results for the hydrodynamical forces for a foil near the free surface in Panship in calm water with a constant forward speed?*

Comparing the results of Panship to experimental results it can be seen that the C_{Di}/C_L^2-curve in Panship is lower in all cases but the same trends are seen. The difference in results might have multiple explanations. First, it is proved to be difficult to determine the induced drag in numerical methods as it is highly dependent on the discretization of the foil and its wake. Second, it is difficult to determine the induced drag in experiments as it cannot be measured directly but is obtained by subtracting the empirical viscous drag from the total drag. An overprediction of viscous drag can easily lead to an underprediction of induced drag. There are signs that indeed the induced drag is overpredicted in the experimental results. In the conclusion of chapter 3 it is stated that the results for induced drag should be used with care. The results of this chapter underscribe this. Especially as a new experimental method, implemented in Panship in the late stage of this thesis, is able to predict the induced drag in much better agreement with the analytic lifting line results. The quality of the results of Panship of a foil near the free surface is poorer than for deeply submerged foils.

If the results of Panship are compared to Refresco, the same overprediction of lift and drag can be seen for the results of Panship as in 3 as for the used foil the viscosity plays an important role. Panship and Refresco show the same trends for lift as the submergence is decreased. However, in Refresco different trends than expected are seen for increased submergence for drag. The LLXM is able to predict the lift and drag better than Panship for a foil with a large viscous effect on lift. For these foils it is more important to include the effects of viscosity than the effects of a free surface.

As introduced in section 2.4, the influence of the hull on the forward foil is very small and therefore the quality of the results of a single foil near the free surface is very similar to the quality of the results of the forward foil. Since the induced drag forms the total drag with the viscous drag, the underprediction of induced drag means

that the total drag of the forward foil will be underpredicted and thus the contribution of the total drag of the forward foil to the total drag of the foil system is too low.

5

Interaction between two foils

After the inclusion of the free surface effects in the previous chapter, in the current chapter the effects of foil interaction are included in the solution and again complexity is added to the problem. As introduced in section 2.3 the wake of a leading foil influences the performance of the trailing foil. The effect of the leading foil can be positive or negative, meaning an increase in lift and reduction in drag or a decrease in lift and increase in drag. In this chapter it is investigated if Panship is able to correctly predict the effects of foil interaction. This chapter gives an answer to the question:

> *What is the quality of the results for the hydrodynamical forces for two foils towed behind each other in Panship in calm water with a constant forward speed, and how does this compare to the results of Hydvlm?*

An answer to this question is provided by comparing the results of Panship to experimental results and two numerical models: the LLXM and Hydvlm. In the experiments two box foils are towed near the free surface. The box foils consist of a foil and three struts of which two are place at the sides of the foil and one in the middle. The goal of this chapter is to use the same configuration as in the experiments in Panship but first the complexity of the problem is reduced by removing the free surface and the struts.

First the LLXM is used to compare the results for foil interaction in Panship to in a controllable environment, without the effects of the free surface. The free surface is excluded from the solution with the same procedure as in chapter 3. Second, the results of Panship are compared to Hydvlm and experimental results to study the behavior for foil interaction near the free surface while neglecting the struts. Third, the struts are introduced to get the same configuration as in the experiments.

At last a study is performed to see if the results of Panship can be improved by using different discretisation of the wake such as determined in chapter 3. However, the foil interaction in the experiments, Hydvlm and the LLXM will be introduced first before the results of Panship can be treated.

This chapter contains the following structure. In this chapter first the used experimental results are described in section 5.1 followed by the results of Hydvlm in 5.2. Third, the foil interaction in the LLXM are treated in section 5.3. Fourth, the foil interaction of two deeply submerged foils in Panship is discussed in section 5.4. Fifth foil interaction of two foils near the free surface is treated in section 5.5 where the influence of the strut is first excluded from the solution and then introduced. At last a conclusion is drawn.

5.1. Experimental data

Experiments to test the effects of foil interaction near a free surface have been performed by Morch in. In that experimental research two different foil configurations where tested. Configuration 1 consisted of two box foils in tandem arrangement whereas configuration 2 consisted of two T-foils up front and a box foil at the rear [19]. In this chapter only configuration 1 is used as the effects of foil interaction in configuration 2 where low.

In the experiments the effects of increasing the distance between the leading and trailing foil for submergences of $h/c = 1.575$ and $h/c = 0.750$ and forward velocities of 3.45 and 5.167 m/s are determined, using a NACA 16-0075 thickness profile with a NACA a = 0.8 mean line. The used foil spacings are 6, 12, 24 and 36 chords.

5.2. Foil interaction in Hydvlm

The experiments described in 5.1 were used by van Walree to validate the foil interaction of the Vortex Lattice Method (VLM) Hydvlm [25]. In this work the foil was interpreted as a NACA 16-008 thickness distribution, instead of a NACA 16-0075 thickness distribution, with a modified NACA a = 0.8 camber.

The differences between the thickness distributions is accounted for by dividing the lift and drag of the trailing foil with influences of the leading foil (C_{Laf} and C_{Daf}) by the lift or drag of the trailing foil without the influences of the leading foil (C_{La} and C_{Da}), as introduced in (2.8). In this way the numerical results can be compared to the experimental result while using a foil with a slightly different thickness distribution. The relations are given here again:

$$C_{Lr} = \frac{C_{Laf}}{C_{La}}$$
$$C_{Dr} = \frac{C_{Daf}}{C_{Da}}$$

(2.8)

The span and chord of the foil are 0.81 and 0.1 m respectively, leading to an aspect ratio AR of 8.1. As this foil has a lift coefficient C_L of 0.3, using equation 2.6 shows that the wake has rolls up very slowly and is rolled up at a distance of 32 chords behind the forward foil.

In the computations in Hydvlm a total of 80 span wise vortex elements M and 4 chord wise elements N are used and for viscous effects on lift can be corrected empirically as in equation 2.56 by means of a viscous reduction factor f_α. A comparison of the lift curve slope determined Hydvlm to the lift curve slope determined by the experiments showed that the lift curve slope in Hydvlm was too low due to viscosity effects. Reducing the effects of viscosity, and thus increasing the reduction factor f_α from 0.91 to 0.97 led to match with the experimental results. Therefore, it can be concluded that almost no viscous effects are present in this situation [25].

The results of the Vortex Lattice Method (VLM) are in good agreement with the results of the experiments and will be plotted with the results of Panship such that the results of Panship can easily be compared to.

5.3. Foil interaction in the LLXM

The Lifting Line - XFoil Method (LLXM) is suitable for use with two foils by extending the influence matrix with three submatrices (2.65) resulting in the model seen in figure 2.7. To perform the calculations, 300 span wise elements M and 1000 iterations where used. As can be seen in figure 5.1 the 1000 iterations where enough to reach a stable condition of for induced velocities on both the leading and the trailing foil. The induced velocities at the foil tips reach a stable condition very fast but the induced velocities at the foil tips take longer. The induced velocities at the foil tip of the trailing foil take the most steps to reach a stable

condition. The same foil as in Hydvlm is used: a foil with a NACA 16-008 thickness distribution and a NACA a = 0.8 mean line.

The resulting lift distributions of the leading and trailing foil can be seen in figure 5.2 where the trailing foil shows the influence of the downwash resultant of the wake of the leading foil. The results for the interaction coefficients C_{Lr} and C_{Dr} of the inviscid and viscous LLXM for increasing foil spacing can be seen in figure 5.3. As the wake of the forward foil goes straight into the trailing foil and it is not corrected with a wake angle α, as in figure 3.13, the C_{Lr} and C_{Dr} are almost constant for increased foil spacing. A very small increase of C_{Lr} and C_{Dr} can be seen for the lowest foil spacing due to the increase of the total force vector. This effect can barely be seen here and is explained into more detail for the results of Panship.

By adding viscous effects in the lift ratio C_{Lr} increases by 18 % and the drag ratio C_{Dr} decreases by 22 %. For the foil velocities of 3.45 and 5.17 m/s the inviscid solution was the same, however for the viscid solution a small decrease in C_{Lr} is seen and a smaller increase in C_{Dr} is seen.
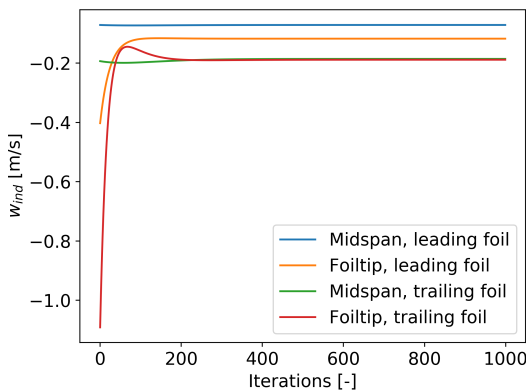

Figure 5.1: Convergence for induced velocities on midspan and the foil tip of the leading and trailing foil
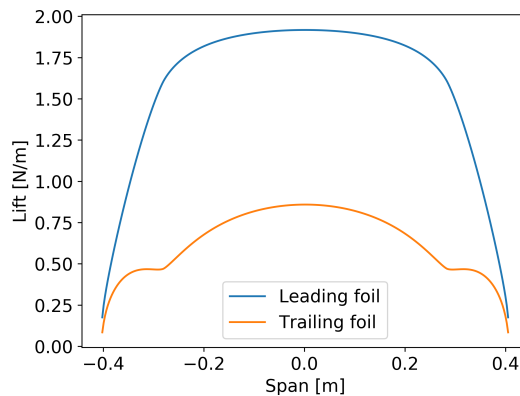

Figure 5.2: Lift distribution on the leading and trailing foil

5.4. Foil interaction in Panship without a free surface

In this section the effect of foil interaction is studied for deeply submerged foils to create a controllable environment and to be able to perform fast calculations without the free surface part of the Green function G^f. In this case the results of Panship can be compared to the results of the LLXM as it also does not contain free
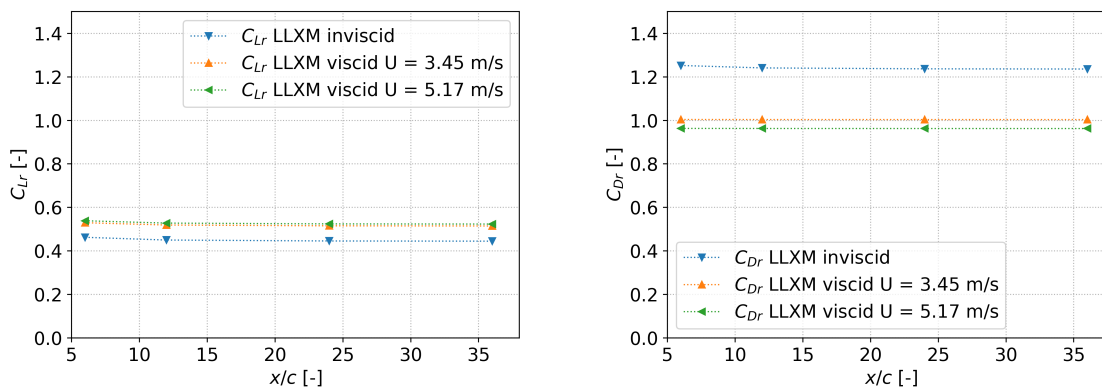

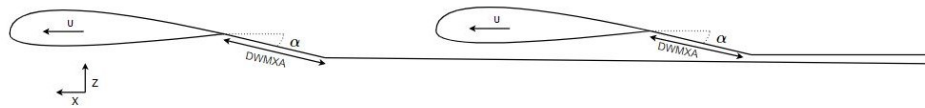Figure 5.3: Effect of increasing foil spacing on C_{Lr} and C_{Dr} for the LLXM

Figure 5.4: Schematical representation of important parameters for foil interaction in Panship.

surface effects. Just as in Hydvlm and the LLXM a foil with a NACA 16-008 thickness distribution and a NACA a = 0.8 mean line is used in Panship instead of the original thickness distribution.

A representation of important parameters for foil-foil interaction can be seen in figure 5.4. This figure is an extension of figure 3.13 where the parameters angle of the second part of the wake β and the length of the first part of the wake DWMXA are left out. The values of these parameters are discussed in section 3.3, resulting in β should be zero such that the wake moves with the uniform flow in the far field. The length of the second part of the wake DWMXB should be long enough, such that the wake sheet ends in the far field. FAKTWE is taken long enough, in this case FAKTWE = 2.5 is used and a further increase did not give a change in solution.

Furthermore, angle of the first part of the wake α is specified by the Kutta condition, where the flow should leave the trailing edge smoothly. The length of the first part of the wake DWMXA is given by (2.6) where the wake moves with the free stream after it is fully rolled up at length e.

For a deeply submerged foil in Panship the same trends should be seen as for the inviscid solution of the Lifting Line - XFoil Method (LLXM) as the free surface effects are excluded from the solution. In figure 5.5 the interaction coefficients for lift and drag C_{Lr} and C_{Dr} for both models are plotted versus the foil spacing x in chords c. To obtain the results in Panship values of 0 and 32 chords for DWMXA are used, such that the wake sheet translates with the free stream when it leaves the foil just as in the LLXM, and such that the wake sheet translates with the free stream as it should be fully rolled up. The struts are neglected in both the solution of the LLXM and Panship. In Panship for each foil 20 spanwise panels M are used and 120 chordwise panels N are used. Using a more detailed discretization of the foil did not lead to an improvement of the solution for lift and only to a very small improvement of the solution for drag.

Figure 5.5 shows that C_{Lr} determined in Panship using DWMXA = 0 is in agreement with the LLXM where C_{Lr} is slightly lower in the LLXM for the three highest foil spacing. Therefore, the reduction of lift in the LLXM is slightly higher. A slight offset from the results of the LLXM results are seen in Panship at the shortest foil spacing. This slight increase is result of the influence of the forward foil and not the wake as the influence of the wake remains constant at increased foil spacing. Therefore, two things can be concluded. The first is that the forward foil, not the wake, has more influence on the results in the Panship and the second is that the forward foil, again not the wake, has a positive influence on the lift generated by the trailing foil.

In figure 5.5 it can be seen that the result of C_{Dr} of Panship with the wake sheet going straight out of the leading foil does not agree with the result of the LLXM. Whereas the LLXM gives an increase of 1.22 of C_{Dr} for the three larger foil spacings including a forward foil, the results of Panship show an increase of 1.43 of C_{Dr}. This can be explained by the fact that the induced drag is severely dependent on the angle of the total force vector. As the induced drag is the cosine of the total force vector and the lift is the sine, a small change in the angle of the total force vector influences the induced drag severely, whereas the effect of lift is smaller. Therefore, a small change in the prediction of the downwash might lead to a large change in induced drag. Just as for C_{Lr}, the results of Panship show an increase in C_{Dr} for the smallest foil spacing. Since both the lift and drag increase the total force vector should have been increased, affecting both the lift and the induced drag. This can be explained by a change in angle of attack due to the flow being curved by the forward foil.

Figure 5.5 shows the results of Panship with DWMXA = 32c as well. This figure shows that as the wake sheet translates with the free stream as the wake should be fully rolled up and the wake sheet is located further
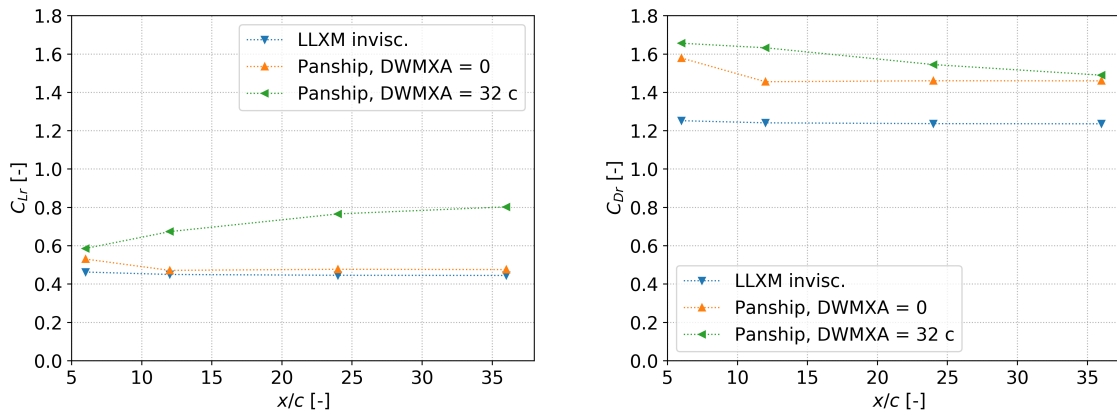
Figure 5.5: C_{Lr} and C_{Dr} for increasing foil spacing for two deeply submerged foils in Panship and the LLXM

away from the trailing foil, C_{Lr} increases. The figure shows that C_{Dr} increases as well, meaning that the total force vector has increased here as well. As the wake sheet is impenetrable, the flow on the wake sheet should be perpendicular to the wake sheet could stir the flow over the trailing foil, resulting in a change in angle of attack affecting both the lift and drag. As the influence of the wake sheet is lower for larger foil spacing, C_{Lr} increases further for larger foil spacing and C_{Dr} is reduced.

5.5. Foils in the proximity of the free surface

Experimental results show that the foil interaction of foils of a hydrofoil vessel highly depend on free surface effects. Therefore, in the free surface part of the Green function G^f is switched on and the foils are placed at the same distance from the free surface as in the experiments. First the results of Panship without struts are used after which the results of Panship with a strut are used to see if the presence of the struts improves the solution. At last the influence of the shape of the wake sheet is determined. In all calculations a NACA 16-008 thickness distribution and a NACA a = 0.8 mean line is used instead of the original thickness distribution.

5.5.1. Foil interaction without struts

In figure 5.7 the foil interaction without struts in Panship is compared to the results of Hydvlm and experiments. The results show a fair agreement for the effect of foil interaction on lift, but the agreement for drag is in much lesser agreement. The simulations have been performed using $M = 20$ and $N = 120$. Increasing the quality of the discretization did not improve the results significantly but increased computational requirements severely, just as described earlier for the deeply submerged foil interaction.

The results for lift are in variable agreement with the results of Hydvlm and experiments. The results for the lowest velocity of $U = 3.45$ m/s, figures 5.7a and 5.7e, are not in agreement for the largest foil spacing for the submergence of $h/c = 0.75$ and for the three largest foil spacing for the submergence of $h/c = 1.575$. However, in both cases the trends seem to be determined correctly. For the velocity of $U = 5.17$ m/s, figures 5.7c and 5.7g, the trends with increasing foil spacing are predicted more correctly and only the smallest foil spacing shows a small deviation of the results.

The results for drag, figures 5.7b, 5.7f, 5.7d and 5.7h, only show the global trends correct for increased foil spacing. The best agreement can be seen for the results for $U = 5.17$ m/s but it seems difficult to predict the reduction or increase in drag correctly. As can be seen in the results of Hydvlm it was difficult to predict the effects of foil interaction correctly as a bigger offset than for lift can be seen for those results. Panship seems to have difficulties in predicting the reduction or increase in drag due to the wake of a leading foil.
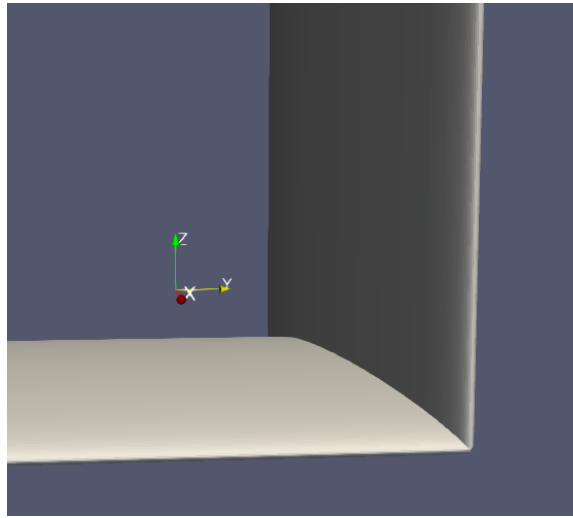
Figure 5.6: The connection between the foil and the strut

As the induced drag is sensitive to the generated downwash, the results might be improved if the effect of the struts is taken into account. Therefore, in the next section the struts are added to the solution of Panship.

5.5.2. Foil interaction with struts

The solution of Panship can be improved by adding a strut to the model. In order to do so, the right connection should be used. Three different connections have been used and only one was able to represent the problem correctly. In the first configuration the strut was not connected with the foil. This lead to a discontinuous pressure distribution between the foil and the strut and the resulting lift and drag were not correct. The second configuration, where the connection was a line of zero thickness, did not give a solution in Panship as the singularities were too close to each other. The third configuration was such that the ending of the inner side of the strut is exactly the same as the ending of the upper side of the foil, see figure 5.6. This was the only connection that gave favorable results and a continuous pressure distribution. Due to limitations in the generator of the mesh it was only possible to use the same amount of panels over the height of the strut as on the width of the foil leading to a very high density of panels over the height of the strut. This lead to unfavorable long time simulations but it is verified that it did not influence the results as the same results were obtained with a lower density of panels on the strut.
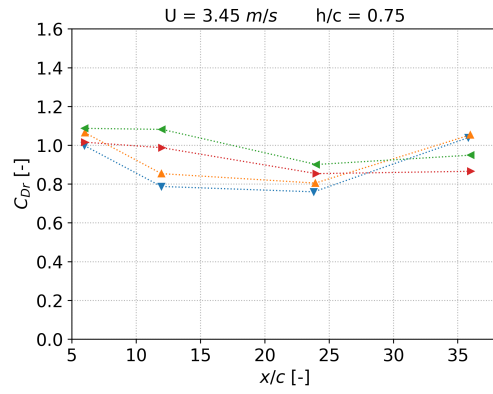
The results for foil interaction with the inclusion of a strut can be seen in the same figures as the results of Panship without the inclusion of a strut. The effect of adding a strut to the solution has a very small influence on the results for lift. The effect of adding a strut are the biggest on the velocity of $U = 3.45 \ m/s$ but negligible on the velocity of $U = 5.17 \ m/s$.

For the lowest velocity the solution is slightly improved for some foil spacings but for other foil spacings the solution is poorer. Especially for the biggest foil spacing the solution is not necessary improved as for the submergence of $h/c = 1.575$ the solution is poorer and for the submergence of $h/c = 0.75$ the solution is better.
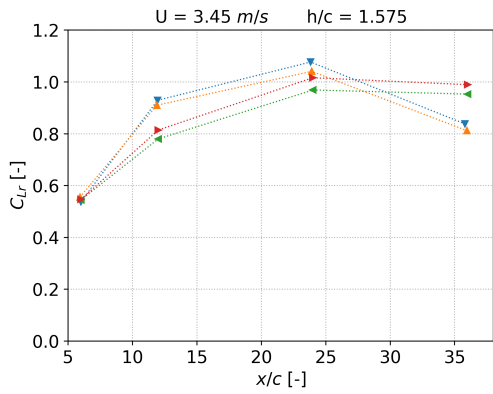
The solution for drag is improved, especially for the velocity $U = 3.45 \ m/s$ where the agreement with the experimental results and Hydvlm is better. For all configurations not exact the same trends are seen as in the experiment and Hydvlm, but the expected order of magnitude and global trends can be seen.
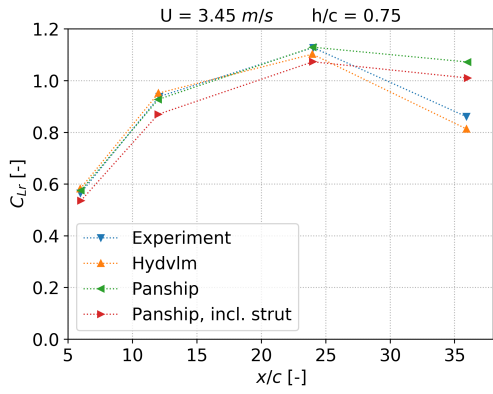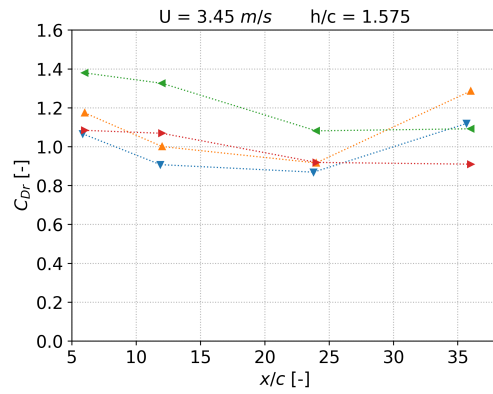
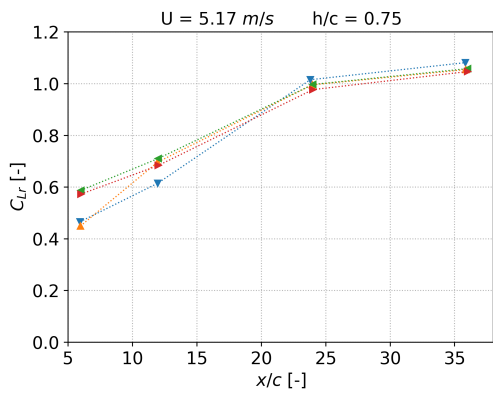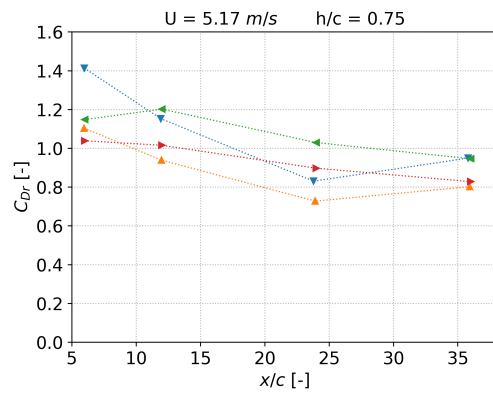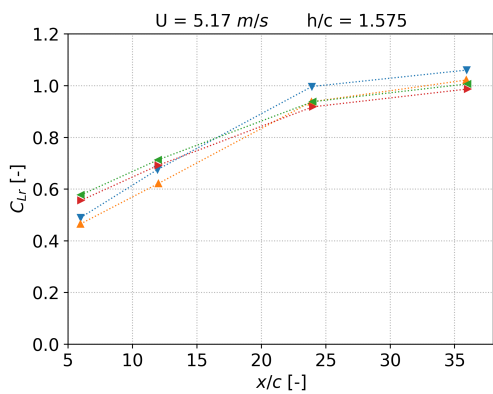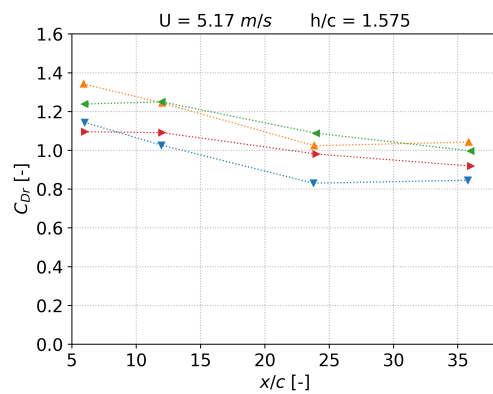Figure 5.7: Foil interaction in Panship, Hydvlm [25] and experiments [19]

5.5.3. Influence of shape of the wake on foil interaction in Panship

The influence of the shape of the wake in Panship on the results for foil interaction is tested by using different angles of the first part of the wake α for the forward foil. By changing α the wake of the forward foil is placed further or closer away from the trailing foil as a long enough length of the first part of the wakesheet DWMXA is used, as can be seen in figure 5.4. Additional to the α used earlier, one such that the wake leaves the trailing edge smoothly, 8°, the angles 0°, 4° and 12° are used. The results of the simulations with other values of α do not show better agreement with the experimental results and Hydvlm than the original results and they are not used furthermore.

5.6. Conclusion

Now the question given at the beginning of this chapter can be answered:

> *What is the quality of the results for the hydrodynamical forces for two foils towed behind each other in Panship in calm water with a constant forward speed, and how does this compare to the results of Hydvlm?*

The results of the LLXM and of Panship for two deeply submerged foils with a wake sheet flowing with the free stream show fair agreement for foil interaction for lift. The agreement for drag is less good, which indicates that both models do not predict the same downwash of the total force.

The foil interaction in Panship shows the same trends for lift for increasing foil spacing as the experiments and Hydvlm, but for some foil spacings Panship has a different result. The differences between the results of Panship, the experimental results and the results of Hydvlm for lift can be result of the lack of viscosity effects in Panship. The zero lift angle and lift curve slope in Hydvlm are corrected for viscous effects and as the results of Hydvlm are in better agreement with the results of the experiment this could play an important role. The results for foil interaction are slightly influenced by the adding struts, but in general, the effect is small.

The results foil interaction for drag show poorer agreement with the experimental results. In chapters 3 and 4 is showed that it is difficult to predict the induced drag of a foil in Panship and this can be seen here as well. The results for drag show the same order of magnitude as the experimental results and Hydvlm and the global trends can be seen more or less. Adding a strut has an effect on the solution by improving the results. The results for foil interaction for drag might be improved with the implementation of the Trefftz plane as introduced in section 4.8.

In general, it can be said that the quality of the results for foil interaction for lift in Panship are good, but are poorer for drag. The results in Hydvlm are of better quality for lift but in Hydvlm it is difficult to determine the drag correctly as well, but the trends are predicted better than in Panship. This means that the lift of the second foil and its contribution to the total lift force determined during the take off in Panship will be predicted fairly well and can for instance be used for optimization of foil spacing. However, the contribution of the drag of the second foil to the drag of the total system will contain extra errors in addition to the errors determined in chapter 4.8.

6

Takeoff in Panship

After studying the effects of foil interaction in the last stage of the validation process the interaction between the hull and the foil system during the takeoff of hydrofoil vessel is studied. During the takeoff, the hydrofoil vessel performs the transition from being hullborne to being foilborne to reduce its resistance. In this chapter the quality of the results during the takeoff of a hydrofoil vessel are studied. The interaction between the hull and the foil system is important if the lift and drag of a hydrofoil vessel is considered during the takeoff as the presence of the hull influences the performance of the foil system and vice versa. This interaction between the hull and the foil system is introduced in section 2.4.

This chapter gives an answer to the subquestion:

> *What is the quality of the results for the hydrodynamical forces of a foil and ship system in Panship during the takeoff in calm water, and how does this compare to the results in Hydres?*

To give an answer to the research question the results of Panship are compared to the results of Hydres and experiments. The results of the experiments are used to compare the results of Panship to but the results of Hydres are mainly used to assess the quality of the results of Hydres and not to directly compare the results of Panship to. The quality of the results of Panship is assessed by comparing the determined drag in Panship to the determined drag in the experiments and by comparing the predicted lift in Panship to the expected lift based on the deadweight of the vessel. Furthermore, to find the source of the differences between Panship and the experimental results, different discretisations of the wake are used in the calculations in Panship. At last, to see if the expected interaction between the hull and the foils is seen, interaction effects are studied.

The experiments, obtained in the early 90s, have been performed at constant speed and therefore the takeoff has not been performed in one single run. In Panship the same is done to be able to compare the results of Panship to the experimental results. It should be possible to perform the takeoff in Panship in one run in the near future, but it has not been done here as it is not possible yet.

The structure of this chapter is as follows. First the experimental results are introduced in section 6.1 followed by an introduction of the results of Hydres in section 6.2. The results of Panship are described in section 6.3 for the resistance and lift during the takeoff and the interaction between the foil and the hull. Last, a conclusion is drawn in section 6.4.

6.1. Experimental data

In Maritime Research Institute Netherlands (MARIN) experimental results for the takeoff of a hydrofoil vessel with an inversed TT-shaped foil are available. The same experimental results have been used to validate the
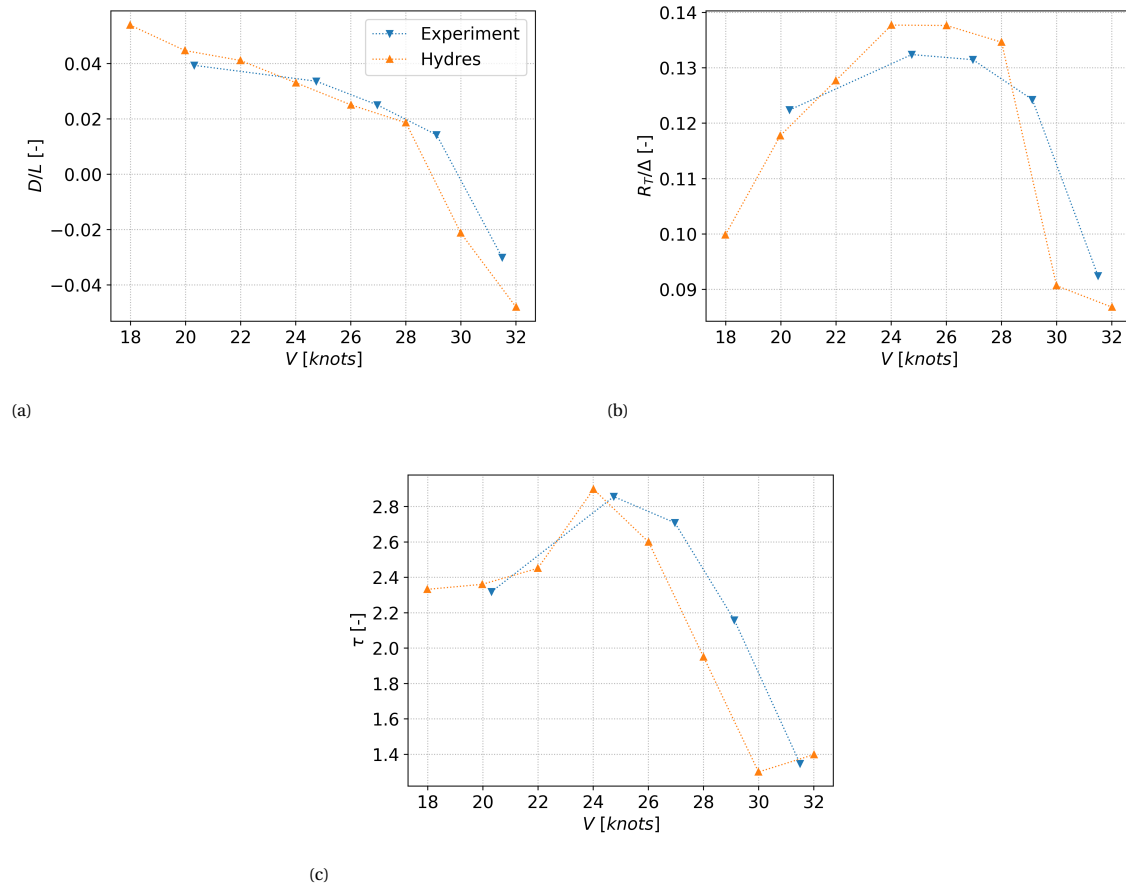
(a)

(b)

(c)

Figure 6.1: Results of Hydres and experiments for the takeoff of a hydrofoil vessel [25]

code Hydres, in which it is possible to perform a takeoff [25]. In the current research, the experimental results scaled to full scale are used of which the flap angles and angles of attack are scaled as well.

During the experiments, only the center flaps of the leading and trailing foil were adjusted and no active flap control was applied. The width of the forward foil is smaller than the width of the leading foil and the chord of the forward foil is 7/9 of that of the trailing foil. The depth of both foils is at least 2.8 chords in the experiments, meaning that the effects of the free surface on the foils are small, but are present. The shape of the struts of the leading foil are reversed V-shaped and the struts of the trailing foil are box shaped. The angle of attack of the leading foil is 0.6° and the angle of attack of the trailing foil is 0.8°. The flap angles are respectively 9.1° and 1.8°.

6.2. Results of Hydres

The results of Hydres and experiments are published in [25] and are given in figure 6.1 for draft D, total resistance R_T and trim τ. The experiments show that the takeoff is predicted too early, which can be seen in the reduction in the resistance and draft between 28 and 30 knots. The results for draft are in very good agreement with the experimental results before the takeoff, after the takeoff the draft is lower than the experimental results, which means that the lift is overpredicted. The resistance is overpredicted before the takeoff and, due to the too early takeoff, underpredicted after the takeoff. The predicted trim is too low for higher velocities than 24 knots, which may be a result of the too early takeoff [25]. The results of Hydres contain a correction for hull-foil interaction but the effect of hull-foil interaction was small [25].
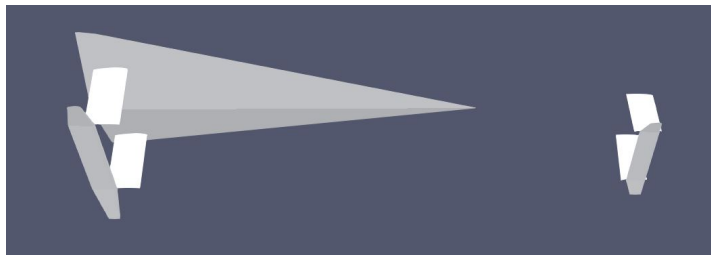
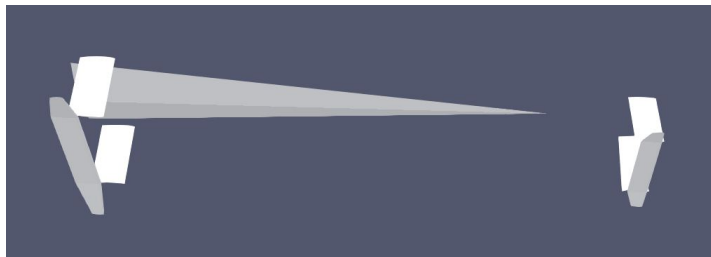Figure 6.2: The submerged hull and foil system at 22.5 knots

Figure 6.3: The submerged hull and foil system at 27 knots

6.3. Results of Panship

Since Panship is not able to determine the equilibrium positions of the hull and foil system itself, the results of the experiments are used to as input for the trim and draft at the given velocity. In order to do so, it is assumed that the accelerations during the takeoff are small and their influence on the results is small.

The experiments were performed in the early 90's and the model is not in the possession of Marin since it was not possible to store it. No 3D-scans are available, thus the exact geometry has to be obtained from available drawings. Based on information of the provided drawings, the complete foil system is discretized with exception of the cigar shaped nacelles at the connections between the foils and the struts. As it is not possible to generate the exact hull shape in the available time based on drawings, it is decided to approximate the hull shape using a constant deadrise over the entire length of the hull. This approximation is only valid during the last part of the takeoff, which contains three data points in the experiments. These data points are the velocities 22.5, 24.7 and 27.0 knots. The resulting geometries can be seen in figures 6.2 and 6.3 at the first data point and the last data point. The geometry only contains the underwater parts of the hull and foil system with respect to the undisturbed water level.

The input for the foil system is based on the conclusions of the previous chapters. The length of the first wake panel l_{w1} is chosen long enough and the shape of the wake is initially based on the roll up and Kutta condition. The length of the first part of the wakesheet, DWMXA, is 7 meters for the leading foil, such that it is rolled up if the wake has passed 33% of the vessel. The length of DWMXA for the trailing foil is slightly longer and is 9 meters. The pressure on the hull is corrected with a transom stern model and the paneling on the hull is such that the solution did not improve for a denser grid. A further increase in paneling for the foil system only gave a very small improvement of the solution. The panels at the connection of the strut and the hull are not taken into account for the calculation of the total force as they contained unrealistic pressure peaks since they are very close to the hull. The foils are corrected for the required flap angle in Panship by rotating the panels around the hinge of the flap.

As the wake influenced the results for drag severely, it is decided to run the simulations using three other discretisations of the wake. In the first the same length for DWMXA is used, but the wake of the struts of the leading foils is neglected in the solution by removing its wake sheet. In the third solution the length of DWMXA is chosen infinitely long such that the wake sheet of the leading foil is further away from the trailing foil. It should be noted that the shape of this wake sheet is unrealistic as it is never force free. In the third discretisation the first two are combined and the influence of the forward foil on the hull and foil is minimized.
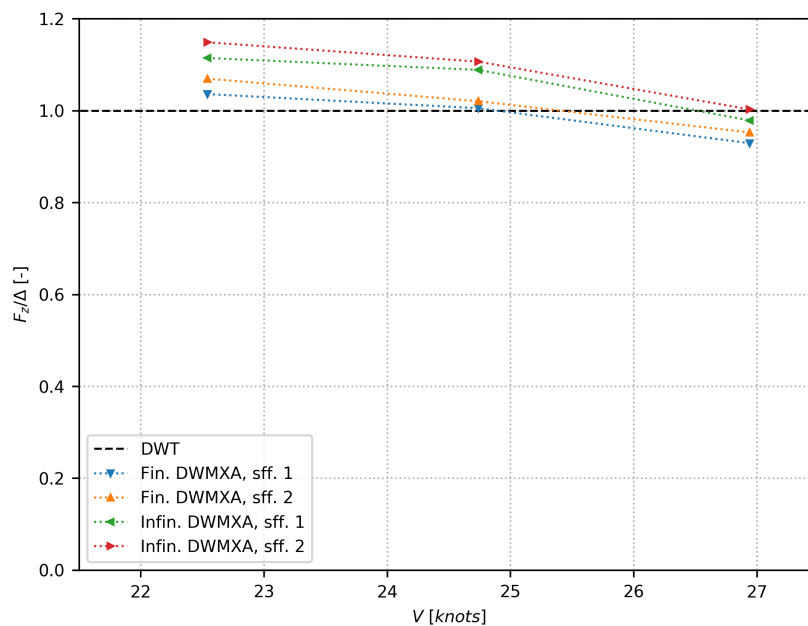
Figure 6.4: Total lift on the hull-foil combination. Fin. DWMXA and Infin. DWMXA denote DWMXA being finite and infinite. ssf.1 and ssf. 2 denote the type of singularity on the forward strut. Singularity type 1 is a source only distribution and does not require a wake sheet. Singularity type 2 is a source and dipole distribution and contains a wake sheet. Therefore, in the case of ssf. 1, the forward struts do not have a wake sheet whereas in the case of ssf. 2 they do.

6.3.1. Lift

Figure 6.4 shows the force in the z-direction F_z for the four different discretisations of the wake and the required force to lift the vessel out of the water, denoted as DWT. It is chosen to not denote this force as lift as it also contains the buoyancy force. The buoyancy forces play an important role in the early stage of the take off, as it is 28% of F_z at a velocity of 22.5 knots. The buoyancy force is much smaller at the higher velocity of 27 knots as it is only 9% of the total force. Figures 6.2 and 6.3 under scribe this as it can be seen that the submerged volume is much smaller at a velocity of 27 knots.

The results show that the predicted F_z for all velocities and discretisations of the wake sheet are similar to the deadweight of the hull-foil combination. The results belonging to the first part of the wakesheet DWMXA being finite, agree better with the deadweight, and thus the required F_z, than the results belonging to an infinite DXMXA.

The results for the finite DWMXA are slightly higher than the required force at the velocities 22.5 and 24.7 knots. This overprediction can be result of an acceleration in z-direction, which the vessel requires to get out of the water and the lack of viscous effects. For the velocity of 27 knots the results for F_z are slightly lower than the required force. This can be explained by a deceleration during the last stage of the takeoff to reach a stationary height above the water. Neglecting the wake of the forward foil gives a small increase in force as the reversed V-shaped struts do not produce downwash.

For the results with an infinite DWMXA, F_z is much higher than for a finite DWMXA. As the wake of the forward foil system is further away from the hull and foil, the system experiences less downwash and produces more lift. In this case the lift is overpredicted. Neglecting the wake of the forward foil has the same effects as when DWMXA is finite, F_z is increased.
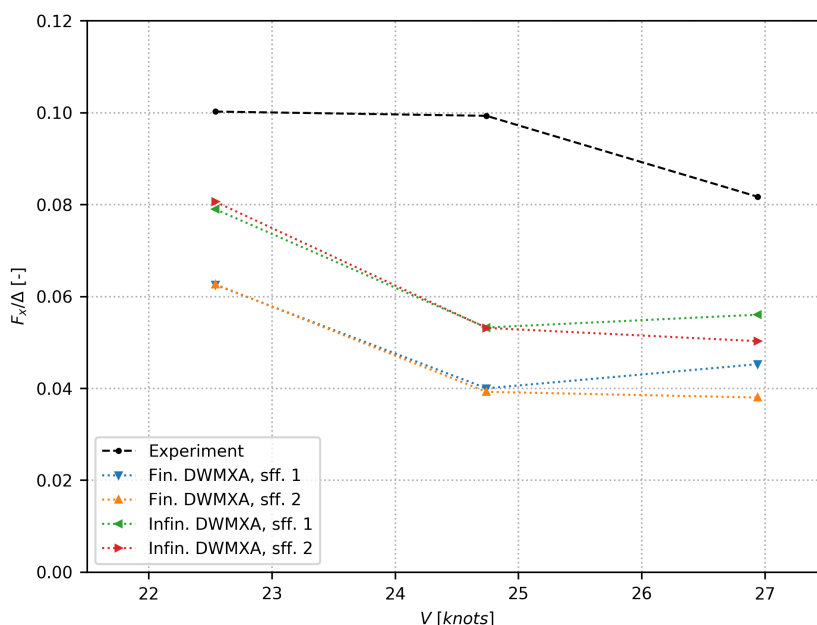
Figure 6.5: Total lift on the hull-foil combination. For the explanation of the legend is referred to figure 6.4

6.3.2. Drag

The results for the resistance are given in figure 6.5 with the experimental results. The figure shows that the resistance is severely underpredicted if compared to the experimental results and that the influence of the wake of the forward foil system is larger on drag than for lift. Removing the wake of the forward struts only has a significant influence on the velocity of 27 knots but the influence of the length of the first part of the wakesheet DWMXA is much larger.

Table 6.1 shows the portions of induced drag of the total drag for the hull only, the foil system only and the total system. The induced drag for the calculations with a finite DWMXA was very small for the foil system and in one case even negative. In that case the induced drag produced trust. As the viscous forces are constant for the same velocity, the difference in resistance for different discretisations of the wake is a result of the induced drag. Unfortunately it is not possible to determine the portions of the induced drag of the hull and foil system separately if the full system is considered.

Based on the results in figure 6.5 and table 6.1 it can be said that the results with an infinite DWMXA are more realistic for induced drag than the finite DWMXA, especially when considering the foil system only. This can be explained by the fact that the wake of the leading foil passes the trailing foil very closely as the forward foil is closer to the free surface due to the trim angle. The wake of the forward foil does not pass the trailing foil this close in foil borne condition and therefore this behaviour is not seen in chapter 5.

The underprediction of the total drag might have four reasons. First, the resistance of spray is not included in the solution. Second, according to the experimental results, the wetted length of the ship was much larger than based on the submerged geometry in Panship. Therefore the wetted area was actually larger and the viscous drag should be higher. Third, as described throughout this thesis, the induced drag is underpredicted in Panship and it plays a role here as well, especially as the total induced drag of the foil system is very low or even provides trust. Fourth, the used form factor may be too low. Equation 2.55 provides a constant form factor per angle of attack, but viscous effects influence the form factor such that it is different per angle of attack [25]. The angles of attack are low in this case, thus the effect of viscosity on the form factor should be small.

	DWMXA	V = 22.5 kn.	V = 24.7 kn.	V = 27.0 kn.
Hull		19 %	24 %	11 %
Foil system	finite	-6 %	2 %	11 % / 4 % [*]
	infinite	46 %	44 %	34 % / 4 % [*]
Total	finite	23 %	12 %	17 % / 0 % [*]
	infinite	40 %	34 %	33 % / 25% [*]

Table 6.1: Portions of induced drag of total drag considering the Hull only, Foil system only and the total system for finite and infinite DWMXA. [*] denotes the cases where the wake of the forward struts plays an important role. The first percentage denotes the portion of induced drag when the wake of the forward strut is neglected in the solution.

6.3.3. Interaction between the hull and the foil

In this section the effects of foil interaction in Panship are studied which is introduced in section 2.4. In order to study the interaction effects, coefficients are used. In this way the effect of the total system on the component is determined. These used interaction coefficients are C_{iz} and C_{ix} for the forces in x and z-direction respectively. The interaction coefficients C_{iz} and C_{ix} are defined as:

$$C_{iz} = \frac{F_{\text{z, component in total system}}}{F_{\text{z, component system only}}} \tag{6.1}$$

$$C_{ix} = \frac{F_{\text{x, component in total system}}}{F_{\text{x, component system only}}} \tag{6.2}$$

The two different components are the hull and the foil system. Therefore, the interaction coefficient for the hull is defined as the force on the hull with the presence of the foil system, the hull in the total system, divided by the force on the hull without the presence of the foil system, the hull only. However, the two foils are considered differently. Thus, the interaction coefficients for the foils always considers effects of two foils, but only uses the force on one foil. In this way the effects of the foil interaction on the two foils can be studied.

The results for foil interaction are shown for the four different wake models in figure 6.6 for the leading foil, the trailing foil and the hull. The interaction coefficients for F_z are treated first. Figure 6.6a shows that, just as expected in section 2.4, the interaction between the hull and the forward foil is very small. The interaction effects for the trailing foil are much larger, as can be seen in figure 6.6c. The discretisation of the wake of the forward foil does influence the performance of the trailing foil, but the effect is small. The reduction of F_z is larger, 40 %, for the two lower velocities than for the highest velocity, where it is 15% to 0%. The interaction coefficient clearly depends on the velocity, just as expected from section 2.4. But in this case it should be noted that the submerged hull on the highest velocity is much smaller than on the lowest velocities as can be seen in figures 6.2 and 6.3, and therefore the interaction can expected to be small. However, based on the results of other studies, the effects are expected to be smaller and more in the order of 0-10 % for the complete foil system [25] [17]. However, this might be case specific.

The interaction coefficients for the hull, given in figure 6.6e, depend much more on the discretisation of the wake. In general, the wake being further away from the hull and removing the wake of the forward strut lead to an increase in F_z. At a velocity of 22.5 knots the interaction coefficient is close to one and the interaction is small. For the velocity of 24.7 knots the interaction coefficient is positive, thus the hull produces more lift, whereas it is negative at 27 knots, producing less lift. The hull produces respectively 19, 24 and 10% of F_z for the increasing velocities, containing hydrodynamic lift and buoyancy forces. Thus, the reduction in F_z at the highest velocity due to the presence of the foil system is small on the total system.

Considering the interaction coefficients for drag, the same is seen for the interaction effects for lift on the forward foil in figure 6.6b, the effect is very small. The interaction coefficients consider the total drag, thus the lift induced drag and the viscous drag. As the viscous drag is constant, the changes seen here are a result of the induced drag. Figure 6.6b shows that the discretisation of the wake influences the interaction coefficient for the trailing foil and that here the interaction coefficient is influenced by the velocity as well. Furthermore,
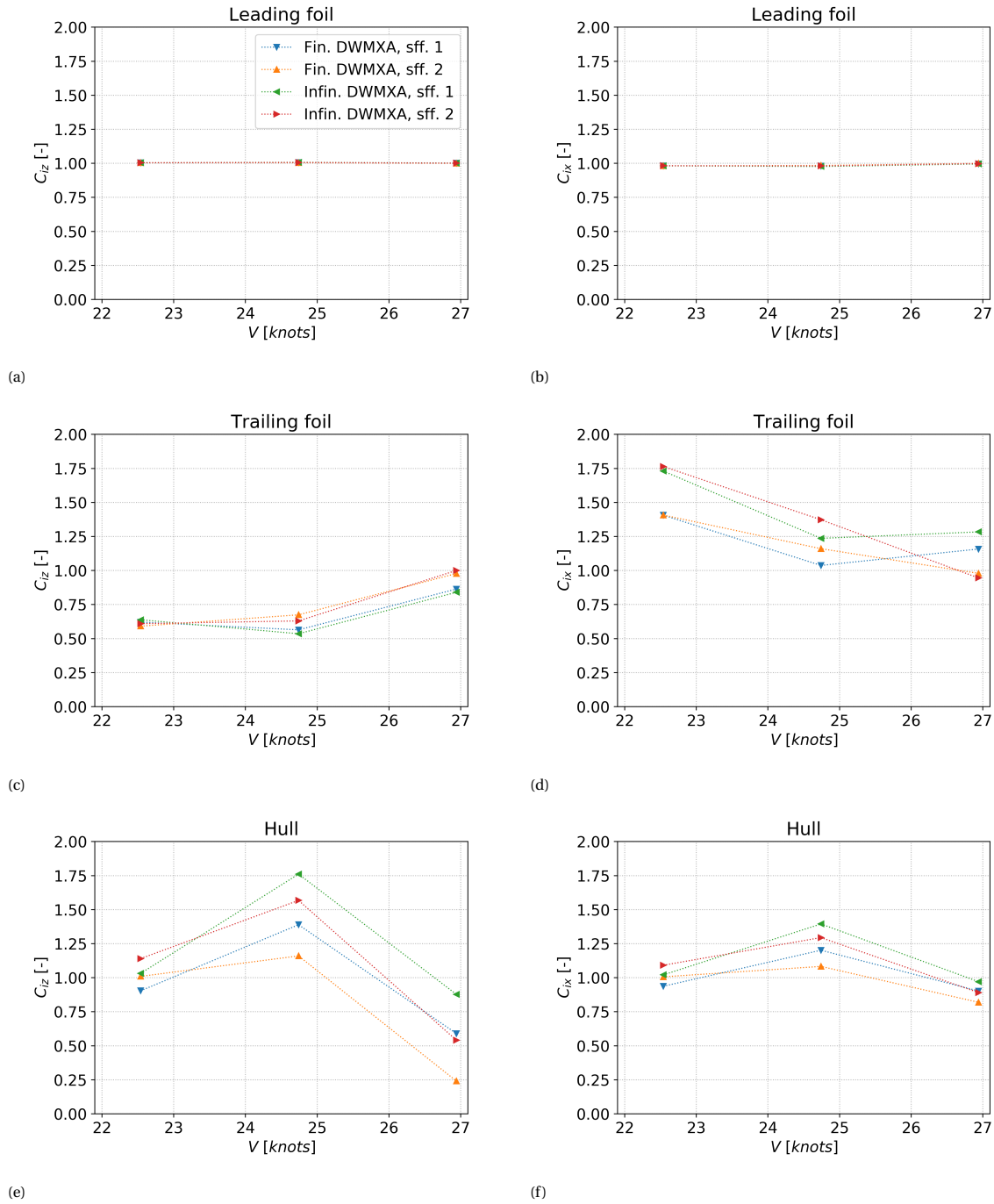
Figure 6.6: Interaction coefficients for interaction between the hull and the foil. For the explanation of the legend is referred to figure 6.4

it can be seen that the influence of the wake of the forward strut is less important than the wake sheet being further away or closer to the trailing foil. The large variation in lift coefficient due to the discretisation of the forward foil under scribes that, according to earlier results in this work, the drag is severely influenced by the discretisation. In this sense it is logical as the inflow of the trailing foil is dominated by the wake of the leading foil.

The drag interaction coefficients for the hull show the same trends as for lift but the variation is smaller. The interaction effect on itself is much smaller and there is only an increase in drag on 24.5 knots.

6.4. Conclusion

Using the results of the experiments, Panship and Hydres an answer can be given to the subquestion provided in the introduction:

> *What is the quality of the results for the hydrodynamical forces of a foil and ship system in Panship during the takeoff in calm water, and how does this compare to the results in Hydres?*

The results of Panship, especially the drag, are influenced by the way the wake of the forward foil is discretised. As expected in the conclusions in 4.8 and 5.6, the results for results for F_z predict the same force as the weight of the ship but the drag is not predicted correct. The drag is severely underestimated if compared to the experimental results. Using an unrealistic shape of the wake, where the effect of the leading foil system on the trailing foil system is smaller, leads to a better prediction of drag, but the drag is still heavily underpredicted. The underestimation of drag can be a result of the underprediction of the induced drag of the foil system, the neglecting of spray, the wrong prediction of the wetted area and a possible underprediction of the form factor.

Panship gives insight into the interaction coefficients of a hydrofoil vessel, however the interaction coefficients for the trailing foil are high if compared to results from the literature. Large variation due to the discretisation of the wake on the interaction coefficients for the drag of the trailing foil and the lift of the hull can be seen.

Comparing the results for drag determined in Hydres to Panship, the quality of the results of Panship for drag is very poor as it is underpredicted severely. The lift in Hydres is overpredicted, as it performs a too early takeoff. A very small overprediction of lift can be seen in Panship as well, which may lead to a slightly too early takeoff. As Panship is not able to predict the correct drag of the hydrofoil vessel during the takeoff, the results of Panship cannot be used to determine the required power during its takeoff. However, as the lift is predicted correctly, the results of Panship can be used for stability calculations and to determine the required takeoff velocity.

7

Conclusions and recommendations

Now all the topics are treated, the research question, given in the introduction of this thesis, can be answered and recommendations for future work can be given. First is started with the research question, given by:

What is the quality of the results for the hydrodynamical forces during the takeoff of a hydrofoil vessel in Panship in calm water, and how does this compare to the results of Hydres?

The subquestions given in the introduction are used to provide an answer to this question. Answers to the subquestions are given in chapters 3, 4, 5 and 6 and are summarized here:

1. *What is the quality of the results for the hydrodynamical forces for a hydrofoil in Panship with a constant forward speed and without free surface effects?* P. 43

   Panship is able to correctly predict the lift of a fully submerged foil in a potential flow but the prediction of lift induced drag is too low. If viscous effects are taken into account Panship overpredicts the lift, and thus the induced drag, as it does not have a correction for viscous effects. Therefore, the quality of the results for lift for a deeply submerged foil in Panship depends on the viscous effect on the lift of the foil. For a low required viscosity the quality is good. The quality of the results for drag is poorer as the induced drag is underpredicted. The discretisation of the foil and its wake influence the quality of the results as well.

2. *What is the quality of results for the hydrodynamical forces for a foil near the free surface in Panship in calm water with a constant forward speed?* P. 53

   The C_{Di}/C_L^2-ratio determined in Panship is too low for all submergences but the right trends are shown. The results of Panship can be used but their quality is limited as the induced drag is undperpredicted. The implementation of a new method to determine the induced drag, using a Trefftz plane, gives a much better agreement with analytic results.

3. *What is the quality of the results for the hydrodynamical forces for two foils towed behind each other in Panship in calm water with a constant forward speed, and how does this compare to the results of Hydvlm?* P. 62

   The effects of foil interaction are predicted well for lift but the results are slightly different from the experimental results and Hydvlm. The difference with the experimental results might be an effect of the

lack of viscous effects in the solution of Panship. The effects of foil interaction on drag are poorer but globally the right trends are shown. Prediction of foil interaction effects on drag is difficult in Hydvlm as well, but the quality of the results is better. The results of Panship may be improved if the induced drag is predicted more correctly using a Trefftz plane.

4. *What is the quality of the results for the hydrodynamical forces of a foil and ship system in Panship during the takeoff in calm water, and how does this compare to the results in Hydres?* P. 70

   Panship slightly overpredicts the lift during the takeoff of a hydrofoil vessel, but the results for drag are of much poorer quality. Results of Panship, especially the drag, are influenced by the shape of the wake of the forward foil-strut system. Using a realistic discretisation of the wake does not give realistic results for induced drag in Panship. Reducing the influence of the wake of the forward foil-strut system on the trailing system gives better results for induced drag, but the results for the total drag are still too low and the shape of the wake is unrealistic. The underestimation of drag can be a result of the following: the underprediction of the induced drag of the total foil system, the neglecting of spray, the wrong prediction of the wetted area and an underprediction of the form factor. Panship gives insight into the effects of foil interaction but comparing the results of Panship with literature, the effects of foil interaction are large.

Now the research question can be answered: The quality of the results for induced drag on the foil system is poor, but if the limits of Panship are taken into account, its results can be used. For a single foil, a foil system and a hull-foil system the prediction of lift is of fair quality. The prediction of drag is more difficult since the induced drag is underpredicted and the effects of foil interaction are predicted poorly. The implementation of a new method to determine the induced drag using a Trefftz plane gives better results and may improve the results for foil interaction and the drag of the total system. Comparing the results for drag during the takeoff determined in Hydres with the results of Panship, it can be seen that the results for Hydres are much better in agreement with the experimental results than the results of Panship.

As Panship is not able to predict the correct drag of the hydrofoil vessel during the takeoff, the results of Panship cannot be used to determine the required power during its takeoff. However, as the lift is predicted correctly, the results of Panship can be used for stability calculations, to determine the required takeoff velocity and optimization of foil spacing.

This version of Panship is not suitable to analyze the hydrodynamical forces during the takeoff of a hydrofoil vessel as the drag is not predicted correctly. Based in the current work, it cannot be said if a BEM in general is not suitable for analysing a takeoff of a hydrofoil vessel. However, using a BEM clearly has its limits. The results of Panship and other BEM can be improved by following recommendations:

1. *Implement a better method to determine the induced drag. Results show that the implementation of a Trefftz plane gives a higher quality of results for a deeply submerged foil. The same method can be extended for use for foils near the free surface.*

2. *Implement a correction for the viscous lift such that the lift and induced drag are determined more precisely for foils with a large influence of viscosity.*

3. *Implement a correction for actual wetted area to determine the frictional forces.*

After these recommendations are implemented, the following should be validated:

1. *Obtain numerical validation data for the takeoff, including viscous effects to determine the interaction coefficients and pressure distributions of the components and use these to validate the hull-foil interaction coefficients in Panship.*

2. *Perform a takeoff in semi-unsteady Panship to validate the hull-foil interaction. In the current work is not accounted for the accelerations during the takeoff as the takeoff is performed in three steady runs.*

In semi-unsteady Panship the actual submerged volume is calculated in every time step such that the takeoff can be performed in one single run.

3. *Perform a takeoff in Panship in waves.*

A

Appendix

A.1. Gauss Theorem

The Gauss' theorem can be used to relate volume integrals to surface integrals and is given by:

$$\iiint_V \frac{\partial Q}{\partial x_i} dV = \iint_A n_i Q dA \tag{A.1}$$

where a volume V is bounded by a closed surface A, having a normal vector $\mathbf{n}$. An elaborate proof of this theorem is provided in [12]. The equation is valid for Q being a tensor, scalar or vector. If Q is a vector, the Gauss' theorem can be rewritten to the Divergence theorem being:

$$\iiint_V \nabla \cdot \mathbf{Q} dV = \iint_A \mathbf{n} \cdot \mathbf{Q} dA \tag{A.2}$$

A.2. Green's theorem

To derive Green's theorem one starts with the Divergence theorem (A.2) [12]:

$$\iiint_V \nabla \cdot \mathbf{Q} dV = \iint_A \mathbf{n} \cdot \mathbf{Q} \, dA \tag{A.3}$$

The first identity of Green's theorem is derived using two scalars which are function of position:

$$\begin{aligned}\psi &= \psi(\mathbf{x}),\\ \phi &= \phi(\mathbf{x})\end{aligned} \tag{A.4}$$

which are used to define the vector field:

$$\mathbf{Q} = \psi \nabla \phi \tag{A.5}$$

This vector field is substituted in (A.3) resulting in:

$$\iiint_V \nabla \cdot (\psi \nabla \phi) dV = \oiint_S \psi \nabla \phi \cdot \mathbf{n} \, dS \tag{A.6}$$

Rewriting the contents of the integral on the left hand side of the equation gives:

$$\nabla \cdot (\psi \nabla \phi) = \psi \nabla \cdot \nabla \phi + \nabla \psi \cdot \nabla \phi \tag{A.7}$$

which can be used to rewrite (A.6) to:

$$\iiint_V \left(\psi \nabla^2 \phi + \nabla \psi \cdot \nabla \phi \right) dV = \oiint_S \psi \nabla \phi \cdot \mathbf{n} \, dS. \tag{A.8}$$

This first result is called the First Identity of the Green's theorem. The Second Identity of the Green's theorem is obtained by substituting another vector field, being:

$$\mathbf{Q} = \psi \nabla \phi - \phi \nabla \psi \tag{A.9}$$

Substituting this vector field in equation A.3 the following result is obtained:

$$\iiint_V \nabla \cdot (\psi \nabla \phi - \phi \nabla \psi) dV = \oiint_S (\psi \nabla \phi - \phi \nabla \psi) \cdot \mathbf{n} \, dS \tag{A.10}$$

which can be rewritten to:

$$\iiint_V \left(\psi \nabla^2 \phi - \phi \nabla^2 \psi \right) dV = \oiint_S (\psi \nabla \phi - \phi \nabla \psi) \cdot \mathbf{n} \, dS \tag{A.11}$$

This result is called the Second Identity of Green's Theorem. Using the definition of a directional derivative:

$$\nabla \phi \cdot \mathbf{n} = \frac{\partial \phi}{\partial n} \tag{A.12}$$

(A.11) can be rewritten to:

$$\iiint_V \left(\psi \nabla^2 \phi - \phi \nabla^2 \psi \right) dV = \oiint_S \left(\psi \frac{\partial \phi}{\partial n} - \phi \frac{\partial \psi}{\partial n} \right) dS \tag{A.13}$$

A.3. Reynolds transport theorem

The Reynolds transport theorem can be used to time differentiate integrals over arbitrary moving and deforming volumes. The derivation provided in [14] is followed which is started with considering a moving volume $V(t)$ having a closed surface area of $A(t)$ with a normal of $\mathbf{n}$. The local velocity of $A(t)$ is given by $\mathbf{b}$.

The derivation is started with the definition of the time derivative of the integral of a function $F(\mathbf{x}, t)$:

$$\frac{d}{dt} \int_{V(t)} F(\mathbf{x}, t) dV = \lim_{\Delta t \to 0} \frac{1}{\Delta t} \left\{ \int_{V(t+\Delta t)} F(\mathbf{x}, t+\Delta t) dV - \int_{V(t)} F(\mathbf{x}, t) dV \right\}. \tag{A.14}$$

The second step is to define ΔV and take a Taylor expansion of $F(\mathbf{x}, t + \Delta t)$ for $\Delta t \to 0$:

$$\Delta V \equiv V(t + \Delta t) - V(t),$$
$$F(\mathbf{x}, t + \Delta t) \cong F(\mathbf{x}, t) + \Delta t \frac{\partial F}{\partial t}. \tag{A.15}$$

Now the integral $\int_{V(t+\Delta t)} F(\mathbf{x}, t + \Delta t) dV$ of (A.14) can be rewritten to:

$$\int_{V(t+\Delta t)} F(\mathbf{x}, t + \Delta t) dV \cong \int_{V(t)} F(\mathbf{x}, t) dV + \int_{V(t)} \Delta t \frac{\partial F(\mathbf{x}, t)}{\partial t} dV + \int_{\Delta V} F(\mathbf{x}, t) dV + \int_{\Delta V} \Delta t \frac{\partial F(\mathbf{x}, t)}{\partial t} dV. \tag{A.16}$$

Substituting (A.16) in (A.14) results in:

$$\frac{d}{dt} \int_{V(t)} F(\mathbf{x}, t) dV = \lim_{\Delta t \to 0} \frac{1}{\Delta t} \left\{ \int_{V(t)} \Delta t \frac{\partial F(\mathbf{x}, t)}{\partial t} dV + \int_{\Delta V} F(\mathbf{x}, t) dV \right\} \tag{A.17}$$

where the first term of (A.16) cancels with the last term in (A.14) and the final term in (A.16) will not contribute as it is second order. $\int_{V(t)} F(\mathbf{x}, t) dV$ in (A.14) can be rewritten using Gauss' theorem:

$$\int_{\Delta V} F(\mathbf{x}, t) dV \cong \int_{A(t)} F(\mathbf{x}, t) (\mathbf{b} \Delta t \cdot \mathbf{n}) dA. \tag{A.18}$$

Substituting (A.18) in (A.17) and taking the limit results in the Reynolds transport theorem, being:

$$\frac{d}{dt} \int_{V^*(t)} F(\mathbf{x}, t) dV = \int_{V(t)} \frac{\partial F(\mathbf{x}, t)}{\partial t} dV + \int_{A(t)} F(\mathbf{x}, t) \mathbf{b} \cdot \mathbf{n} dA \tag{A.19}$$

A.4. Kutta-Joukowski lift theorem

Under the assumptions of potential flow, the flow around a shape can be reproduced by using a uniform flow, a dipole and a circulation around the shape. As example a cylinder is used, where the lift resulting of flow around the cylinder can be determined by integrating the pressure over the wall [14]. The pressure is a result of (2.22) where the potential is the sum of the potential of a vortex, a uniform flow and a dipole:

$$\Phi = U_\infty \cos\theta \left(r + \frac{R^2}{r} \right) - \frac{\Gamma}{2\pi} \theta \tag{A.20}$$

The resulting pressure of (2.22) is given by:

$$p(r = a, \theta) = p_\infty + \frac{1}{2} \rho \left(U^2 - \left(-2U \sin\theta - \frac{\Gamma}{2\pi a} \right)^2 \right) \tag{A.21}$$

Integration of (A.21) in the vertical direction over the surface of a circle results in the following equation for lift per unit width:

$$L = -\int_0^{2\pi} p(r = a, \theta) \, \sin\theta \, a \, d\theta = -\rho U \Gamma \tag{A.22}$$

This relation between lift and circulation is known as the Kutta-Joukowski lift theorem and can be used for any 2D shape. Equation A.22 can be rewritten in vector form, as the force is directly proportional to the circulation and acts normal to the free stream:

$$\mathbf{F} = \rho \mathbf{U} \times \Gamma \tag{A.23}$$

A.5. The Biot-Savart Law

The derivation of the Biot-Savart Law as given in [13] is given here which starts with the assumption of incompressible flow and constant viscosity. The velocity field is taken as a result of the curl of a vector $\mathbf{B}$:

$$\mathbf{q} = \nabla \times \mathbf{B}. \tag{A.24}$$

Now the vorticity becomes:

$$\zeta = \nabla \times \mathbf{q} = \nabla \times (\nabla \times \mathbf{B}) = \nabla(\nabla \cdot \mathbf{B}) - \nabla^2 \mathbf{B}. \tag{A.25}$$

As the curl of a gradient vector is zero, $\mathbf{B}$ should be chosen such that:

$$\nabla \cdot \mathbf{B} = 0 \tag{A.26}$$

This equation can be used to rewrite (A.25) into:

$$\zeta = -\nabla^2 \mathbf{B} \tag{A.27}$$

which can be solved using Green's theorem (A.13). In order to solve the Green's function the following definitions for ϕ and ψ are used:

$$\phi = \mathbf{B},$$
$$\psi = \frac{1}{\left|\mathbf{r_0} - \mathbf{r_1}\right|}$$

and the singularity point $\mathbf{r_0} = \mathbf{r_1}$ is excluded from the integral [12]. The vector $\mathbf{r_0} - \mathbf{r_1}$ is the vector from the vortex segment to the location of interest. The solution of (A.27) is given by:

$$\mathbf{B} = \frac{1}{4\pi} \int_V \frac{\zeta}{\left|\mathbf{r_0} - \mathbf{r_1}\right|} dV \tag{A.28}$$

Using (A.25) this can be rewritten to:

$$\mathbf{q} = \frac{1}{4\pi} \int_v \nabla \times \frac{\zeta}{\left|\mathbf{r_0} - \mathbf{r_1}\right|} dV \tag{A.29}$$

Before the integration is started, the following identities have to be defined where dS is selected such that it is normal to ζ.
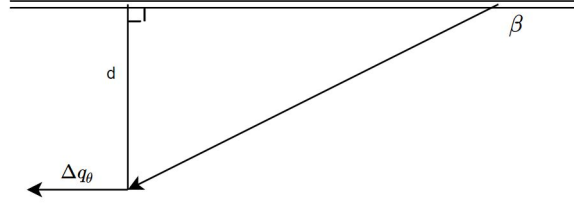
Figure A.1: Induced velocity of a constant strength vortex line

$$d\mathbf{l} = \frac{\zeta}{\zeta} dl \tag{A.30}$$

$$\Gamma = \zeta dS \tag{A.31}$$

$$dV = dSd \tag{A.32}$$

Using (A.30), (A.31) and (A.32) for the integral part of A.29 and carrying out the curl operator gives:

$$\nabla \times \frac{\zeta}{|\mathbf{r}_0 - \mathbf{r}_1|} dV = \nabla \times \Gamma \frac{d\mathbf{l}}{|\mathbf{r}_0 - \mathbf{r}_1|} = \Gamma \frac{d\mathbf{l} \times (\mathbf{r}_0 - \mathbf{r}_1)}{|\mathbf{r}_0 - \mathbf{r}_1|^3} \tag{A.33}$$

Substituting the result of (A.33) into (A.29) leads to the Biot-Savart Law:

$$\mathbf{q} = \frac{\Gamma}{4\pi} \int \frac{d\mathbf{l} \times (\mathbf{r}_0 - \mathbf{r}_1)}{|\mathbf{r}_0 - \mathbf{r}_1|^3} \tag{A.34}$$

In differential form the Biot-Savart Law states:

$$\Delta\mathbf{q} = \frac{\Gamma}{4\pi} \frac{d\mathbf{l} \times (\mathbf{r}_0 - \mathbf{r}_1)}{|\mathbf{r}_0 - \mathbf{r}_1|^3} \tag{A.35}$$

A.6. Induced velocity of a constant strength vortex line

To determine the induced velocity of a constant strength vortex line, the differential form of the Biot-Savart Law is rewritten to a form which is convenient for numerical use. The derivation is provided by [13] and is started with rewriting (A.35) to a scalar form:

$$\Delta q_\theta = \frac{\Gamma}{4\pi} \frac{\sin\beta}{r^2} dl \tag{A.36}$$

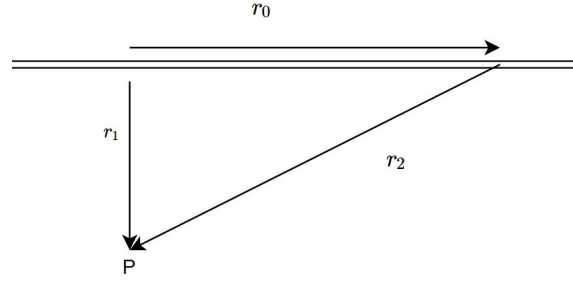Based on figure A.1 the following relations can be given:

$$d = r\sin\beta \tag{A.37}$$

Figure A.2: Definitions of vectors $\mathbf{R_0}$, $\mathbf{R_1}$ and $\mathbf{R_2}$

$$\tan(\pi - \beta) = \frac{d}{l} \tag{A.38}$$

Leading to:

$$l = \frac{-d}{\tan \beta} \tag{A.39}$$

$$dl = \frac{d}{\sin^2 \beta} d\beta \tag{A.40}$$

Substituting A.37 and A.40 in A.36 gives:

$$\Delta q_\theta = \frac{\Gamma}{4\pi d} \sin \beta d\beta \tag{A.41}$$

Integrating this equation from point 1 to point 2 on the vortex segment leads to:

$$q_{\theta 1,2} = \frac{\Gamma}{4\pi d} \left(\cos \beta_1 - \cos \beta_2 \right) \tag{A.42}$$

This equation can be modified for use in 3D form using the vectors from point 1 and point 2 on the vortex line to the influence point such that (see figure A.2):

$$\mathbf{r}_0 = \mathbf{r}_1 - \mathbf{r}_2 \tag{A.43}$$

Using the relations for the distance from a point to a line and the angle between two vectors [12]:

$$d = \frac{\left| \mathbf{r}_1 \times \mathbf{r}_2 \right|}{\left| \mathbf{r}_0 \right|}, \tag{A.44}$$

$$\cos \beta_1 = \frac{\mathbf{r}_0 \cdot \mathbf{r}_1}{\left| \mathbf{r}_0 \right| \left| \mathbf{r}_1 \right|}, \tag{A.45}$$

$$\cos \beta_2 = \frac{\mathbf{r}_0 \cdot \mathbf{r}_2}{\left| \mathbf{r}_0 \right| \left| \mathbf{r}_2 \right|} \tag{A.46}$$

and the direction of the normal on the plane of the influence point and start and end of the vortex line:

$$\mathbf{n} = \frac{\mathbf{r}_1 \times \mathbf{r}_2}{\left|\mathbf{r}_1 \times \mathbf{r}_2\right|} \tag{A.47}$$

As final result the induced velocity of a vortex line is:

$$\mathbf{q}_{1,2} = \frac{\Gamma}{4\pi} \frac{\mathbf{r}_1 \times \mathbf{r}_2}{\left|\mathbf{r}_1 \times \mathbf{r}_2\right|^2} \mathbf{r}_0 \cdot \left(\frac{\mathbf{r}_1}{r_1} - \frac{\mathbf{r}_2}{r_2}\right) \tag{A.48}$$

B

Appendix

B.1. Grid convergence
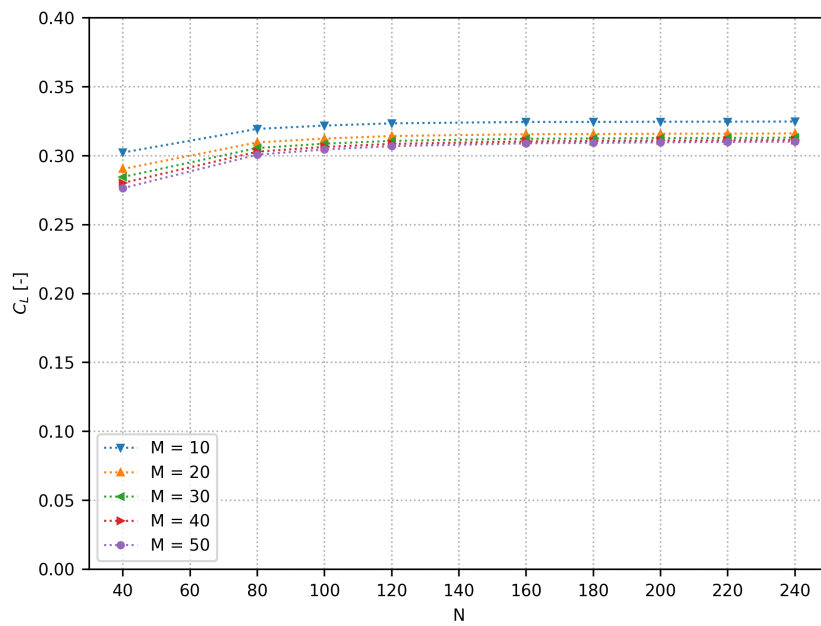
Figure B.1: Effect of amount of spanwise M and chordwise panels N on lift of a NACA64A010 foil
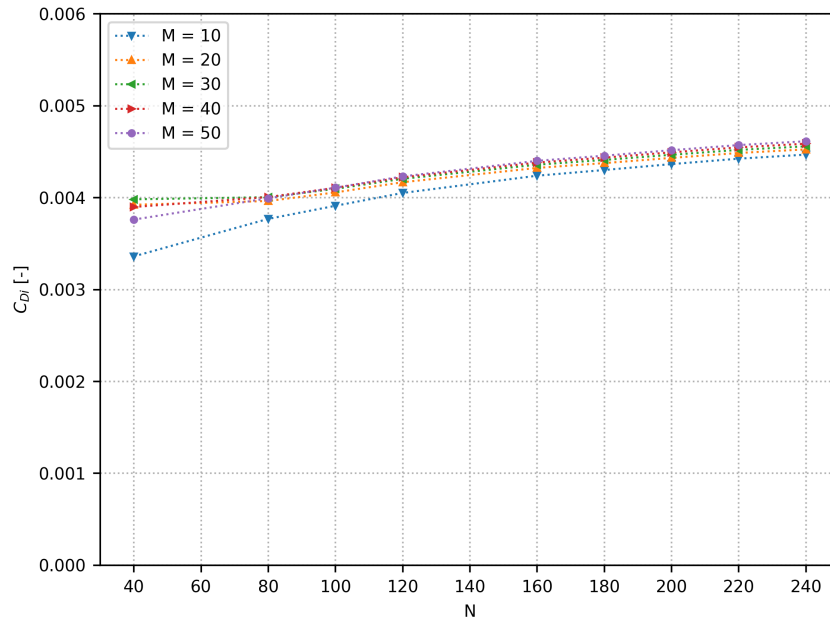
Figure B.2: Effect of amount of spanwise M and chordwise panels N on drag of a NACA64A010 foil
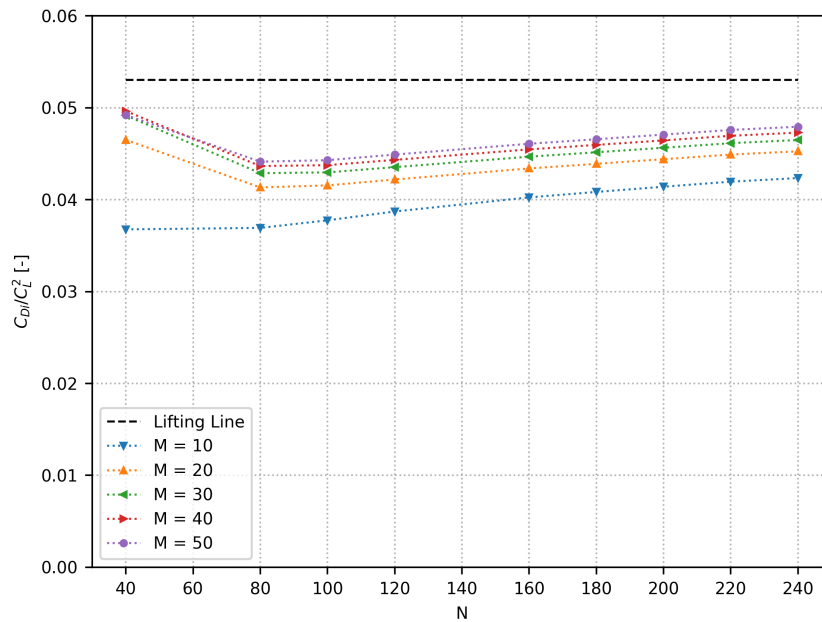
Figure B.3: Effect of amount of spanwise M and chordwise panels N on C_{Di}/C_L^2 of a NACA64A010 foil
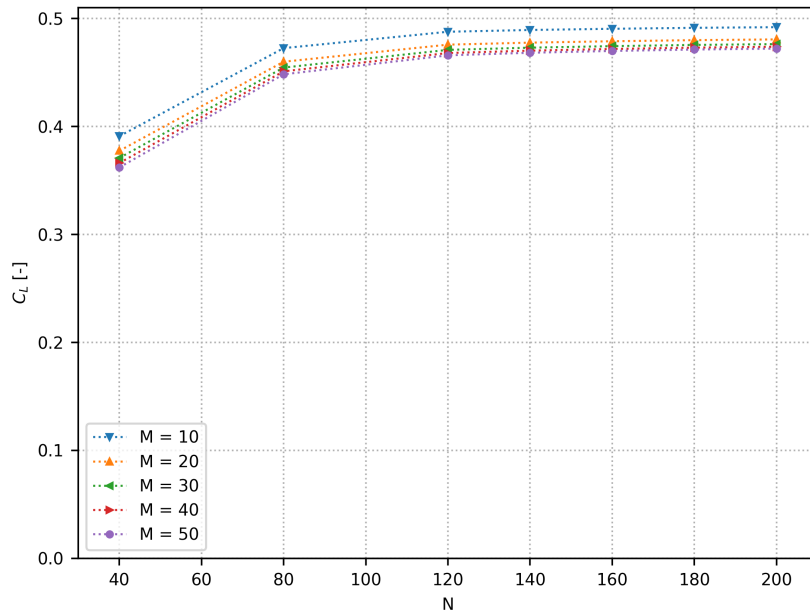
Figure B.4: Effect of amount of spanwise M and chordwise panels N on lift of a NACA16-008 with a NACA a = 0.8 modified camber line
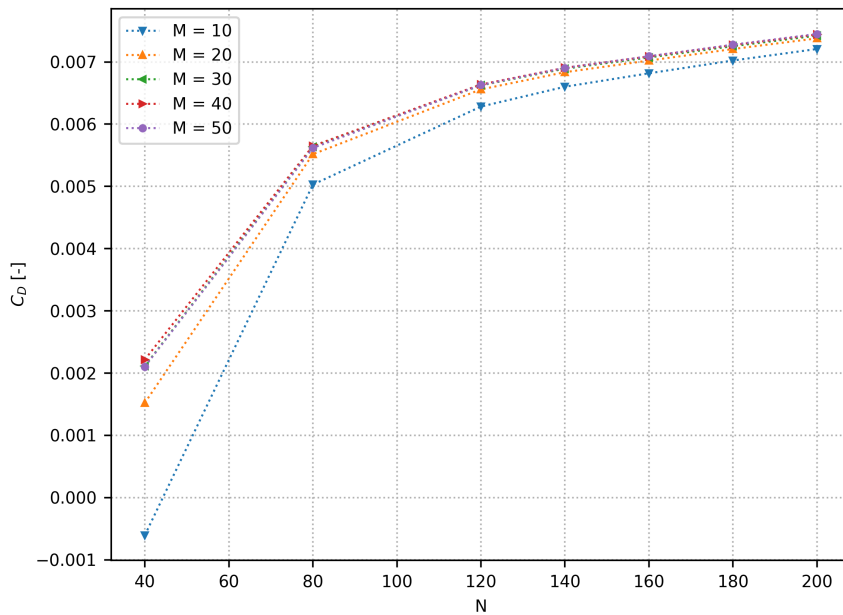
Figure B.5: Effect of amount of spanwise M and chordwise panels N on drag of a NACA16-008 with a NACA a = 0.8 modified camber line

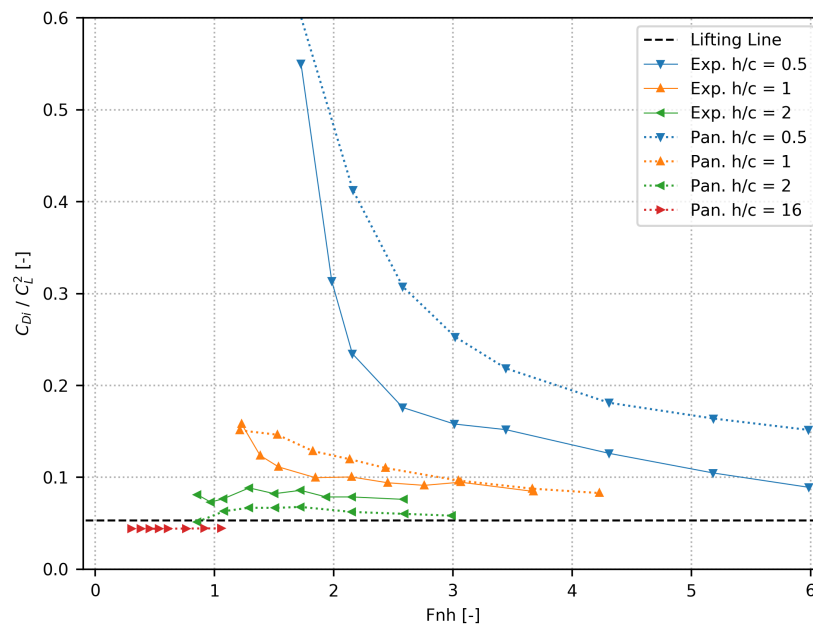## B.2. Influence of length of first wake panel on free surface effects

Figure B.6: Results of Panship and experiments [27] for the C_{Di}-C_L^2-curve for an angle of attack of 4°, the results for an elliptical lift distribution in an analytical lifting line method are shown as well. The used value of FAKTWE is 0.1.
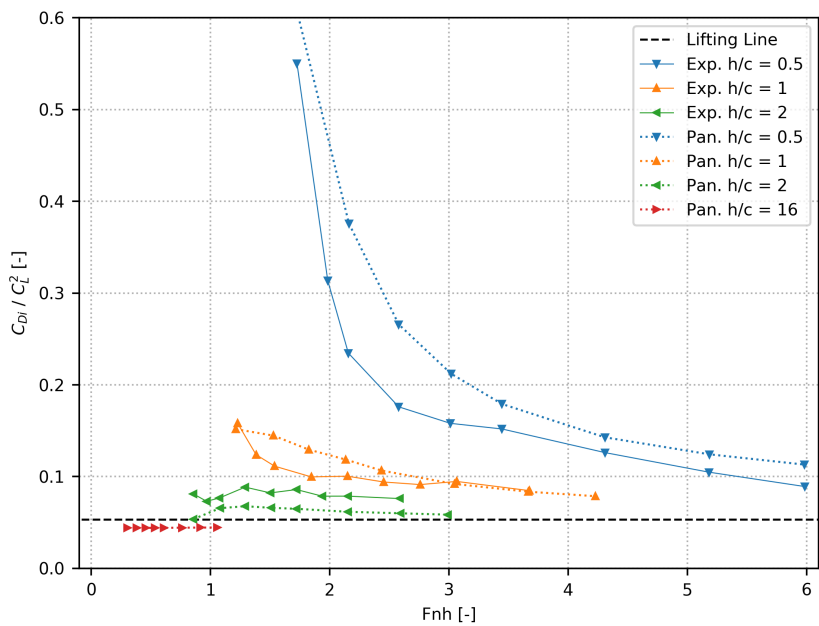
Figure B.7: Results of Panship and experiments [27] for the C_{Di}-C_L^2-curve for an angle of attack of 4°, the results for an elliptical lift distribution in an analytical lifting line method are shown as well. The used value of FAKTWE is 0.5.

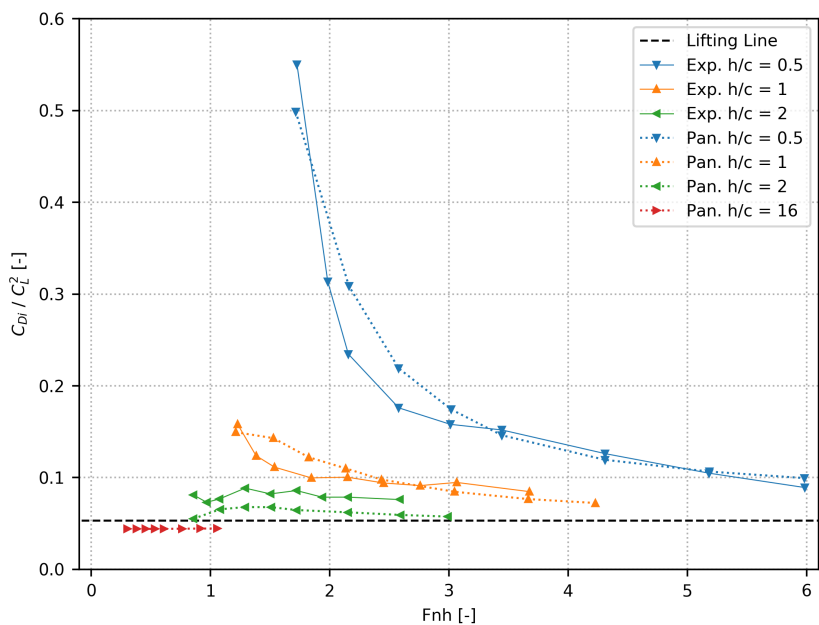Figure B.8: Results of Panship and experiments [27] for the C_{Di}-C_L^2-curve for an angle of attack of 4°, the results for an elliptical lift distribution in an analytical lifting line method are shown as well. The used value of FAKTWE is 1.0.
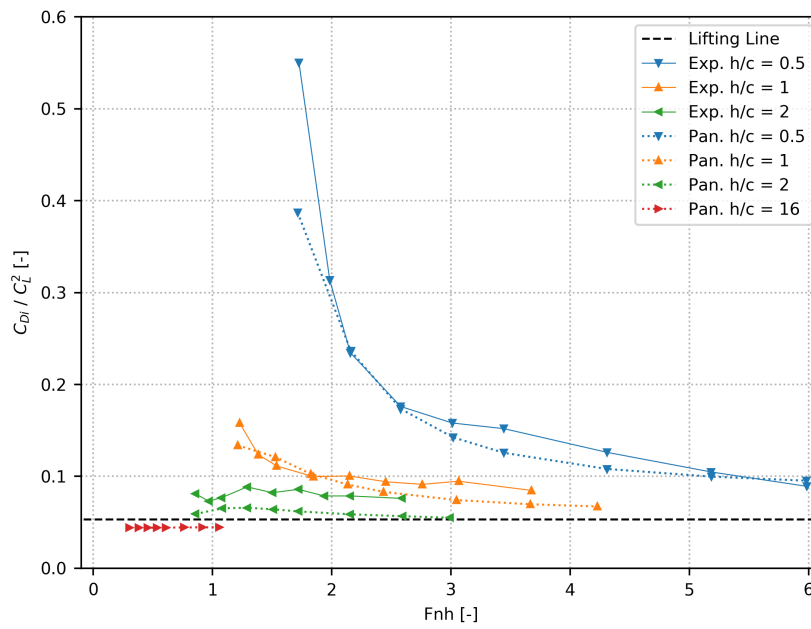
Figure B.9: Results of Panship and experiments [27] for the C_{Di}-C_L^2-curve for an angle of attack of 4°, the results for an elliptical lift distribution in an analytical lifting line method are shown as well. The used value of FAKTWE is 2.5.

Bibliography

[1] D. Amadori. *A CFD study of morpho butterflies*. Master's thesis, Politecnico di Torino, 2019.

[2] J. Anderson. *Introduction to flight*. McGraw-Hill, 7th edition, 2012.

[3] P. de Jong. *Seakeeping behaviour of high speed ships*. PhD thesis, Technical University of Delft, 2011.

[4] M. Drela. XFoil: An analysis and design system for low reynolds number airfoils. In *Low Reynolds Number Aerodynamics: Proceedings of the Conference Notre Dame*, pages 1–12, 1989.

[5] M. Drela and M. Gilest. Viscous-inviscid analysis of transonic and low reynolds number airfoils. *AIAA Journal*, 25(10):1347–1355, 1987.

[6] M. Drela and H. Youngren. *XFOIL 6.9 user primer*, 2001.

[7] O. Faltinsen. *Sea loads on ships and offshore structures*. Cambridge University Press, 6th edition, 1998.

[8] O. Faltinsen. *Hydrodynamics of high-speed marine vehicles*. Cambridge University Press, 1st edition, 2005.

[9] J. Grisolia and J. de Dios Ortuzar. Forcasting vs. observed outturn: studying choice in faster inter-island connections. *Transportation Research*, pages 159–168, 2010.

[10] S. Hoerner. *Fluid-dynamic drag: Practical information on aerodynamic drag and hydrodynamic resistance*. Hoerner Fluid Dynamics, 2nd edition, 1992.

[11] S. Ishikawa. Study on hydrodynamic interaction between hull and submerged foils. In *Spring Meeting of The Society of Naval Architects of Japan*, pages 135–142, 1991.

[12] K. Karamcheti. *Principles of ideal-fluid aerodynamics*. John Wiley and Sons, Inc., 1st edition, 1966.

[13] J. Katz and A. Plotkin. *Low-speed aerodynamics*. Cambridge University Press, 2nd edition, 2001.

[14] P. Kundu, I. Cohen, and D. Dowling. *Fluid Mechanics*. Academic Press, 6th edition, 2016.

[15] M. Mahmud. The applicability of hydrofoils as a ship control device. *Journal of Marine Science and Application*, 14(3):244–249, 2015.

[16] M. Martin. The stability derivatives of a hydrofoil boat. Technical report, Hydrodynamics Incorporated, 1963.

[17] G. Migeotte. *Design and optimization of hydrofoil-assisted catamarans*. PhD thesis, University of Stellenbosch, 2002.

[18] S. Mohammad and M. Mehmet. Effect of thickness-to-chord tatio on aerodynamics of non-slender delta wing. *Aerospace Science and Technology*, 88:298–307, 2019.

[19] H. Morch. Aspects of hydrofoil design; with emphasis on hydrofoil interaction in calm water. Technical report, Institutt for Marin Hydrodynamikk Trondheim, 1992.

[20] J. Newman. The rolling up of the trailing vortex sheets and its effects on the downwash behind wings. *Proceedings of the 4th International Conference on Numerical Ship Hydromechanics*, pages 1–19, 1985.

[21] A. Smith and N. Gamberoni. Transition, pressure gradient, and stability Theory. Technical report, Douglas Aircraft Company, inc., 1956.

[22] S. Smith. A computational and experimental study of nonlinear aspects of induced drag. Technical report, NASA Ames Research Center, 1996.

[23] J. Spreiter and A. Sacks. The rolling up of the trailing vortex sheets and its effects on the downwash behind wings. *Journal of the Aeronautical Sciences*, 18(1):21–32, 1951.

[24] R. Timman and J. Newman. The coupled damping coefficients of a symmetric ship. *Journal of Ship Research*, 5(4):1–7, 1962.

[25] F. van Walree. *Computational methods for hydrofoil craft in steady and unsteady flow.* PhD thesis, Technical University of Delft, 1999.

[26] F. van Walree and P. de Jong. *Panship: User manual.* MARIN, 6700 AA Wageningen, The Netherlands, 3rd edition, 11 2018.

[27] M. Wilson. Experimental determination of low froude number hydrofoil performance in calm water and in regular waves. In *Proceedings of the Twentieth General Meeting of the American Towing Tank Conference*, pages 517 – 540, New Jersey, 1983.